NASA CR-121000
2420-N03

BASIC FAILURE MECHANISMS IN ADVANCED COMPOSITES

BY

J. V. Mullin, V. F. Mazzio and R. L. Mehan

GENERAL ELECTRIC COMPANY
SPACE SCIENCES LABORATORY

prepared for

NATIONAL AERONAUTICS AND SPACE ADMINISTRATION

NASA Lewis Research Center

Contract NASw-2093

Tito T. Serafini, Project Manager

NASA CR-121000
2420-N03

BASIC FAILURE MECHANISMS IN ADVANCED COMPOSITES

BY

J. V. Mullin, V. F. Mazzio and R. L. Mehan

GENERAL ELECTRIC COMPANY
SPACE SCIENCES LABORATORY

prepared for

NATIONAL AERONAUTICS AND SPACE ADMINISTRATION

NASA Lewis Research Center

Contract NASw-2093

Tito T. Serafini, Project Manager

1. Report No.	2. Government Accession No.	3. Recipient's Catalog No.
NASA CR-121000		

4. Title and Subtitle	5. Report Date
Basic Failure Mechanisms in Advanced Composites	6. Performing Organization Code

7. Author(s)	8. Performing Organization Report No.
J. V. Mullin, V. F. Mazzio and R. L. Mehan	2420-NO3
	10. Work Unit No.

9. Performing Organization Name and Address	11. Contract or Grant No.
General Electric Company Space Sciences Laboratory Valley Forge, Pa.	NASw-2093
	13. Type of Report and Period Covered
12. Sponsoring Agency Name and Address	Contractor Report
National Aeronautics and Space Administration Washington, D.C. 20546	14. Sponsoring Agency Code

15. Supplementary Notes

Project Manager, Tito T. Serafini, Materials and Structures Division, NASA-Lewis Research Center, Cleveland, Ohio

16. Abstract

The purpose of this effort was to identify failure mechanisms in carbon-epoxy composites as a basis for more reliable prediction of the performance of these materials. The approach involved both the study of local fracture events in model specimens containing small groups of filaments and fractographic examination of high fiber content engineering composites. A good deal of emphasis has been placed on the correlation of model specimen observations with gross fracture modes. The effects of fiber surface treatment, resin modification and fiber content were studied and acoustic emission methods were applied. Some effort was devoted to analysis of the failure process in composite/metal specimens.

17. Key Words (Suggested by Author(s))	18. Distribution Statement
failure mechanisms, composites, carbon fibers, fracture modes, acoustic emission	Unclassified - unlimited

19. Security Classif. (of this report)	20. Security Classif. (of this page)	21. No. of Pages	22. Price*
Unclassified	Unclassified	113	3.00

* For sale by the National Technical Information Service, Springfield, Virginia 22151

FOREWORD

This is the final report for NASA Contract NASw 2093 "Basic Failure Mechanisms in Advanced Composites". The program was accomplished during the time period April 1971 to March 1972 and initiated through NASA Headquarters under Mr. Bernard G. Achhammer. During the year the program was transferred to Lewis Research Center with Dr. Tito T. Serafini as NASA Program Manager.

The individuals who contributed to the program are:

Mr. E. Muziani and Mr. R. Grosso in the preparation and testing of specimens.

Dr. E. Feingold, Mr. E. Castagliuolo Mr. T. Harris and Mr. M. Birenbaum in characterization.

The authors also wish to thank Mr. Achhammer and Dr. Serafini for their helpful technical suggestions. Interesting and fruitful technical discussions with Mr. R. Pride and Dr. H. Herring of NASA-Langley Research Center are also appreciated.

The requirements of NASA Policy Directive NPD 2220.4 (September 14, 1970) regarding the use of SI units have been waived in accordance with the provisions of paragraph 5d of that Directive.

BASIC FAILURE MECHANISMS IN ADVANCED COMPOSITES

by

J. V. Mullin, V. F. Mazzio and R. L. Mehan

SUMMARY

This final report covers the period 25 April 1971 to 25 March 1972 performed under Contract NASw-2093 and initiated through NASA Headquarters under Mr. Bernard G. Achhammer. During the year the program was transferred to Lewis Research Center with Dr. Tito Serafini assigned as NASA Program Manager.

The purpose of this effort is to identify failure mechanisms in carbon-epoxy composites as a basis for more reliable prediction of the performance of these materials. The approach involves the study of fracture phenomena at two levels:

a) local fracture events in model specimens containing small groups of fibers where individual fiber failure, interface and matrix response can be observed and photographed.

b) fractographic examination of engineering composite specimens where the fiber content is on the order of half the specimen volume to establish gross fracture modes.

Much of the effort has been directed toward tensile behavior but some experiments have also been conducted in compression. Parameters such as resin toughness, fiber surface treatment and variations in fiber properties and volume fraction have been considered.

A good deal of emphasis has been placed on the correlation of single fiber and tow observations with gross fracture modes. This phase of the program has been particularly fruitful with clear evidence that single fiber tests are very good indicators of gross composite fracture modes. The relation between fiber content and bulk fracture modes is particularly interesting with lower fiber contents resulting in more localized fracture

zones for the most part. Further, there is strong evidence that weaker composites, regardless of fiber content, tend to cleave on a single plane while the stronger specimens exhibit extensive fracture zones as a result of cumulative damage.

Other aspects of the program include the study of failure processes in composite/metal specimens and the use of acoustic monitoring to reconstruct the failure process. Although most of the effort described here involved DEN 438 epoxy-novolac as the matrix, some experiments were performed with the ERL 4617 cycloaliphatic system and BP 907 elastomer modified epoxy in the tube studies.

TABLE OF CONTENTS

LIST OF TABLES

LIST OF TABLES (continued)

LIST OF FIGURES

FIGURE Page

FIGURE Page

FIGURE Page

1.0 INTRODUCTION

This report covers the period April 1971 through March 1972 and supplements the progress report submitted in October 1971 on NASA contract NASw-2093. The research described herein is an outgrowth of efforts initiated under NASw-1543 where failure mechanisms in boron/epoxy were investigated. In the first year of the current efforts emphasis was shifted to carbon fibers with the major focus on matrix and interface response to fiber fracture. Comparisons were made between different fibers, various fiber coatings and different degrees of matrix crack sensitivity. In each case the approach was to first identify basic fracture mechanisms for model single and multiple fiber specimens and then to explore means for controlling the failure process to prevent sudden catastrophic failure. The utility of such an approach is of course dependent on how translatable are the model specimen observations to those made on heavily reinforced engineering composites. Therefore this year's efforts emphasized correlation between fracture phenomena for model and engineering composites subjected to tensile loading. Specific attention is given to the effects of standard fiber surface treatments, differences in behavior for two batches of the same fiber and the effect of fiber content on fracture modes. In every case both a modified and unmodified resin formulation was used to evaluate the effects of crack sensitivity of the matrix.

Unfortunately, there are few characterization techniques which allow systematic and detailed monitoring of the critical events in the fracture process of composite specimens. This need has led to the monitoring and analysis of acoustic emissions from the specimens during the entire load history. Since there is little reference data with which to compare such observations, the use of the technique is as much a contribution to the further development of acoustic analysis as it is to a fundamental understanding of material performance. Only by isolating and identifying specific failure mechanisms and sequences of events in the failure process can we hope to establish reference data which will serve our needs in the future.

A part of the current effort has also been focused on the failure mechanisms in composite/metal specimens because of their increased use. Both flat sandwich specimens and tubes of carbon/epoxy bonded to aluminum alloy were fabricated and tested in this phase of the effort. Primary emphasis was placed on fracture modes rather than on collection of strength data so that relatively few specimens were involved for any single material system or specimen geometry. However, both compressive and tensile fracture modes were examined.

The research described here is fundamental in nature but essential to the accurate prediction of composite performance. It demonstrates how fracture observations made on isolated fibers in model systems can yield valuable insight into composite failure modes in the engineering composite specimens tested thus far. Effects of fiber property changes, surface treatments and environmental exposure on interface and matrix response are readily examined by these methods. Only through an understanding of such phenomena can we hope to design reliably with advanced fiber reinforced composites.

2.0 MATERIALS CONSIDERATIONS

2.1 Fundamental Failure Mechanisms

Two distinct characteristics have been observed in the fracture surfaces of most composites; fibers fractured at the surface and those which have fractured elsewhere and pulled out. When the first mode dominates the surface resembles cleavage in homogeneous materials while the latter mode suggests interface failure as a major element in the failure process. Unfortunately, in a densely packed composite we have no easy means of determining the order or significance of the individual elements in the fracture process. Further, the validity of post fracture observations depend on the tortuous nature of the failure process and dynamics of specimen rebound.

This points up the desirability of observing certain elements in the local failure process in very simple model specimens. Since carbon fibers are used in tow form, the interaction between individual filaments within the tow and the overall response of the tow are both of major concern in establishing these local failure mechanisms. We are concerned here with the first evidence of failure in the fibers and the role which the matrix plays in propagation or containment of these initiated cracks.

First experiments (1)* were performed on boron/epoxy model specimens and three distinct failure sources were observed to occur in the matrix at the fiber fracture site. These are illustrated in Figure 1 and can be summarized as follows:

(1) In the upper picture the broken filament has remained strongly bonded to the matrix on either side of the break. This results in the disk-shaped crack normal to the fiber which grows suddenly; its size is determined by the magnitude of the strain energy released when the fiber fails and the crack sensitivity of the matrix surrounding it.

* Numbers in brackets correspond to references at end of this report.

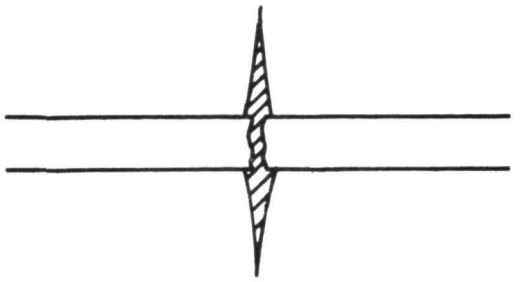

HIGH ENERGY RADIAL
CRACK NORMAL TO FIBER

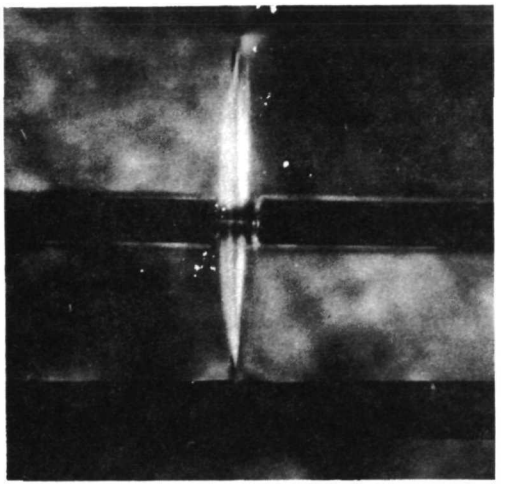

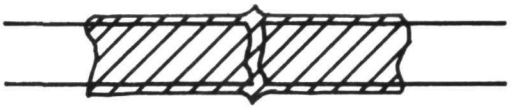

INTERFACE UNBONDING DUE TO HIGH
SHEAR STRESS AT NEWLY FORMED
ENDS

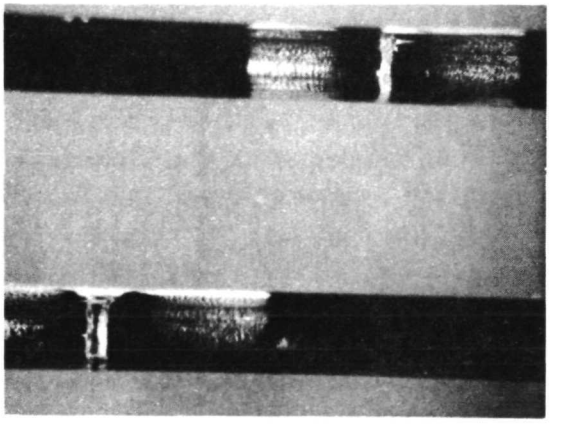

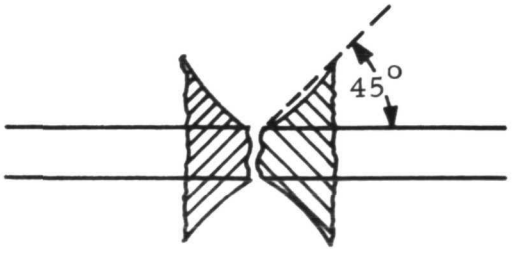

LOW ENERGY RESOLVED SHEAR
STRESS INDUCED TENSILE
CRACKS IN THE MATRIX

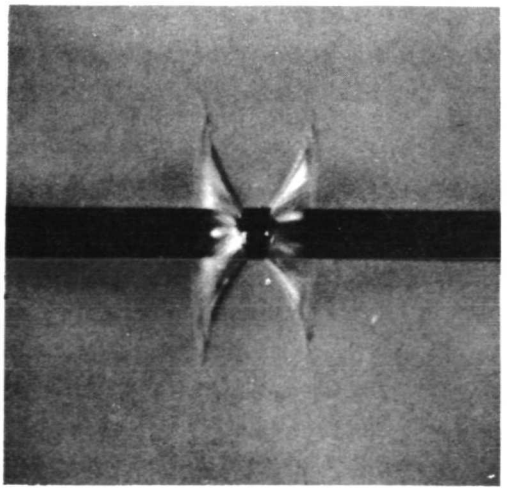

Figure 1. Diagrams and Photographs of Failure Mechanisms in Boron-Epoxy

(2) When the filament is not so strongly bonded to the matrix, the high shear stress concentrations at the interface adjacent to the fiber break can cause debonding to occur. This is illustrated in the center photo of Figure 1 where the boron filaments had been coated to obtain such behavior.

(3) If the bond strength is sufficient but the matrix is weak in tension, a tensile crack may propagate in the high shear transfer region beginning at the interface and growing at about 45° to the fiber axis at its source as shown in the lower photo of Figure 1. Note that this crack becomes nearly normal to the fiber axis as it propagates. This is consistent with the nature of the tensile stress field around the fiber break as determined photoelastically by several earlier studies (2, 3).

Analysis of such failure mechanisms can help to discern whether a particular fiber/matrix combination is fiber, matrix or interface limited. However, because only isolated fibers are being observed, we have, at best, only an indication of the elements which contribute to the failure of engineering composites. Therefore the approach is to examine both single and multiple fiber interactions in simple model specimens and then to correlate these data with the fracture process in heavily reinforced (engineering) specimens. In this way the effects of matrix modification, fiber surface treatment, and the like on composite performance can be more readily understood.

The remainder of this section will describe the nature of the fibers, matrix characteristics and specimen preparation and test techniques.

2.2 Nature of the Fibers

2.2.1 Mechanical Properties

It has been noted in the last progress report (5) that two different failure mechanisms have been observed in composites consisting of the two batches of untreated HT fibers. The original batch of fibers displayed a gross failure mode consisting primarily of cleavage in both the modified and unmodified resin, while the new batch displayed a marked tendency to undergo splitting and fiber pull-out. It was hypothesized at that time that this difference was due to either a strength difference between the fibers or a difference in the bond strength. In order to determine which of these two possible reasons was responsible for the composite behavior, a series of tensile tests on

individual filaments was performed. In addition to tests of the HT fibers, tensile tests were performed on Type A fibers (original batch - PPC53/733) in order to verify the manufacturer's data.

Tensile tests were performed on a Tecam micro-tensile machine, illustrated in Figure 2. The machine uses a torsion balance to apply the loads and a mirror autocollimating telescope system to measure extensions. Loads may be applied from 1.0 mg to 400 g, and extensions may be measured to $5 \times 10^{-3} \mu$. In application, the fiber specimen is glued on small anvils in the machine and aligned by means of alignment screws. The load is applied incrementally until the specimen fractures. A detailed discussion of the operation of this device may be found in the original article by March (4).

To determine the tensile strength of fine fibers, it is necessary to measure the cross-sectional area of each fiber either before or after test. Because the present objective was merely to ascertain if differences existed between several batches of fibers, a simpler method was used. The strength was calculated using the manufacturer's value of the elastic modulus and the experimental value of the failure strain by the relation:

$$\sigma \text{ calculated} = (E \text{ assumed}) \quad (\epsilon \text{ measured})$$

This approximation allows for the fact that the fibers cross-sectional areas can vary. The method requires an accurate value of the experimental failure strain, and it has been found in this laboratory that good strain values are obtained using the Tecam machine if the gage length is kept above about 10 mm.

The data are presented in Table I, and a comparison between the manufacturer's values and ours is shown below:

Fiber	Manufacturer's Data	Measured Filament Strength
HT-original	387 KSI	359 KSI
HT-new	379 KSI	366 KSI
A-original	346 KSI	295 KSI

It may be seen that fairly good agreement with the manufacturer's data is found, with the possible exception of the Type A fibers, which we find weaker than reported. Specifically, very little difference exists between the two batches of

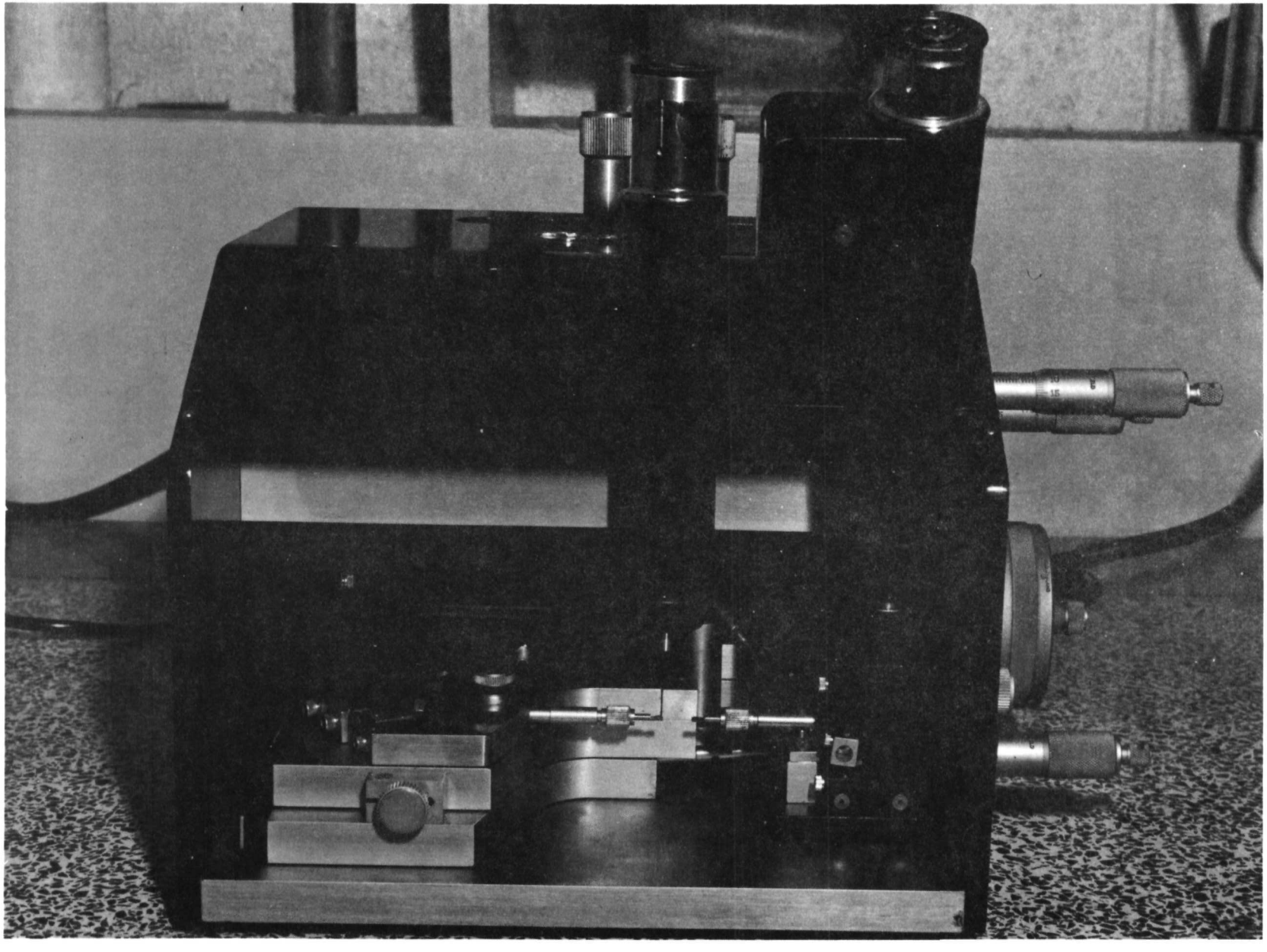

Figure 2. TECAM Micro Tensile Machine

TABLE I. STRENGTH OF INDIVIDUAL CARBON FIBERS

Fiber	Measured Strength, KSI	
HT-original	475	326
	278	309
($E = 37.1 \times 10^3$ ksi)	438	266
	408	353
	266	407
	430	201
	453	364
	416	
Average:	359	
HT-new	282	387
	387	418
($E = 36.0 \times 10^3$ ksi)	434	378
	269	326
	411	
Average:	366	
AU	298	342
	268	241
($E = 29.5 \times 10^3$ ksi)	267	274
	327	306
	327	297
Average:	295	

HT fibers. From this, it may be inferred that differences in composites failure modes between these two fiber types are due to differing bond strength, and not to fiber strength.

Besides the fundamental properties of the fibers, there are the additional considerations of surface chemistry and morphology which can affect the wetting and bonding characteristics and, therefore, the bond strength. In every instance experiments were undertaken on a comparative basis in an attempt to isolate the effects of a single variable.

During the past year major emphasis was focused on evaluating untreated fibers because it was planned to modify the interfacial bond strength in order to control the fracture process. The untreated fibers provide an excellent reference base for this purpose. Even though interlaminar shear strength values have been improved by oxidative surface treatments, the effects on other properties are still not completely understood. Composites made with treated fibers have shown some strength deterioration after a period of time and this problem is of major concern. Therefore, a comparison of the mechanical response of treated and untreated fibers represented a significant part of the work reported here as did fiber variation from one batch to another.

Carbon fibers are available in multi-filament tow form ranging from 48 inches to 3,000 feet long without splices. Tows contain approximately 10,000 individual fibers which average about 8 microns in diameter. The number of fibers, varying lengths and their extremely small diameter present some handling difficulty as far as fiber spacing and orientation are concerned. The number of filaments of Type A and HT fibers used during the course of this work was reduced considerably in model specimens. This presents some problems in fiber handling and specimen preparation because the fibers, being extremely lightweight, have a tendency to move about freely when placed in a heated resin matrix during processing. This fiber movement sometimes results in specimens ranging from a loose distribution of fibers to a compacted bundle with some fiber crossover.

The properties of the Type A and HT fibers used in this work, are shown in Table II.

TABLE II MANUFACTURER'S TOW TEST DATA

Fiber Type & Batch No.	Date Rec'd	Tensile Strength Ksi	Tensile Modulus millions of psi	Filament Diameter microns
Original HT	7-69	387	37.1	7.4
HT-U (New) (PPH 42/124)	7-71	379	39.1	8.1
HT-S (New) (PT117/201Z)	9-71	364	36.0	8.3
Type A (Original) (PPC53/733)	1-71	346	29.5	8.1
Type A (New) (PA1/19)	7-71	315	28.5	8.4
Type A-S (New)	7-71	326	28.9	8.6
HM (Original) Courtauld's Type B	None	375	55	8.2
HM-S (New) (QM123/306W)	9-71	296	62.5	7.4

2.2.2 Surface Characteristics

All previous work performed on fiber surface characterization in this program was done mainly to examine and compare surfaces of various untreated and treated carbon fibers. This was done through the use of electron microscopy. The surfaces and structures of PAN-based and cellulose-based fibers, covering a wide range of moduli and strength, were examined and the series of figures presented in previous program reports (5, 6 and 7) show comparisons between two lots of untreated HT fibers, untreated versus treated HT, Type A fibers and untreated HM fibers.

During this period of study we concentrated on the observed differences in local fracture behavior between the two batches of untreated HT fibers designated original and new, as well as on the behavior of untreated versus treated HT and Type A fibers in both modified and unmodified epoxy-novolac and ERLA 4617 resins. Detailed comparisons of mechanical behavior are discussed in Section 3.

Since the physical structure of the carbon surfaces is important in determining the interfacial area available for bonding between fiber and matrix in a composite, additional techniques were investigated to ascertain whether any micro-surface differences existed. Infra-red analysis (I.R.) of the original and new HT fibers produced no apparent difference because either (a) the carbon fibers, being black bodies, absorbed most of the energy, or (b) the concentration of functional groups was too low to be detected by IR.

Bundles of each fiber type used in this program were examined using electron probe x-ray microanalysis (EPXM). This analytical technique, which is used in the determination of elemental (chemical) compositions and distributions in small specimens or in small regions of large specimens, was used in hope of determining the composition or variations in composition of surface films in individual fibers; and to compare the surface composition between the various fiber types. When individual fibers in a bundle were studied a 0.5μm diameter electron beam was used. When bundles of fibers were studied the diameter of the electron beam was adjusted to about 100μm. The x-ray spectrometers permitted analysis to be made extending from atomic number 5 (boron) upward in the periodic table of elements. The sensitivity of EPXM as it was employed in these studies is probably better than 100 ppm.

We were unable to detect any element except carbon from any fiber-type using EPXM. We must therefore conclude from these analyses that either:

(a) the fibers are clean and do not contain surface films, or (b) the fibers contain surface films and are composed of elements beyond the limits of detectability of the EPXM spectrometers and detectors (below atomic number 5 - H, Li, Be), or (c) surface films do exist on the fibers and are composed of elements of atomic number 5 and greater, but the films are extremely thin and therefore contain insufficient material for EPXM detection. We believe the latter to be the case.

Of the techniques used to date to characterize the carbon fiber surfaces, electron microscopy provides the best comparison of fiber surface features. Other techniques which should be investigated in the future are emission and Raman spectroscopy.

2.3 Matrix Characteristics

The principal functions of the matrix in a composite system are to transfer stress to the fibers and isolate fiber fractures. When the matrix is capable of being modified without degrading its load transfer function, one can develop the toughness and flexibility to prevent rapid and catastrophic crack propagation.

2.3.1 Mechanical Properties

Resin flexibility or toughness is the major control parameter selected for this study. On the basis of ease of modification to cover a wide range of properties, handling and cure, as well as excellent optical characteristics for microscopic examination, epoxy-novolac (DEN 438) was chosen. The unmodified version has good strength and modulus at room temperature, and good strength retention after exposure to humidity and water environments. For example, on tests done in this laboratory, room temperature tensile strength of DEN 438 was 9.0×10^3 psi; and after 1 month exposure at 95% relative humidity and $77^{\circ}F$ there was no change in strength. On the other hand, it was reported (8) that composite specimens of carbon fibers and DEN 438 lost about 20% of their original flexural strength in 22 weeks of "wet-loading".

Modification of DEN 438 is accomplished by using plasticizers such as polypropylene glycol (PPG 425). In both the unmodified and modified form nadic methyl-anthydride-(NMA) is used as the curing agent and benzyl dimethylamine (BDMA) is used as the accelerator. Both formulations, along with their mechanical properties, are shown in Table III.

Table III. Properties of Epoxy-Novolac Formulations

FORMULATION	Unmodified (Phr)	Modified (Phr)
DEN 438	100	100
MNA	72	72
BDMA	2	2
PPG 425	---	60
PROPERTY		
Ultimate Tensile Strength, ksi	6.5 - 10	3.7 - 4.5
Modulus of Elasticity, millions of psi	0.40 - 0.45	0.20 - 0.25
Elongation, %	2.5	15 - 25
Toughness, $in.lb/in^3$	150 - 250	650 - 700
Specific Gravity	1.22	1.21

Note that the toughness of the modified resin is higher by a factor of three, while elongation is greater by an order of magnitude. Tensile strength and modulus are greatly affected by modification, and this can be expected to have a more significant effect on transverse properties. Another shortcoming of the modified system is that the combined curing agent and modifier moderately reduce the elevated temperature properties, and the modifier; although a co-reactant, is hygroscopic causing reduced strength under humidity and moisture conditions. After 1 month at 95% relative humidity and 77°F, the tensile strength retention was only 54 percent.

The unmodified DEN 438 system, an inherently rigid system, can be very crack sensitive in uniaxial tension in single and multiple-filament specimens depending upon fiber strength, bond strength and load rate. In some cases incremental uniaxial tensile loading produces no cracking or debonding until the ultimate load is reached. At this point a single crack may appear, and will often cause catastrophic failure, regardless of fiber surface condition. On the other hand, the modified formulation allows small cracks to accumulate at lower load levels. The ductility of the resin in the modified sense is therefore beneficial to absorbing energy released when each fiber breaks, and containing the crack with each occurrence until gross damage occurs. Arridge (9) has shown that toughness is an important parameter in fiber reinforced composites but suggests that in a real composite the flexible or toughened matrix acts like a rigid system because of fiber constraint.

Another consideration is the difference in modulus between the matrix system and fibers. The ratio of fiber modulus to that of the matrix is so great (100 : 1) that modulus is not an important matrix parameter in uniaxial tension compared to toughness and total elongation. In transverse tension the situation is not the same however. Under this load condition high matrix strength and modulus are often required. The problem of mechanical compatibility is immediately evident under different loading conditions, and suggests that a great deal still has to be done to optimize a combination of matrix properties in order to achieve greater composite performance.

Only a limited amount of work has been done in this program to date with the more widely used cycloaliphatic epoxy resin - ERLA 4617. This system unmodified has 20% higher strength and 100% higher modulus than many

other epoxy resins. However, it has been reported (8) that the unmodified cast resin resulted in weight gains of 9.7% after 72 hours water boil as compared with 1 to 3% for systems such as unmodified DEN 438. Properties of the ERL 4617 system are shown in Table IV. Here the difference in properties relate to the different curing agents used with each formulation. ERLA/m-PDA and ERLB/MDA have quite different toughness and elongation properties but only slight differences in modulus. This system is more opaque than the epoxy-novolac system but with careful control of lighting clear pictures of the local fracture patterns can be obtained.

2.3.2 Shrinkage Characteristics

All thermoset resin systems, regardless of chemical composition or molecular configuration undergo volume shrinkage as a result of crosslinking (cure), post-cure, and cooldown after cure. In the case of epoxies shrinkage resulting from processing is caused by the chemical reaction and rearrangement of the molecules into a more compact configuration; essentially without release of volatile material. Condensation resins undergo greater shrinkage by evolution of a higher percentage of lower molecular weight components. Epoxy resins behave in much the same way when modified by unreactive modifiers, and to a lesser degree when reactive modifiers are used. Our concern then was more with the modified version during the preparation of single and multiple fiber specimens. Non-uniform shrinkage places single strands and individual fibers in a stressed condition which can result in fiber crimping and/or debonding. Because of this concern cure techniques were developed to minimize shrinkage and fiber distortion. Also, a modification of the mold set-up was made in order to provide a more uniform resin shrinkage and eliminate or minimize fiber crimping in the preparation of simple specimens. Further details of preparation are given in Section 2.5.1. There has been no indication in our work that high shrinkage or fiber crimping occur in high fiber volume composites.

2.4 Metal Substrates

In addition to the analysis of failure processes in composites there is interest in unidirectional fiber composites combined with metals as a result of work initiated by NASA-Langley. Those efforts were focused on boron-epoxy tape bonded uniaxially to aluminum tubes in an effort to improve column strength. This approach offers great advantages for truss and strut applications since the boron-epoxy greatly increases the stiffness and strength while the aluminum

Table IV. Properties of Cycloaliphatic Epoxy Formulations

PROPERTY	FORMULATION	
	ERLA 4617-114.0 PBW m-PDA-Curing Agent 27.0	ER:A 4617-11.4 PBW MDA Curing Agent 43.0
Ultimate Tensile Strength, ksi	20	16-20
Modulus of Elasticity millions of psi	0.815	0.78
Elongation, %	2.8	6-7
Toughness, in. lb/in^3	320	832
Specific Gravity, gms/cc	1.27	1.26

provides an efficient means for making connections. Certainly the bond between the composite and metal is a critical link in this approach and the failure process can be limited by either of the two constituents or the interface between them. For this reason an analysis of the basic failure mechanisms which occur in these composite-metal elements is necessary to optimize their performance. The following sections outline some of the fundamental considerations in fabricating both flat and tube-type specimens.

2.4.1 Mechanical Properties

The aluminum used for the flat face sheet material was 2024 aluminum 1/16 inch thick. The stress-strain curve in the region of interest (up to 1.0% strain) is given in Figure 3. The material can be well represented in this range by two straight lines, one of which is the line representing Young's modulus (10.3×10^6 for the specimen measured in Figure 3), and the other is the tangent modulus. The representation was used in the analysis to be discussed in Section 3.4.1.

After several flat specimen metal/composite specimens were tested, it was decided that the aluminum would behave in a more reproducible manner if it was pre-strained to 0.6% strain. This procedure decreased the region where the stress-strain curve heels over, and also made the yield point determination quite precise. Most of the flat plate composite specimens prepared used aluminum face sheets in the pre-strained condition.

The aluminum tubing used for the metal/composite tubes was 1/32" wall-2024, which has essentially the same properties as the sheet material, except that the tubing was cold drawn during manufacture.

2.4.2 Surface Preparation for Bonding

Flat and tube adherend metal surfaces to be bonded were prepared by mechanical abrasion (liquid-honing). This method provides an oxide-free, satin finish surface as shown in Figure 4 that enhances bond strength. The honed surfaces are then solvent cleaned with hexane to remove greases and dust particles.

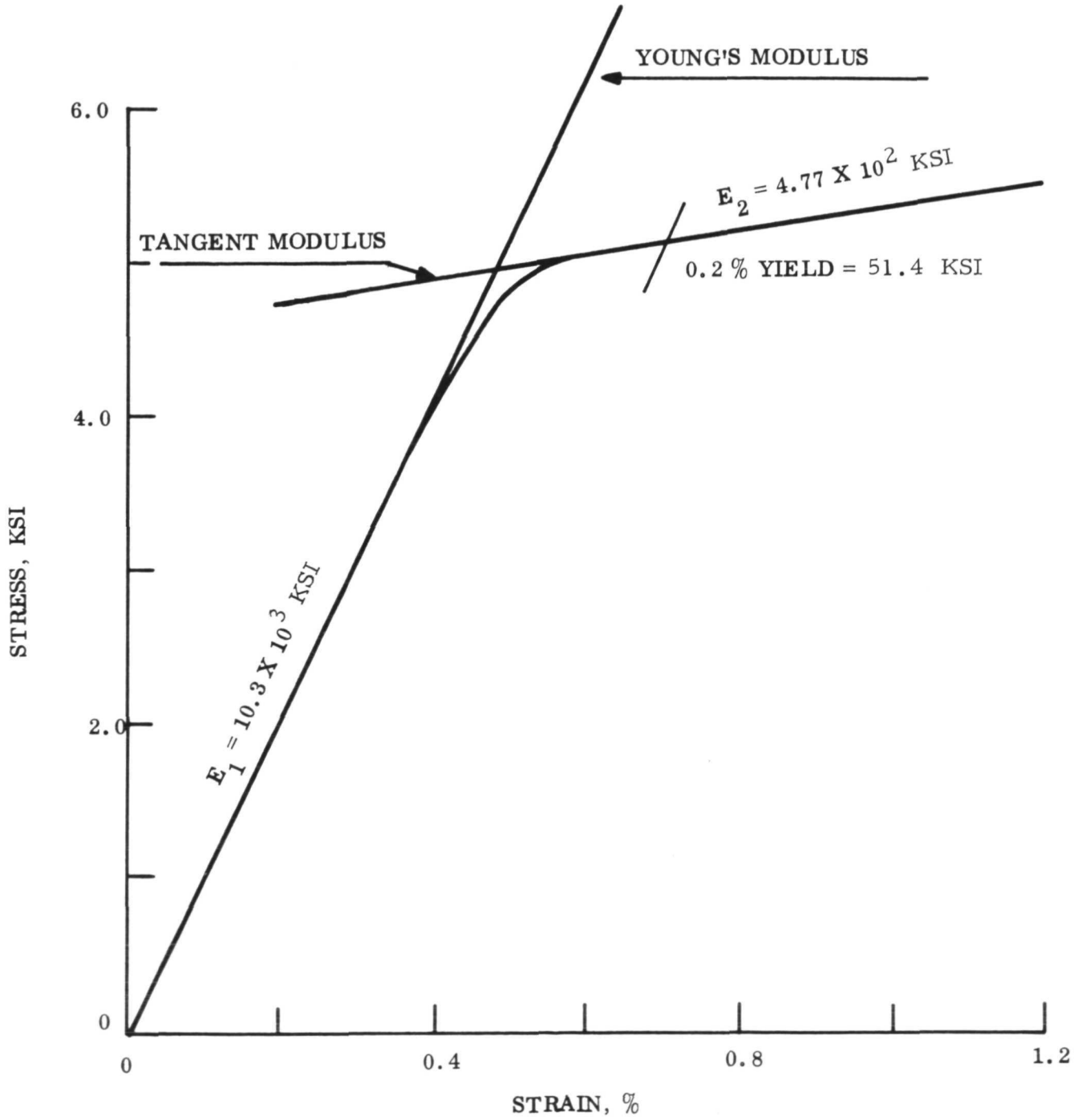

FIGURE 3. STRESS-STRAIN CURVE TO 1.0% STRAIN FOR 2024 ALUMINUM

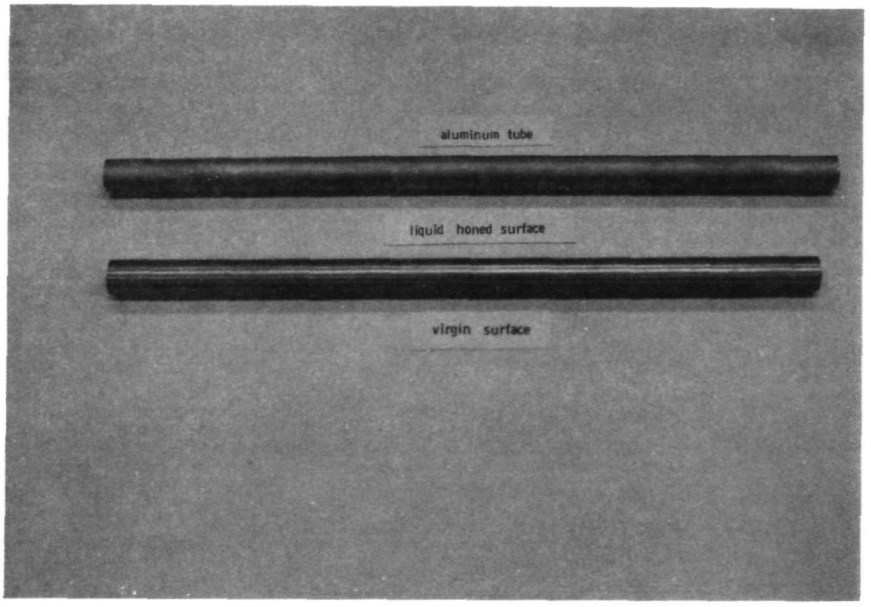

Figure 4. Comparison of Adherend Aluminum Surfaces Before and After Liquid Honing

2.5 Specimen Preparation and Testing

2.5.1 Model Composite Specimens

Separate cure schedules were used in the preparation of single and multiple fiber specimens using the modified and unmodified epoxy-novolac. This was necessary because of the different shrinkage characteristics of the two resin formulations, and the different gel time properties. The unmodified formulation shrinks less during cure because of increased cross-linking density; also, the gel time is shorter. In the modified formulation the opposite is true. Therefore, the initial gel time cycle was short for the unmodified resin and longer for the modified resin.

In addition to varying the cure, the mold configuration was important to achieving uniform resin shrinkage. The most effective mold set-up for good uniformity was a multiple cavity open mold with spacers at regular intervals. This arrangement reduced the resin mass and helped to distribute shrinkage evenly, as opposed to shrinkage toward the center bulk as in the case of larger resin castings.

The model composite specimens were prepared according to the following procedure:

1. A shallow 4 inch square mold assembly with 1/4 inch square brass rods, spaced 1/4 inch apart, was coated with a thin film of RAM 225 mold release agent. The solvent was evaporated out of the RAM at room temperature. The film was then baked onto the mold for one hour at 250°F to provide a stable film which will not diffuse into the matrix during cure.

2. A thin layer (1/16 inch) of epoxy resin was poured into the mold and partially cured (effectively "B" staged) as follows:

   1 hour at 180°F for the unmodified system; 2 hours at 180°F for the modified system.

   This rendered the resin sufficiently tacky to prevent fiber movement during final cure.

3. After the first cure, the filaments were laid down parallel with one another, at the desired spacing. Additional epoxy (1/16 inch) was poured over the filaments.

4. The composite, regardless of matrix state, was then cured for 2 hours at 180°F followed with a stepwise increase in temperature to 350°F at which point post-cure was carried out for 2 hours.

5. The 4" long by 1/4" wide specimens were removed from the mold, sanded to desired thickness and ground to provide a 1" long gage section.

Microscopic examination was carried out on a Bausch and Lomb microscope for the most part, with magnifications between 20 and 300x. The details of the failure process for various test parameters are presented in Section 3.

Specimens were also made with unmodified ERLA 4617 epoxy resin and tested. The curing agent was methylenedianiline (MDA). Initially specimens were prepared much the same as the epoxy-novolac. Gel time for the first 1/16 inch layer lasted for 4 hours @ 200°F. At the end of this time the resin was fairly well gelled, but it was noted that shrinkage began to occur as soon as the resin began to cool. Fibers were placed on this layer immediately, and another 1/16 inch layer of resin was applied over the fibers. The assembly was then placed in the oven again for final cure for 4 hours at 250°F plus 16 hours at 325°F.

The ERL 4617 system is more reactive than the epoxy-novolac resin making the working time shorter and less reproducible from batch to batch. Therefore another technique was used to establish more uniformity. Utilizing the same molds as before, holes (.010" diameter) were drilled at each end to accommodate 4 complete specimens. The ends of the single or multiple fibers were then secured in the holes with RTV Silicone rubber. This kept the fibers straight and tight, and also resealed the drilled holes. The resin was then introduced into the mold cavities slowly until the level of the resin was equal on both sides of the fiber. Cure was then achieved in one continuous cycle, thus eliminating uneven cure and shrinkage. After cure the same cutting, grinding and polishing procedures were used as in previous specimens.

All model specimen tests were conducted at the same strain rate (0.02 in/in/min). To obtain a complete picture of the fracture events to ultimate failure it was necessary to interrupt the test at regular intervals for thorough microscopic examination. This introduces some complications since the interruption of the failure process may in itself introduce extraneous effects which would not occur during continuous loading. However, the lack of sufficient magnification and scanning control on a machine mounted microscope dictated this approach. All tests were carried out on an Instron testing machine with complete recording of load and deformation.

2.5.2 Controlled Volume Fraction Specimens

Engineering composites containing Type A fibers were prepared and tested, using both the unmodified and modified epoxy-novolac resins. Similar specimens were prepared using treated and untreated HT fibers in both resins. These specimens were prepared and tested to complete the work on the effects of surface treatment on fracture mechanisms, and to compare different fiber batches, respectively. Since the quantities of materials used for this work were so small, wet pre-pregging and curing was done by hand instead of using commercially tailored prepreg materials. All such specimens contain high volume fractions (.55 to .60) in order to assess the effects of resin modification and fiber treatment on engineering composites.

Briefly, the process used for preparing all such specimens with both resin systems was to immerse a preweighed amount of fibers in the matrix and place the bundle in a 9 inch long x 0.5 inch wide mold, then pre-staging in a circulating air oven for a prescribed time (45 minutes at 180°F for the modified system and 20 minutes at 180°F for the unmodified system). This was followed by placing the male section of the mold on the prepreg, placing the assembly in a press and curing for 2 hours at 180°F, followed by a stepwise increase in temperature to 350°F and held for 2 hours. The mold used for curing specimens is shown in Figure 5. The specimens were removed from the mold, cleaned of mold flash, tabbed on the ends with 1 1/2 inch x 0.5 inch Scotchply 1002 tabs and tested in an Instron testing machine at a strain rate 0.02 in/in/min. The results of these tests are discussed in Section 3.1 and Section 3.2.

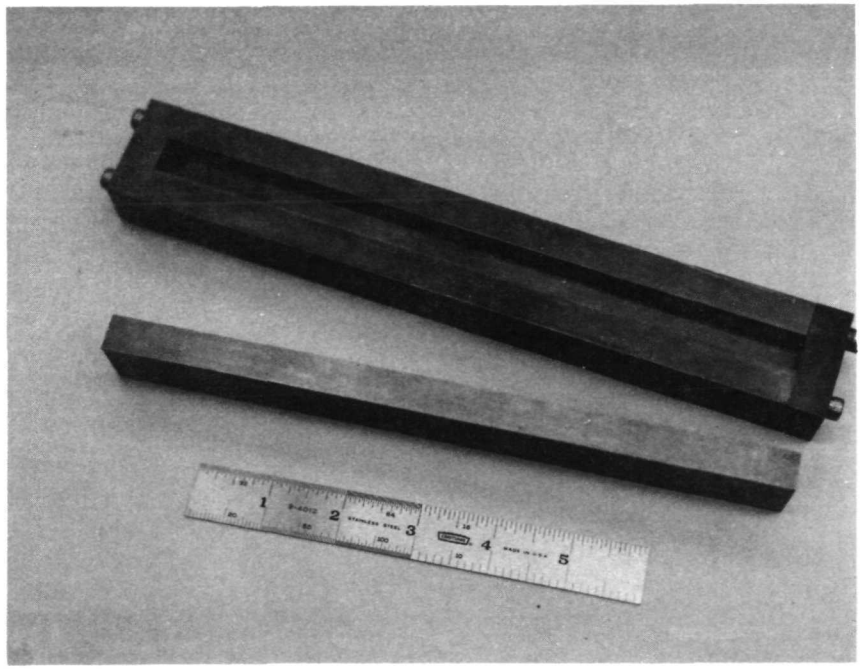

Figure 5. Hardened Steel Mold Used in Specimen Preparation

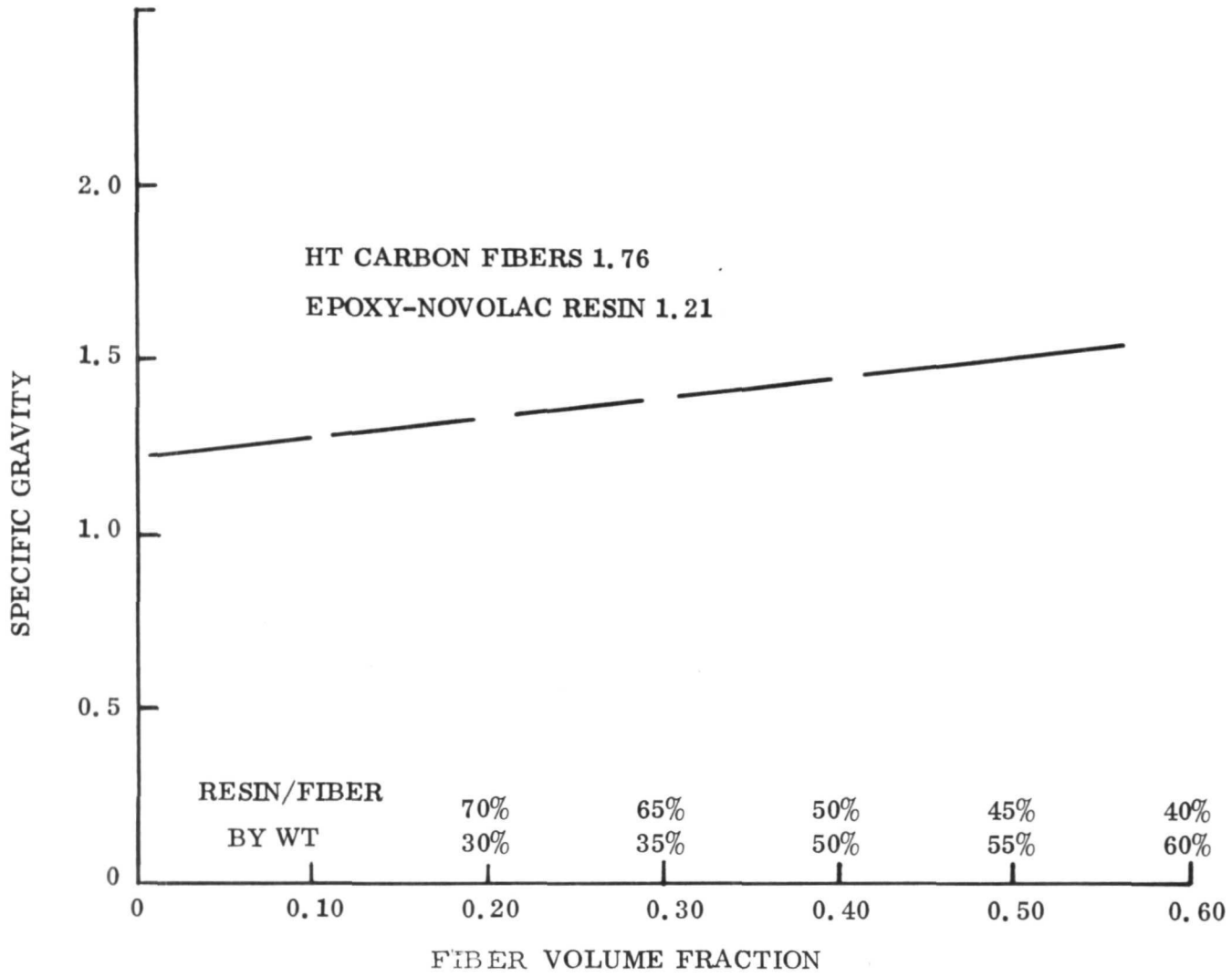

Figure 6. Composite Specific Gravity as a Function of Fiber Volume Fraction

Major effort during this period was concentrated on the preparation of specimens containing fiber volume fractions in the range of .20 to .60, so that the effects of fiber content on the fracture of bulk composites could be evaluated. Normally, the procedure for preparing such specimens would be to mold panels from prepregged materials to the desired thickness, representing each volume fraction level, and then to machine the desired tensile specimens from these panels. The main reason this technique was not used here is that there is no commercial prepreg available with unmodified and modified DEN 438. Therefore, a hand lay-up technique was used in order to be consistent with prior work. The use of tailored prepreg materials would not have been economical at this point in the work.

Several means were considered to achieve good uniformity, and the most logical approach was to prepare specimens at each V_f level on a density-to-weight basis. In this approach the weight ratio for each volume fraction level was calculated in order to achieve a finished composite with a desired specific gravity. With the known fibers and resin densities, and specimen volume, the theoretical composite specific gravities were plotted and are shown in Figure 6.

Specimens were then fabricated on the basis of these calculated weights in the 9" x 0.5" molds shown previously in Figure 5. One layer of fibers was placed into the mold and then a small amount of resin was poured over the fibers. The procedure was repeated until all constituents were used. The filled molds, without the male inserts were then placed in an air circulating oven at 180°F to "B" stage the resin to a more viscous or semi-fusible state. The time was 20 minutes for unmodified resin and 45 minutes for modified resin. After B staging the resin the male die inserts were placed into the molds, and the assembled molds were then placed into a pre-heated press at 200°F with contact pressure. These conditions were applied for 10 minutes for unmodified and 15 minutes for modified resins, at which time pressure was increased to 1000 psig. At the same time the temperature was increased at the rate of 15°F per minute. This heating rate was selected so that at the time maximum pressure was applied the final cure could begin. Cure was then continued for 3 hours at 350°F, and at the end of this period the heat was turned off to begin cooldown. Cooldown was slow (16 hours overnight) and under pressure. The specimens were removed from the mold and molding flash was scrapped from the edges. Specimen thickness, weight and specific gravity were determined in order to ascertain the uniformity of the specimens and process.

The entire preparation procedure was repeated for all specimens made for all fiber volume levels, and the only variable was the constituent weights at each level. The end result of this effort was that uniform fiber distribution was achieved at each volume fraction level. Even with this degree of control, resin flow during cure sometimes resulted in deviations from the expected fiber volume fraction so that final grouping was determined by measured modulus and rule of mixture calculations.

An indication of the fiber distribution uniformity achieved within a specimen, and between one V_f level and another is shown in Figure 7. The photo at the top of the figure is an entire cross-section of the composite to show where the lower micrographs were taken. From left to right at each volume fraction level there appears to be good uniformity of fiber distribution. And also, there appears to be good fiber packing with increased fiber content (from .40 to .60). Note also the uniformly increasing strength and modulus with increased volume fraction. Further details of mechanical behavior are discussed in Section 3.3.

2.5.3 Flat Composite/Metal Specimen Preparation

The effects of thermal mismatch between the composite and metal substrate are dependent on a number of factors such as thermal expansion coefficient for the composite, adhesive and metal. The composite thermal expansion coefficient is in turn dependent on lay-up angles and stacking sequence of plies which have a nearly zero coefficient in the fiber direction. To minimize distortions which can result from thermal mismatch in flat specimens, alternate layers of composite and metal must be used with symmetry with respect to the midplane through the thickness.

The two approaches taken in the preparation of composite/metal flat specimens were: first, to prepare the complete specimen in one operation using the matrix resin to bond to the metal; second, to cure the carbon/epoxy composite separately and bond it to the metal adherends after cure.

In the first approach there is the problem of obtaining sufficient resin at the bond line between the prepreg and the metal. Low prepreg resin content in such an approach can result in discontinuities in the bond line or the formation of voids near the bond line in the composite. In either case, a weakened region

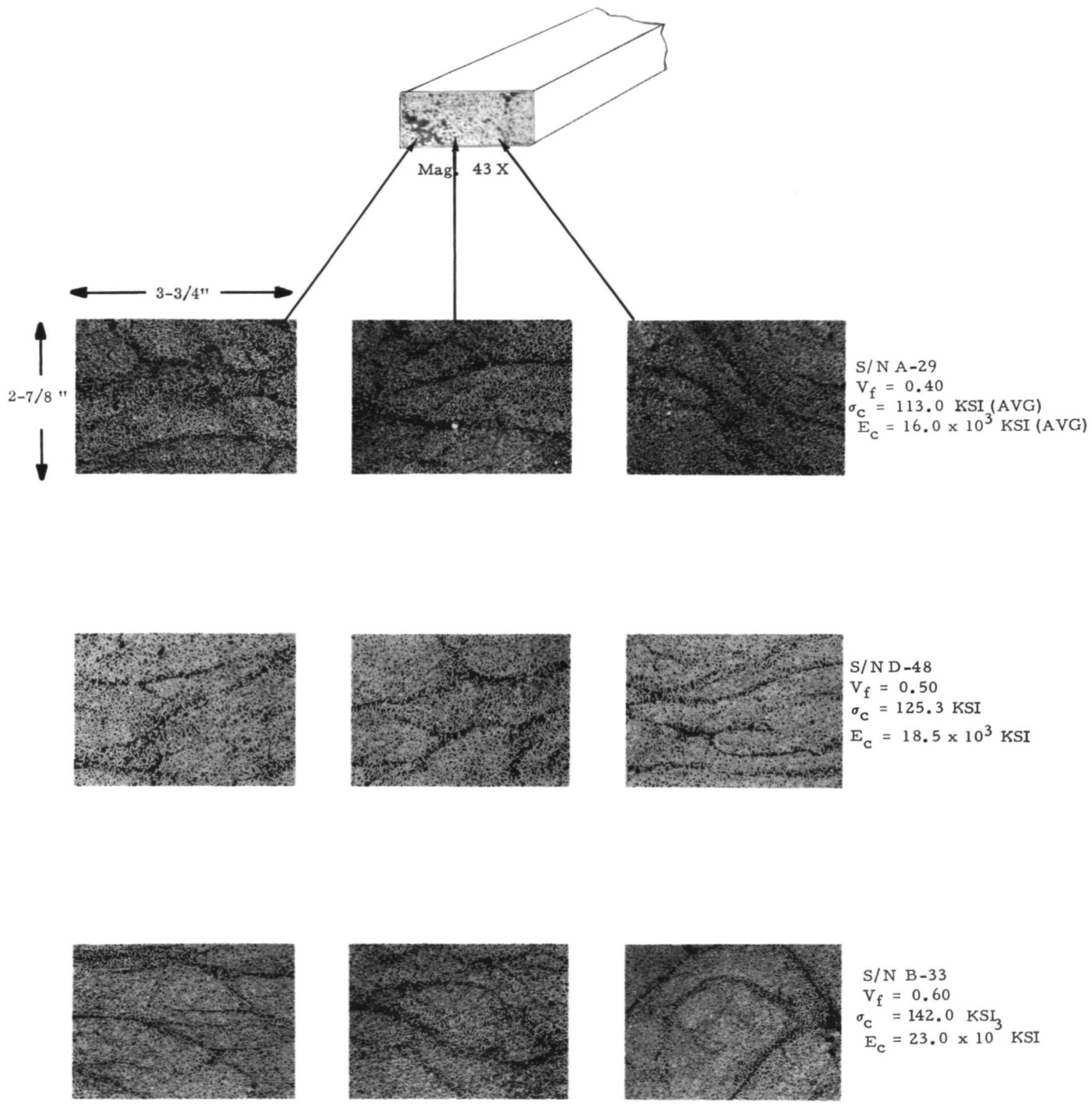

Figure 7. Typical Fiber Distribution in Specimen Cross-Sections for a Range of Volume Fractions (Untreated HT Carbon Fibers in Unmodified Epoxy-Novolac) 100 X Mag.

is formed which is likely to fail under the high shear stresses which develop on cooling back to room temperature. Although this approach presents some difficulties, it is precisely the kind of process used for the fabrication of some composite/metal parts. Therefore it was considered necessary to evaluate the failure mechanisms of parts produced using this process.

The second approach - fabricating the composite and then bonding to the metal - requires more time and is limited to certain configurations but provides better control of the bonding process. There are several advantages to this approach. First, better control of resin flow was possible when the composite material was cured alone. The cure cycle was less likely to impair the properties of the resin because the composite was first cured alone, and the resin was not required to perform a dual function as in the first approach. Because lower temperature cures can be used with certain adhesives and the choice of adhesives is less constrained, there is much less danger of introducing fabrication stresses.

Briefly, the procedure used for preparing flat composite/metal specimens is as follows:

1. Lay-up the required number of layers of prepreg 0.5 inch wide x 9 inch long in the mold. Place the male section of the mold into the cavity.

2. Cure in a press for two hours at 350^{o}F; cool slowly to room temperature.

3. Lightly sand both composite surfaces for better bonding. Degrease surfaces with solvent.

4. Prepare the two adherend metal surfaces by vapor-honing. Degrease surfaces with solvent.

5. Apply room temperature cure adhesive in a thin layer to both prepared composite and metal surfaces.

6. Assemble the composite/metal specimen in the bonding fixture and place under clamp pressure.

7. Allow to stand at room temperature for ~ 16 hours. Complete cure in an air circulating oven for 2 hours at 200°F.

8. Allow a slow cooldown to room temperature.

Figure 8 shows tensile specimens prepared by this process. Note in the top specimen-edge view - the individual outside layers of 1/32 inch thick 2024 aluminum and the uniformity of the 1/16 inch thick layer of composite material in the center. The lower specimen simply shows a top view of the specimen surface with end grips. Tensile testing and acoustic analysis were done on some of these specimens and data is discussed in Section 3.4.1.

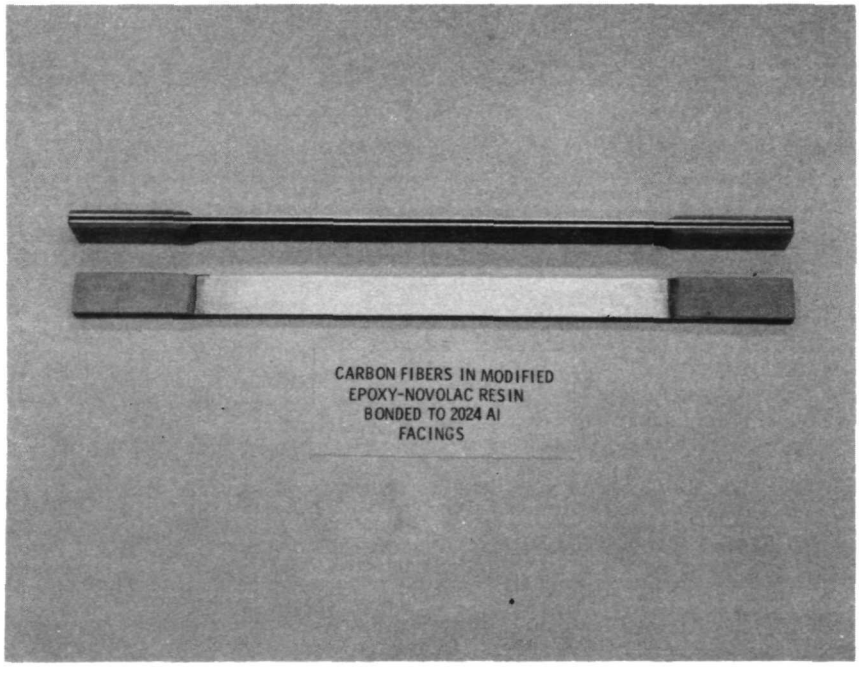

FIGURE 8. TYPICAL FLAT CARBON - EPOXY/METAL TENSILE SPECIMENS

2.5.4 Tube Composite/Metal Specimen Preparation

The preparation of tube specimens is essentially restricted to the curing in-situ approach described in the previous discussion of flat specimens. One major difference is the fact that the composite is not constrained on both surfaces in the tube specimens as it had been when sandwiched between two metal surfaces. Since the composite is external to the tube and the specimen is axisymmetric, this does not result in distortion and the composite is better able to accommodate to shrinkage during cure.

During this period of work tube composite metal specimens were prepared from both the unmodified epoxy-novolac used throughout this program and elastomer modified epoxy (BP907) prepreg. The following procedure was used: the surface of the tube to be wrapped was liquid honed, and then degreased with hexane. An epoxy resin was then painted on the surface and staged to a highly tacky state. The prepreg was wrapped unidirectionally over the tube to the desired thickness. Teflon shrink tube was then placed over the tube, and the complete assembly was cured in an air circulating oven for 4 hours @ 350°-360°F. Cooldown took place overnight ($\sim$ 16 hours). During the cooldown time the shrink tube remained in place over the specimen. Photographs showing the stepwise-procedure are contained in Reference 5.

2.5.5 Characterization of Tube Specimens

After the two different tubes were cured, they were visually examined for fiber alignment and porosity. The unmodified resin/carbon tube showed longitudinal splitting through one or more layers of materials. This is obviously due to stresses resulting from shrinkage. The elastomer modified epoxy/carbon tube, on the other hand was uniformly tight and solid. Because of its elastomeric nature it was better able to absorb the shrinkage stresses.

Approximately 1" was cut from each end of both tubes. The tube with the unmodified resin began to crack immediately after cutting. The longitudinal splits mentioned earlier opened up sufficiently to expose the metal tube. Loud cracking noises also accompanied the stress relieving. The tube with the elastomeric matrix produced no cracking or sounds after the edges were trimmed. Acoustic emission analysis was carried out on subsequent tube specimens and the discussion of this analysis is given in Section 3.4. As indicated in Reference 5, a one inch segment of tube was taken from the specimen fabricated using the elastomeric matrix. Microscopic examination showed no debonding along the interface of metal tube and composite, nor longitudinal splitting. Compression testing was performed on the one tube (elastomeric matrix) and the details are given in Section 3.5.

2.5.6 Acoustic Emission Studies

When metals, polymers, composites, or other materials are subjected to a load, local failure events such as slip, twinning, fiber fracture, etc., results in the sudden release of energy. The elastic wave produced by this energy release is transmitted through the material and can be detected by suitable instrumentation. The study of such events, either by counting them or analyzing by other means, constitutes the area of acoustic emission. The first systematic work in this area was performed by Kaiser in 1950 (10), and further fundamental work has been conducted by Schofield (11), Liptai (12), and Tatro (13).

Acoustic emission techniques have been in use in the Space Sciences Laboratory for about two years, and primary emphasis has been placed on the analysis of the failure modes in composite materials and ceramics. The equipment is illustrated in Figure 9 (with the exception of the counting device which will be described later), and a block diagram of the instrumentation is given in Figure 10. The transducer used in all cases was an Endevco Model 2226C accelerometer. The acoustic data is stored on an Ampex tape recorder operating at 15 ips, which allows frequencies up to about 80 kHz to be recorded. An oscilloscope is used to monitor both the input and output signals. Depending on how the data is to be treated, output read-out devices can be a spectrum analyzer (for frequency analysis), a high speed oscillograph, or a counting and summation system for recording acoustic events.

Although some of the past work performed in this laboratory on boron epoxy specimens has involved the use of frequency analysis of the acoustic events (14), this technique was not found to be applicable for carbon epoxy specimens. Because of the lower amplitude level for these specimens, the predominate frequency observed was the transducer resonant frequency of 48 kHz. With boron epoxy, sufficient energy was available to excite lower frequency modes such as specimen vibration. In addition, the number of events for carbon epoxy was much greater than before. Because of these factors, techniques involving counting the acoustic events were utilized. The details of the instrumentation used to perform this function has been described previously (5).

Most acoustic emission instrumentation records several counts for an individual event such as a fiber fracture. This is illustrated in Figure 11. For small amplitude events, the transducer is set into resonance by the travelling elastic wave as described previously, and will produce the damped sinusoidal signal shown in Figure 11. The amplifier which converts the data to digital form has an adjustable discriminator level, below which the data is not counted. In the example shown in Figure 11, the discriminator level is set such that the particular acoustic event shown is "counted" three

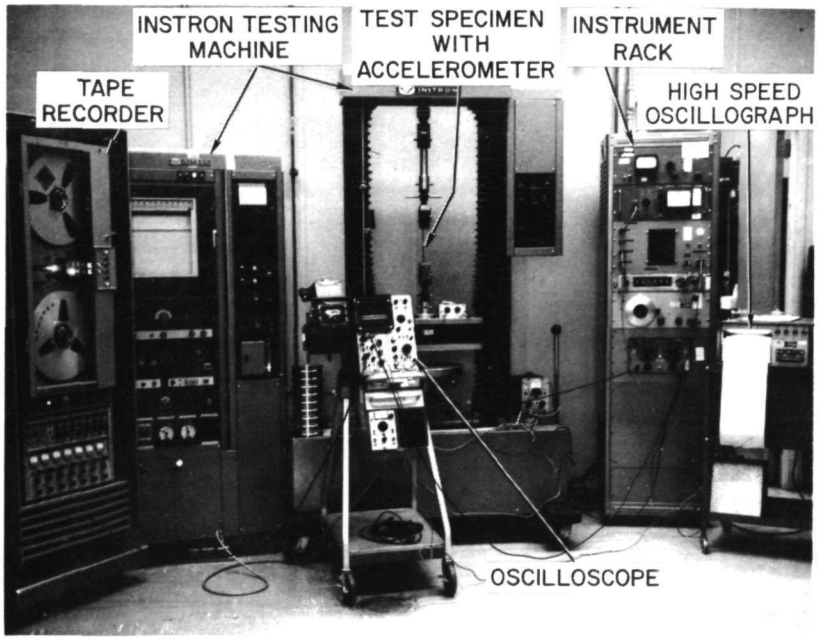

Figure 9. General View of Acoustic-Emission Test Equipment and Associated Readout Devices

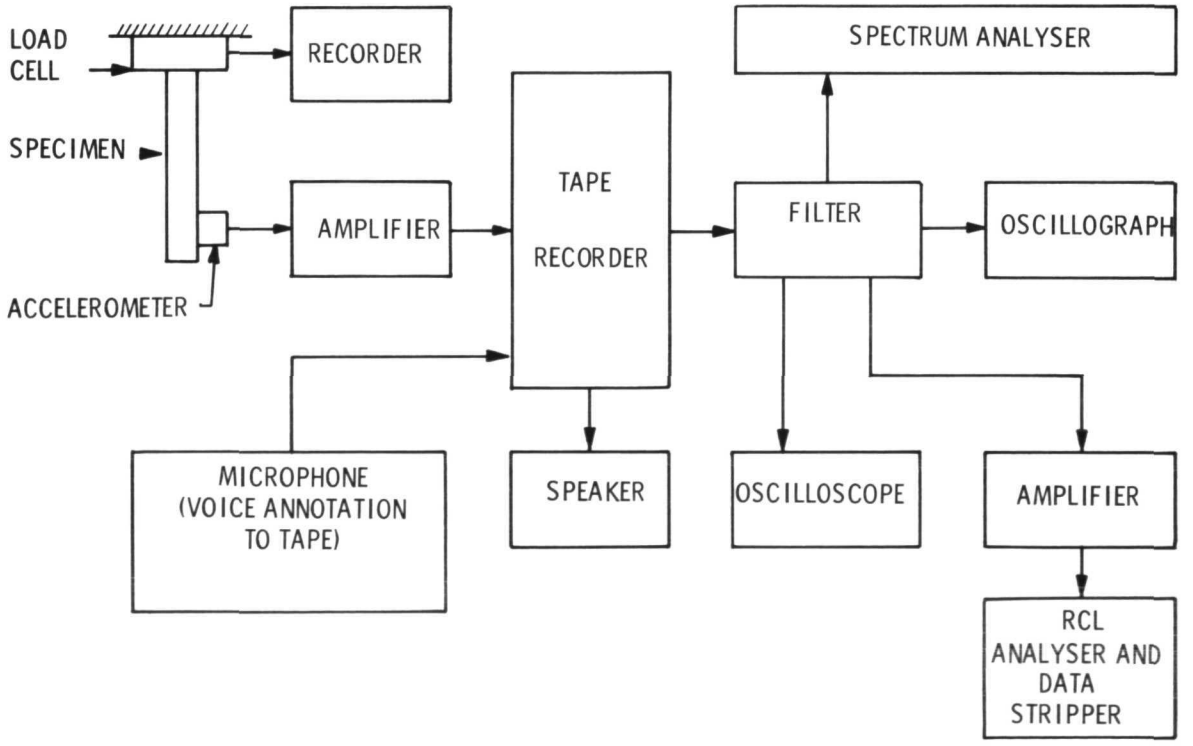

Figure 10. Schematic of Acoustic Emission Test Equipment

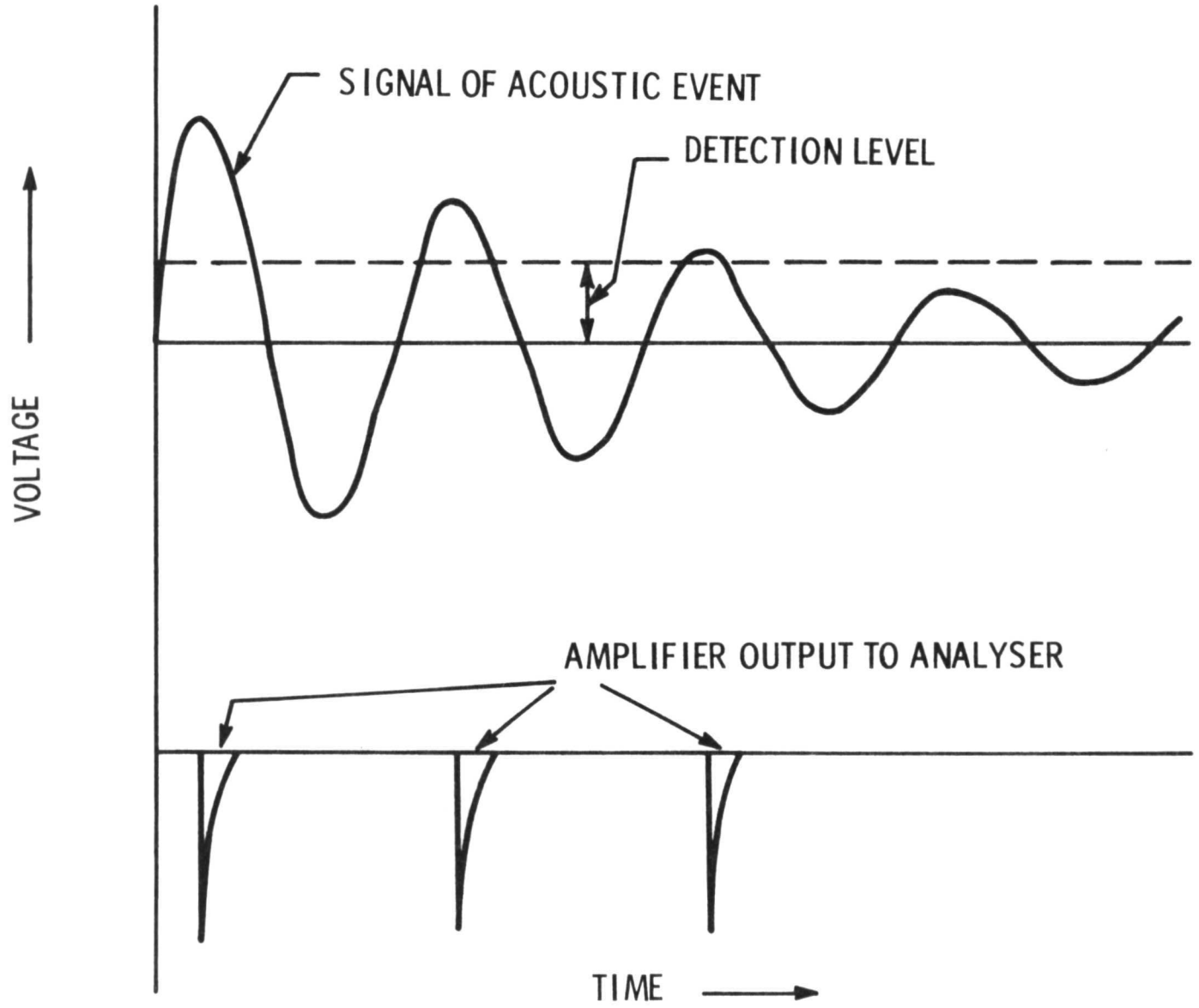

Figure 11. Schematic Illustrating Conversion of an Acoustic Event to Digital Form

times. Obviously, higher energetic events will result in a higher count, as will events which physically occur in the specimen near the transducer as contrasted to those occurring at some distance from it. These factors must be kept in mind when analyzing count data obtained from a particular test.

When working at reasonably high gain levels (greater than, say, 50 db), considerable care must be taken to prevent the introduction of spurious acoustic noise introduced by the gripping system. Metal-metal contact produces copious emissions under load, presumably because of the interaction of surface asperities. Similarly, wedge-type grips using serrated surfaces are unsuitable because the deformation introduced by them causes such spurious acoustic signals. Finally, the adhesive bond between the end tabs and the specimen can produce acoustic signals as the bond line is deformed.

The factors detailed above were not important when working with boron-epoxy composites because of the relatively low gain used. However, when carbon epoxy composites were being evaluated, it was evident that a different load train and gripping system had to be used. Wedge grips were replaced with pin-loaded grips, and rubber coated pins were used to avoid metal-metal contact between the pin and metal end tabs. In addition, teflon tape was wrapped around all thread connections in order to further reduce metal-metal contact.

Experimentally, noise produced by the bond line and the deformation introduced by the pins bearing against the specimen and end tabs proved the most difficult to eliminate. Dunegan, et al, (15) have described a method of prestressing the pin area to eliminate extraneous noise in metal specimens, but this was found to be unsatisfactory for the case of adhesively bonded end-tabs because of the acoustic noise generated by the bond line deformation. The method adopted for this system is shown schematically in Figure 12, and the assembly itself is shown in Figure 13. The area between the two loading pins was subjected to a preload, while at the same time the upper pin (used to hold the specimen during test) was firmly seated and the area around it preloaded. Although the area below the lower loading pin was not subjected to load until the specimen was actually tested, the number of emissions from this area were not large and could be ignored, as discussed in the previous report (5).

A specimen after preloading and prior to tensile testing is shown in Figure 14, with the accelerometer bonded to it. The reduced gage length was 3 inches long and 0.175 inches wide, and the fillet had a 4-inch radius. The end tabs were 2-1/2 inches long. The entire specimen was 9 inches long, 1/2 inch wide, and about 1/16 inch thick and was made by the procedure described earlier in this report.

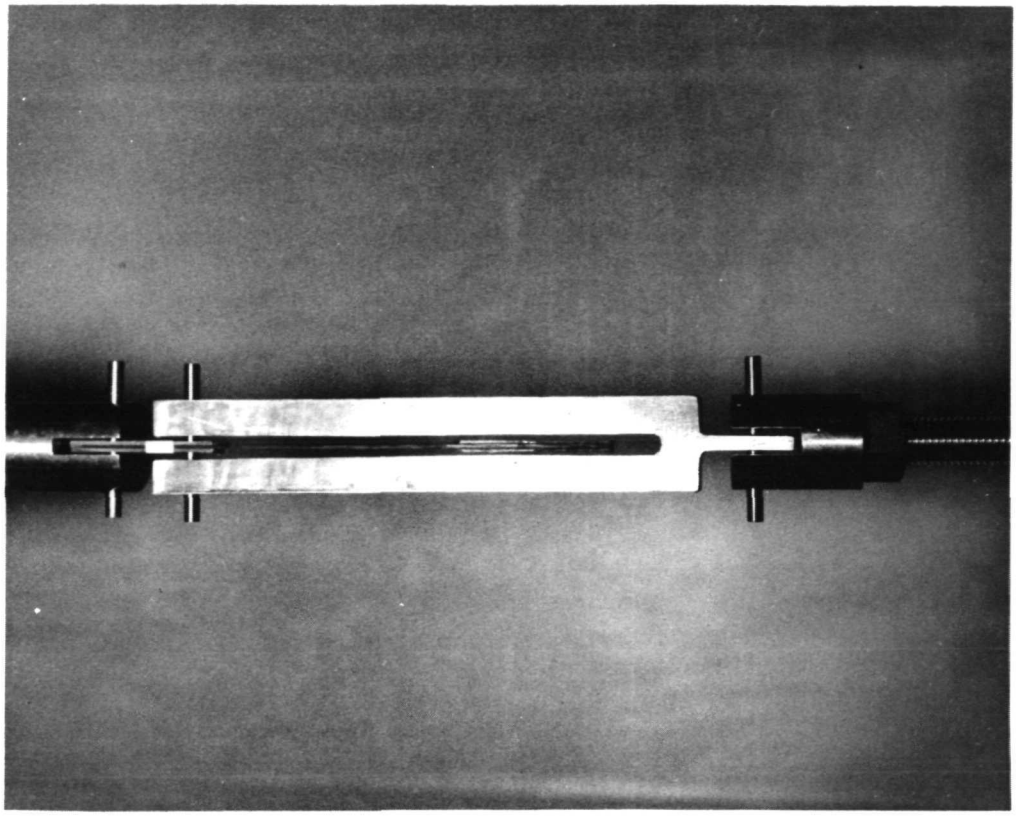

Figure 13. Photograph of Pre-Loading Fixture

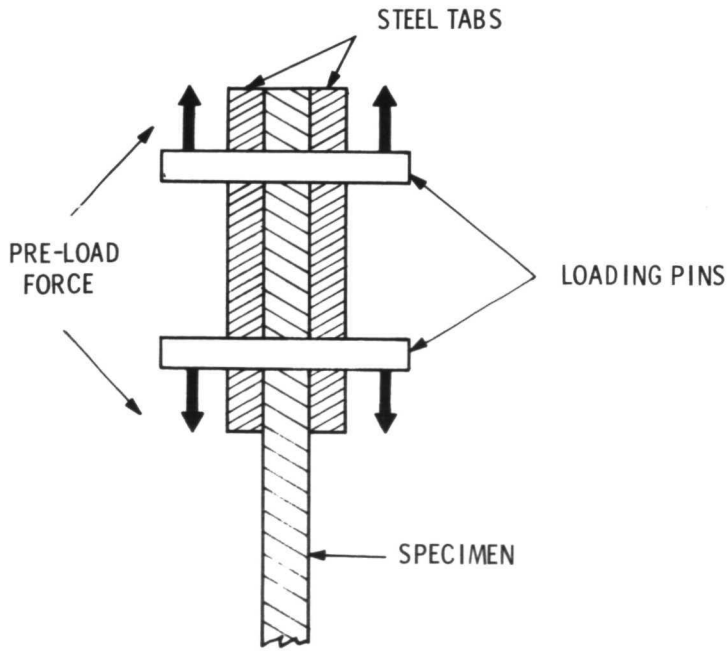

Figure 12. Schematic of Pre-Loading Fixture

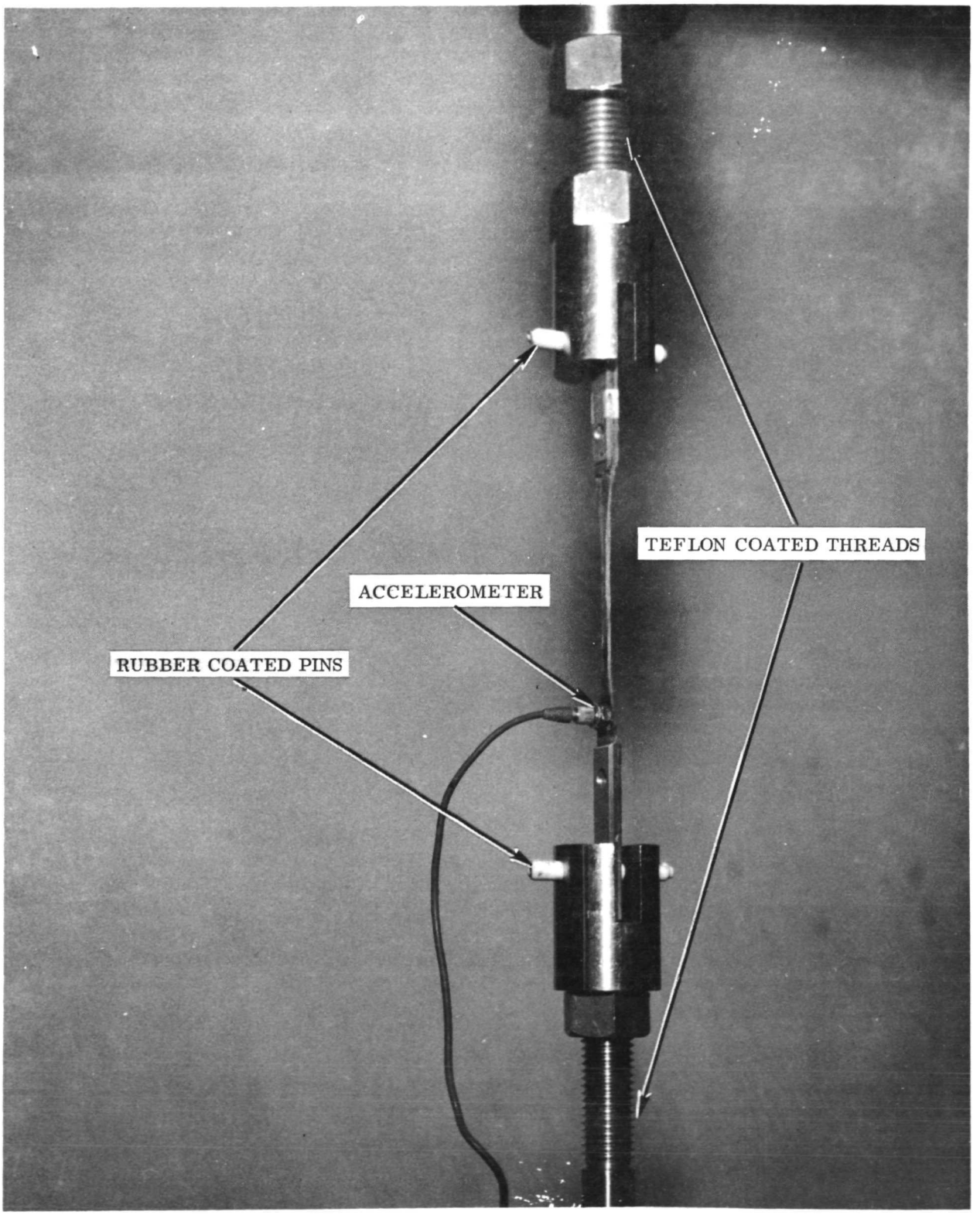

Figure 14. Photograph of a Test Specimen Ready for Test

In spite of the care and effort devoted to preparing these specimens, a fair amount of them still broke in the grips. The most usual mode of failure was either a bearing failure in the pin hole, or a grip failure associated with the lower loading pin hole. It seems clear that an even narrower gage length should be used in order to reduce the stress in the grip section. Slightly smaller diameter pins would also be desirable, as would a larger head width. However, in spite of the grip failures, and possible extraneous acoustic noise associated with bond line deformation and fracture in the grip, enough data has been generated to gain an insight into the failure mechanisms of carbon epoxy composites. This data is discussed in Section 3.2.3.

3.0 EXPERIMENTAL PROCEDURES AND OBSERVATIONS

3.1 Effect of Surface Treatment on Fracture Mechanisms

All previous tests were conducted on untreated fibers because this provided a useful reference basis for comparison with subsequent interface control studies. Most prepreg material sold commercially contains surface treated fibers to enhance interlaminar shear strength properties but the effect of this surface treatment on local fracture mechanisms has not yet been determined. The following discussion compares the behavior of treated and untreated HT and Type A fibers in the modified resin formulation since their behavior in the unmodified resin is essentially the same.

3.1.1 Comparison of Treated and Untreated HT Fibers

The comparisons presented here involve only the new batch of HT fibers in the treated and untreated condition. Differences in behavior between fiber batches will be discussed in Section 3.2.

Consider first the local fracture mechanisms shown in Figure 15 for small groups of fibers encapsulated in the modified resin formulation and tested in tension. The untreated fibers in the upper photos of Figure 15 failed with no evidence of matrix cracks normal to the fiber but instead, localized debonding extending a few fiber diameters on either side of the fiber fracture site. This behavior is in sharp contrast to that of the surface treated (HTS) fiber specimen shown in the lower photos where there is definite evidence of matrix cleavage normal to the fibers and little evidence of debonding. Clearly, the fiber surface treatment has strengthened the interfacial bond and changed the local energy dissipation from an interfacial separation to a matrix fracture mode. This behavior is not unexpected since the surface treatment was developed to enhance the bond strength and thus improve both interlaminar shear and transverse composite strength.

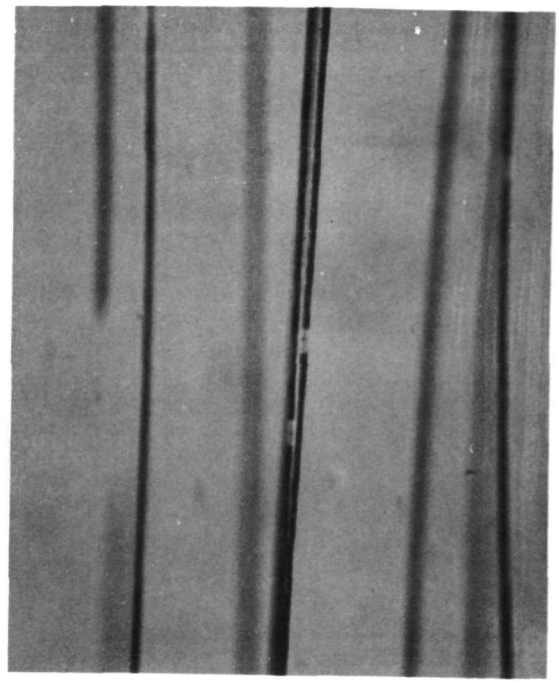

60X 150X

Untreated HT Fibers in Modified Resin Formulation

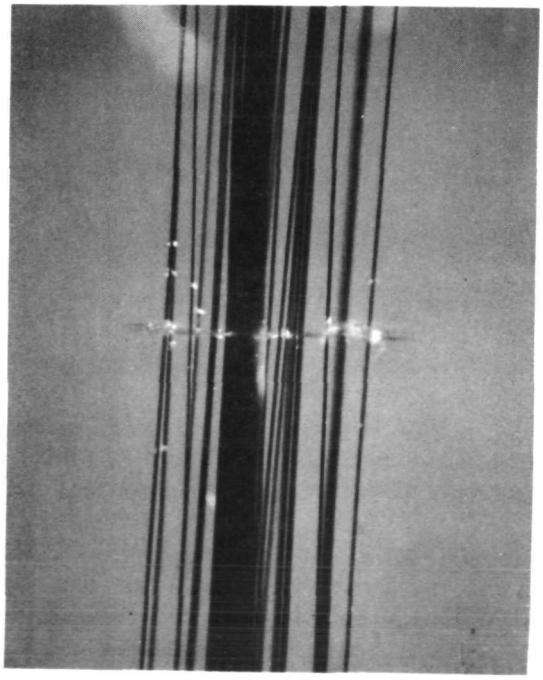

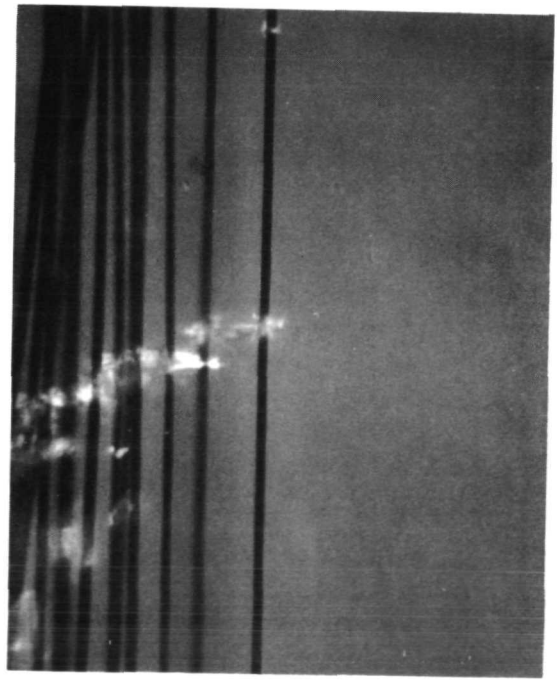

60X 150X

Surface Treated HT Fibers in Modified Resin Formulation

Figure 15. Comparison of Fracture Mechanisms for Treated and Untreated HT Fibers

More significant is the degree of correlation between microfracture mechanisms and bulk composite fracture modes. Figure 16 shows how bulk composite tensile specimens made with treated and untreated HT fibers compare. Note in the upper photo how the untreated fiber specimens have failed over an extensive area with much of the fracture surface parallel to the fibers indicating interface failure. By contrast, the surface treated fibers in the lower photograph show much more localized fractures with relatively little interface oriented fracture surface but a good deal of cleavage. This behavior of the engineering composite is consistent with the model specimen fracture observations for these treated and untreated fibers in that the surface treatment was expected to result in more cleavage because of the stronger bond it provides. The untreated fiber fractures, on the other hand, were better isolated from adjacent fibers by the interface failure allowing more random spacing of fiber fractures and more splitting along the interfaces in the bulk composite. Although the average strengths of these small groups of tensile specimens were about the same (even though the failure modes differed greatly,) the scatter in strength for the treated fiber specimens is somewhat higher than that for the untreated fiber specimens. This suggests that the cleavage failure mode associated with the stronger bond results in greater strength variation, possibly due to stress concentration effects once a microcrack is initiated normal to the fibers. However, these differences in fracture modes do not appear as significant when we take a somewhat more detailed look at strength as a function of fiber surface treatment given in Table V. Each resin formulation is represented for treated and untreated fibers. Both treated and untreated fibers gave about 20 percent higher average strengths in the modified resin system but no significant effect of the surface treatment was evident in either resin system. This is interesting in the light of the previous observations on failure modes. It appears that any effect of these fracture mode changes on composite strength are lost in the statistical variation which is inherent in the nature of fibrous composites when relatively small numbers of specimens are tested.

3.1.2 Comparison of Treated and Untreated Type A Fibers

Following the same procedures outlined previously for the HT fibers, model composite specimens containing single fibers and tows of the treated and untreated Type A fibers were tested using modified resin formulation. Figure 17 shows in the upper photographs how the untreated Type A fibers generate very small cleavage cracks normal to the fibers accompanied by a significant amount of unbonding. In the lower photos the surface treated fibers have generated very large

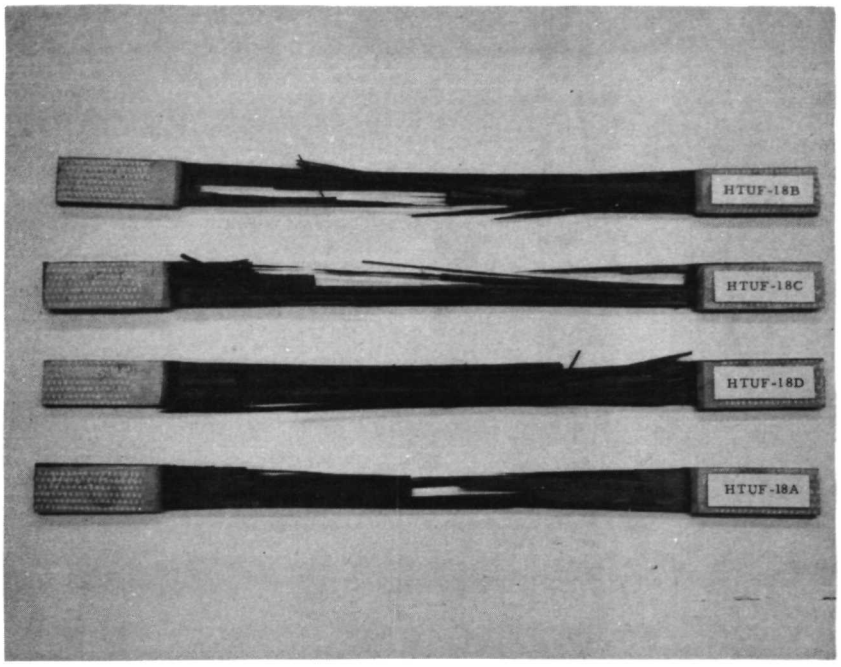

	Tensile Strength Ksi	V_f
	195.3	0.55
	184.0	0.54
	179.5	0.57
	173.6	0.50
avg	183.1	0.54

Range = 21.7 Ksi

Untreated HT Fibers in Modified Resin Formulation

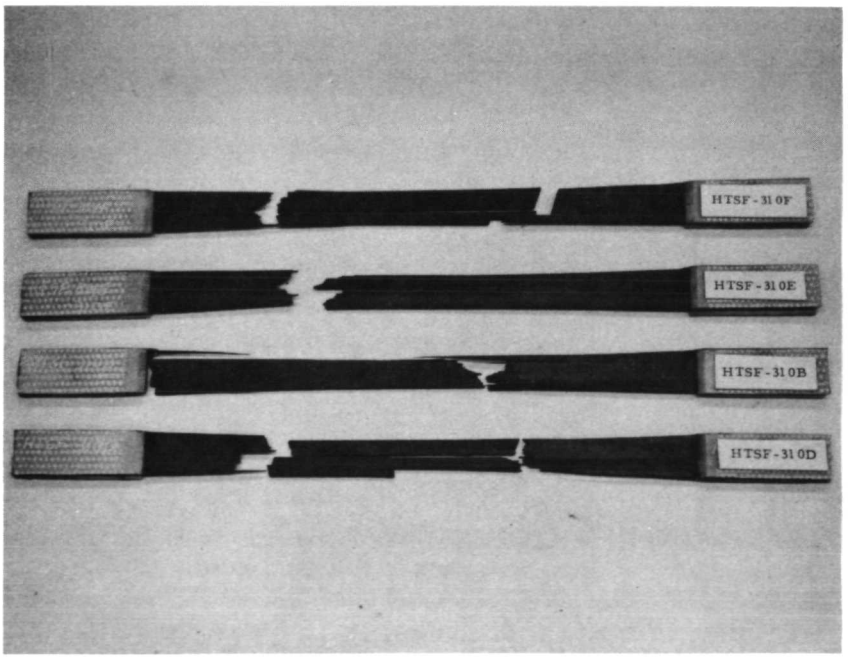

	176.0	0.56
	180.0	0.56
	202.0	0.62
	210.0	0.63
avg	192.0	0.59

Range = 26.0 Ksi

Surface Treated HT Fibers in Modified Resin Formulation

Figure 16: Fracture Modes for HT Fibers in Epoxy-Novolac

Table V. Comparison of Composite Tensile Strength Data for Treated and Untreated HT Fibers in Both Resin Formulations.

UNTREATED HT FIBERS

UNMODIFIED RESIN				MODIFIED RESIN			
Specimen Number	Tensile Strength Ksi	Tensile Modulus $x10^3$Ksi	V_f	Specimen Number	Tensile Strength Ksi	Tensile Modulus $x10^3$Ksi	V_f
HTUR* 1	171.0	21.9	0.55	HTUF 18A	173.0	19.4	0.50
3	157.0	22.0	0.56	18B	195.0	21.6	0.55
4	139.0	19.6	0.50	18C	184.0	21.1	0.54
33	158.0	26.4	0.63	18D	179.0	22.5	0.57
39	113.0	19.2	0.51	24B	153.0	20.0	0.51
46	123.0	20.6	0.55	24C	168.0	19.6	0.50
48	159.0	20.8	0.55	24D	167.0	18.5	0.47
Avg.	146.0	21.5	0.55	Avg.	174.0	20.4	0.52

TREATED HT FIBERS

UNMODIFIED RESIN				MODIFIED RESIN			
Specimen Number	Tensile Strength Ksi	Tensile Modulus $x10^3$Ksi	V_f	Specimen Number	Tensile Strength Ksi	Tensile Modulus $x10^3$Ksi	V_f
HTSR 313A	159.0	22.5	0.62	HTSF 310A	166.0	19.7	0.54
313B	152.0	19.5	0.54	310B	202.0	22.6	0.62
313C	139.0	19.0	0.52	310C	152.0	20.0	0.55
313D	143.0	17.6	0.49	310D	210.0	23.0	0.63
313E	139.0	19.0	0.52	310E	180.0	20.4	0.56
313F	160.0	19.5	0.54	310F	176.0	20.5	0.56
Avg.	149.0	19.5	0.54	Avg.	181.0	21.0	0.57

* The specimen designation uses the last letter to describe resin modification. R denotes unmodified resin and F denotes modified. U denotes untreated fibers and S denotes treated fibers.

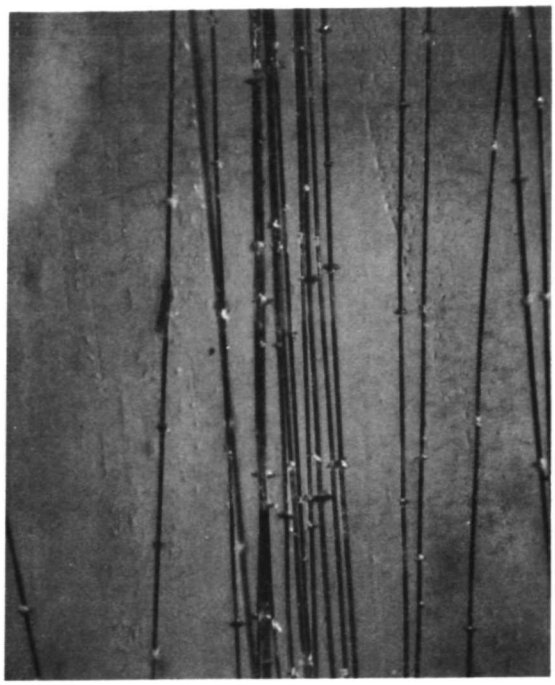

60X

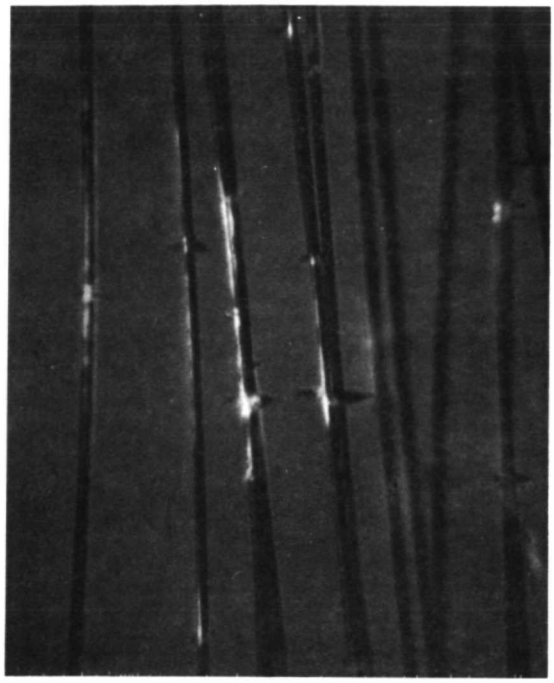

150X

Untreated Type A Fibers in Modified Resin Formulation

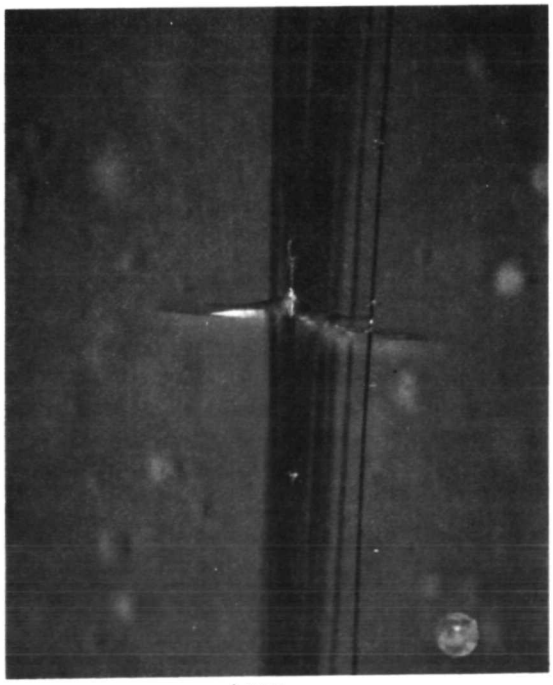

60X

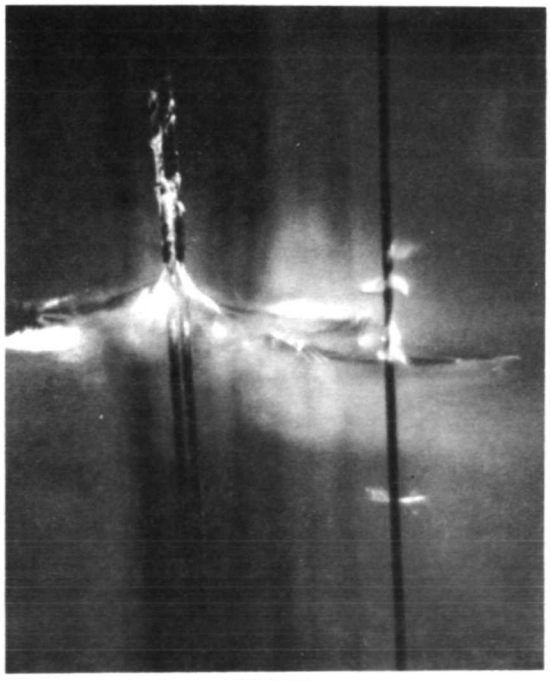

150X

Surface Treated Type A Fibers in Modified Resin Formulation

Figure 17 : Comparison of Fracture Mechanisms for Treated and Untreated Type A Fibers

and concentrated cleavage fractures with no evidence of unbonding at the interface. Only a few very large cracks were evident along the entire specimen length for the treated fibers, while hundreds of small fractures were evident in the untreated fiber specimen. Once again we see that the fiber surface treatment with its enhanced bond strength eliminates the alternative of energy absorption through interface failure and prevents the cumulative damage process from continuing. This is clearly demonstrated in the composite failure modes shown in Figure 18. Note that the specimens made from untreated Type A fibers in the upper photo exhibit a great deal of interface failure with the fractures extending over the entire length of the specimen. Very little cleavage normal to the fibers is evident and most of these specimens did not separate into two pieces even though they were extensively damaged.

The surface treated Type A fibers shown in the lower photo exhibit much more localized fracture surfaces with a somewhat jagged appearance. The significance of the jagged fracture of the lower photo compared to the interface splitting in the upper photo seems to be related to the degree to which an interface initiated crack is retarded. When the interface is weak the initial interface separation seems to run the entire length of the specimen allowing the fiber to separate from the matrix in an unstable manner over its entire length. When surface treated the bond is stronger and the interface initiated crack tends to stop at some uniform distance from the fiber break. Adjacent fibers are overloaded along that unbonded length and sometimes fail in that region causing turning of the crack normal to the fibers. This process of controlled debonding and fiber fracture causes the step type fracture surface which is seen from close inspection of the lower photo in Figure 18. The length of the steps parallel to the matrix/fiber interface should vary inversely with bond strength between fiber and matrix.

Table VI gives a comparison of the tensile strengths of specimens prepared from both treated and untreated fibers in each resin formulation. Just as in the case of HT fibers, there is no clear evidence of a bulk strength effect due to surface treatments for either resin formulation in this series of tests. When normalized to the same volume fraction, the average strengths are quite similar with the scatter greatest for untreated fibers in the modified resin.

In general the average composite strengths for the Type A fibers are considerably lower than those for the HT fibers discussed in the previous section. However, we must be cautious in drawing any far-reaching conclusions from these limited data. This series of tests was performed

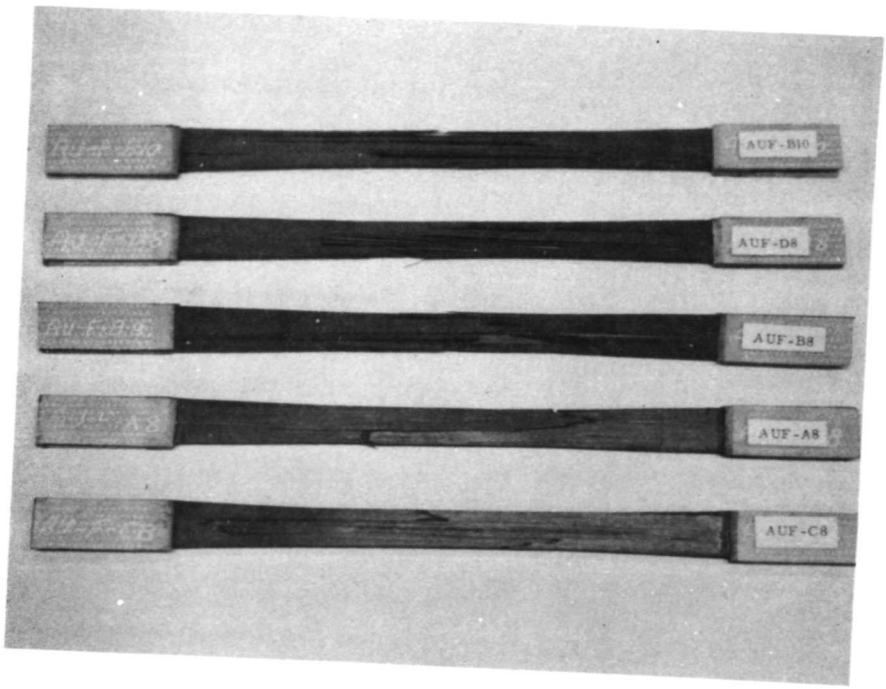

Tensile Strength Ksi	V_f
139	0.60
134	0.60
127	0.58
99.5	0.52
88	0.55
σ_{avg} =117.5	0.58

Range = 51 Ksi

Untreated Type A Fibers in Modified Resin Formulation

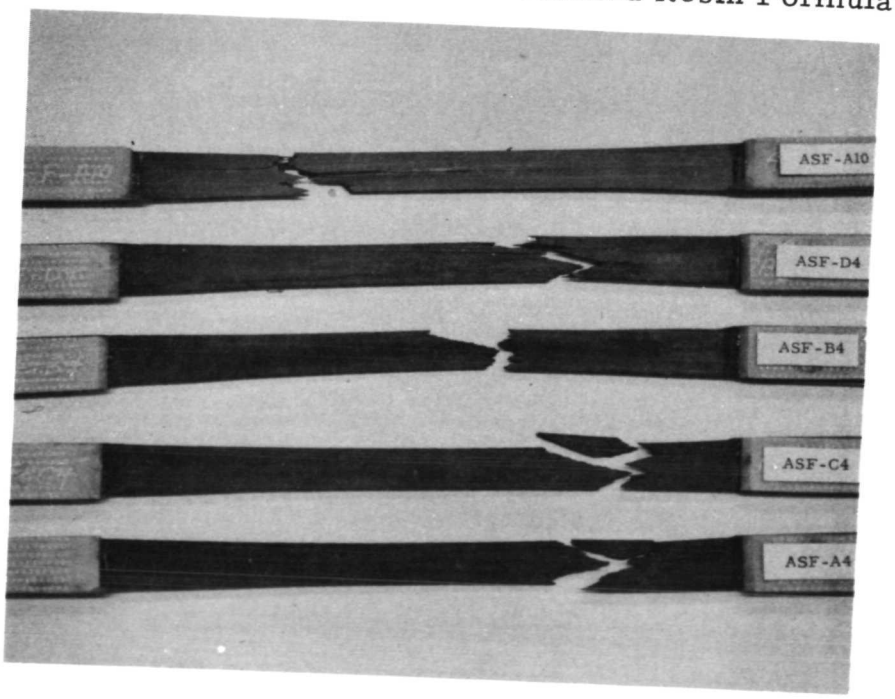

120	0.57
118	0.54
111	0.51
100	0.56
99	0.45
109.6	0.53

Range = 21 Ksi

Surface Treated Type A Fibers in Modified Resin Formulation

Figure 18: Fracture Modes for Type A Fibers in Epoxy-Novolac

Table VI. Comparison of Composite Tensile Strength Data for Treated and Untreated Type A Fibers in Both Resin Formulations.

UNTREATED TYPE A FIBERS

UNMODIFIED RESIN				MODIFIED RESIN			
Specimen Number	Tensile Strength Ksi	Tensile Modulus x10^{3}Ksi	V_f	Specimen Number	Tensile Strength Ksi	Tensile Modulus x10^{3}Ksi	V_f
AUR-A7	91.0	15.0	0.50	AUF - A8	99.5	15.5	0.52
B7	99.0	15.4	0.52	B8	127.0	17.3	0.58
C7	93.5	14.7	0.49	C8	88.0	16.4	0.55
D7	86.0	15.9	0.53	D8	134.0	17.9	0.60
B9	112.0	16.8	0.56	B10	139.0	18.6	0.63
Avg.	96.3	15.6	0.52	Avg.	117.5	17.1	0.58

TREATED TYPE A FIBERS

UNMODIFIED RESIN				MODIFIED RESIN			
Specimen Number	Tensile Strength Ksi	Tensile Modulus x10 Ksi	V_f	Specimen Number	Tensile Strength Ksi	Tensile Modulus x10 Ksi	V_f
ASR-A3	110.0	13.7	0.47	ASF - A4	99.0	13.1	0.45
B3	124.0	15.7	0.54	B4	111.0	14.9	0.51
C3	99.0	13.7	0.47	C4	100.0	16.2	0.56
D3	104.0	16.3	0.56	D4	118.0	15.6	0.54
A9	108.0	13.5	0.46	A10	120.0	16.5	0.57
Avg.	109.0	14.6	0.50	Avg.	109.6	15.3	0.53

to analyze gross fracture modes and is not intended as a statistical study of composite strength. The strength data is included for completeness and as an indicator of specimen uniformity.

3.1.3 Comparison of Treated and Untreated HT Fibers in Cycloaliphatic Epoxy

The ERL 4617 resin system has generated a good deal of interest because of its high strength, moduli and heat distortion properties. Further, the system can be modified much the same as the DEN 438 system although the total elongation to fracture is significantly less than that of the DEN system. Both treated and untreated HT and Type A fibers were encapsulated in the MDA cured resin which has a total elongation of 6-7% and is designated as ERLB 4617. In every case the tensile specimen failed at the location where the single fiber fracture occurred. There were no fiber fractures at any other location along the specimen length in these specimens. This behavior is very similar to that of the unmodified resin system at first glance and is shown in the upper photo of Figure 19. However, when we examine the fracture surfaces there is a very significant difference between the HT and HTS fiber specimens as shown in the lower photo where the left section contains the treated HT fibers and the right section contains untreated HT fibers. Note in the lower left photo that the treated (HTS) fiber initiated the fracture in the specimen. However the specimen on the right shows that the untreated fibers did not initiate the crack. In the specimen on the right, the fracture initiated at the specimen edge and passed through the fibers as it traversed the specimen. Both specimens were machined and polished in an identical manner and showed no evidence of surface defects.

This same behavior was observed for the Type A fibers as shown in Figure 20. This upper photo is typical of the single fracture site failure mode observed in profile for both the treated and untreated fiber specimens. However, the lower photo shows how the surface treated fibers (on the left) initiated the fracture while the untreated fibers (on the right) were broken by an edge initiated crack. This consistent difference in response for the two types of treated and untreated fibers suggests that the surface treated fibers with their higher bond strength are much more damaging stress concentration sources than the untreated fibers. Further tests will determine whether the observations made on these model composite specimens are significant in engineering composite performance.

3.2 Comparison of Fracture Mechanisms for Different Fiber Batches

Very early in this program (6) it had been shown that untreated HT and Type A fibers behaved differently in model composite specimens with the HT fibers generating cleavage cracks normal to the fibers and the Type A

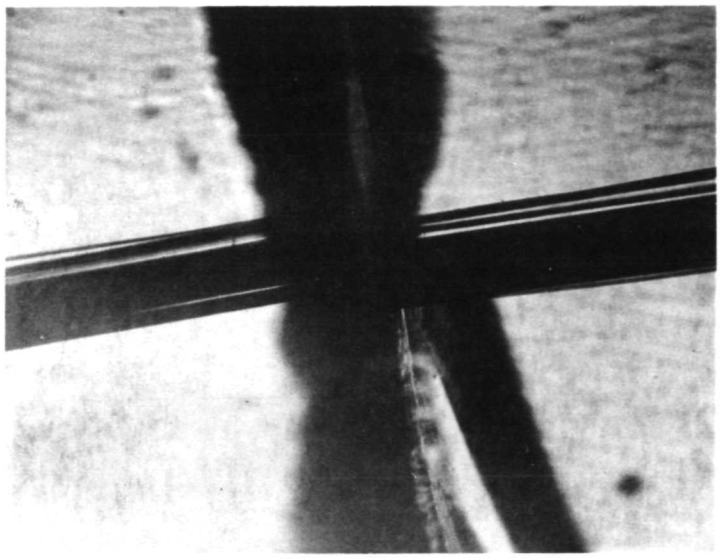

Typical Fracture Profile for Both Treated and Untreated HT Fibers

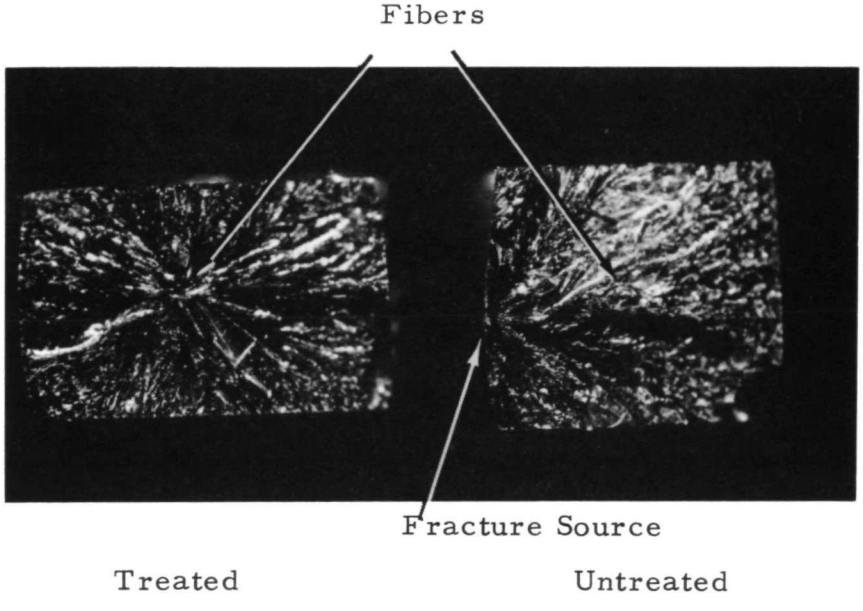

Figure 19. Comparison of Fracture Surfaces for HT Fibers in ERLB 4617 Resin

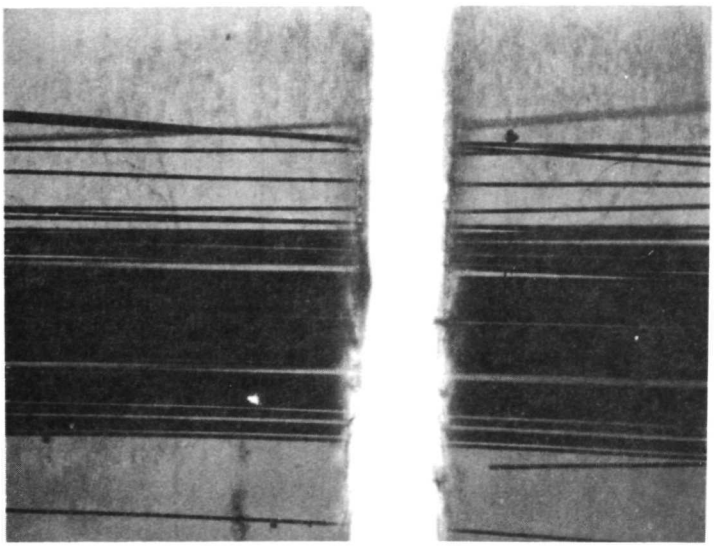

Typical Fracture Profile for Both Treated and Untreated Type A Fibers

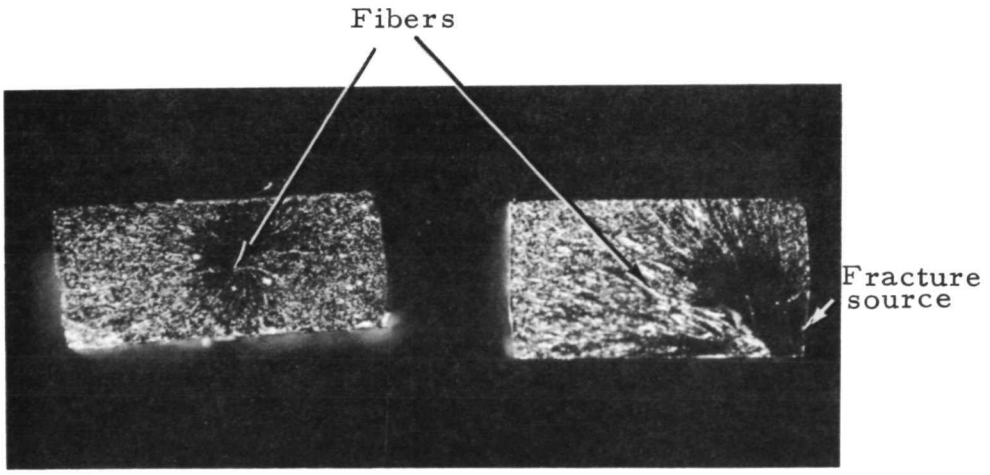

Figure 20. Comparison of Fracture Surfaces for Type A Fibers in ERLB 4617 Resin

fibers debonding at the fiber fracture site. These observations were made using untreated HT fibers obtained from Courtaulds in 1969 and having the designation "Original" in this report. In July of 1971 a new batch of untreated HT fibers was obtained from Hercules, Inc. who are licensed to produce Courtaulds fiber in the United States. The two batches of fibers were identical in properties and processing according to the manufacturer's data. Since the failure mechanisms for the two batches of the same type fiber showed distinct differences in model specimen behavior, this section will describe both microscopic observations and engineering composite tensile properties for the two batches of fibers.

Following the procedures established in earlier experiments, tensile specimens were prepared with a small number of carbon fibers encapsulated in both modified (15 to 25 percent strain to failure), and unmodified resin (2.5 percent strain to failure). The fracture mechanisms observed in the unmodified resin are shown in Figure 21. The upper photo shows typical behavior of the original batch of fibers where no accumulation of fiber fractures was evident and the first fiber fracture resulted in failure of the specimen. There was no evidence of fiber pullout or debonding which indicates that the bond was strong.

The lower photo in Figure 21 shows the typical behavior of the new batch of untreated HT fibers in the unmodified resin system. Although the failure was essentially the same with only one matrix crack, there was evidence of fiber pullout near the fracture. This is evident in the lower photo of Figure 21 and suggests some difference in the interfacial bond strength between the two batches of fibers when tested in the same resin system. A comparison of the two batches of untreated HT fibers in the modified resin systems shows much more dramatic differences in the fracture modes. The upper photos in Figure 22 shows how the original batch of fibers initiated cleavage cracks normal to the fibers as they failed in tension. By contrast, the lower photo shows no such cracks even after separation of fibers due to fracture. Since the resin tends to recover after loading and close these separations, it is difficult to photograph fiber fractures which do not cause matrix cracking. The presence of these cracks is substantiated by the large debonded areas observed along the length of the fibers and the fracture strain of the specimen which greatly exceeded that of the fibers.

Since examination at 30,000 X shows no difference in surface characteristics (5) this difference in interfacial behavior between two batches of the same fiber cannot be attributed to surface morphology. To determine whether this difference in local behavior would affect engineering composite properties a series of tensile specimens were prepared and tested.

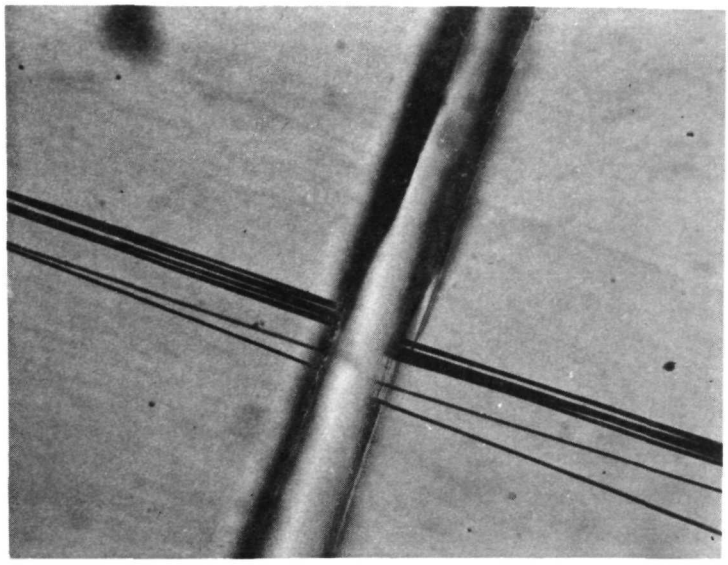

(a) Original Untreated HT Fibers in Unmodified Resin-60 X

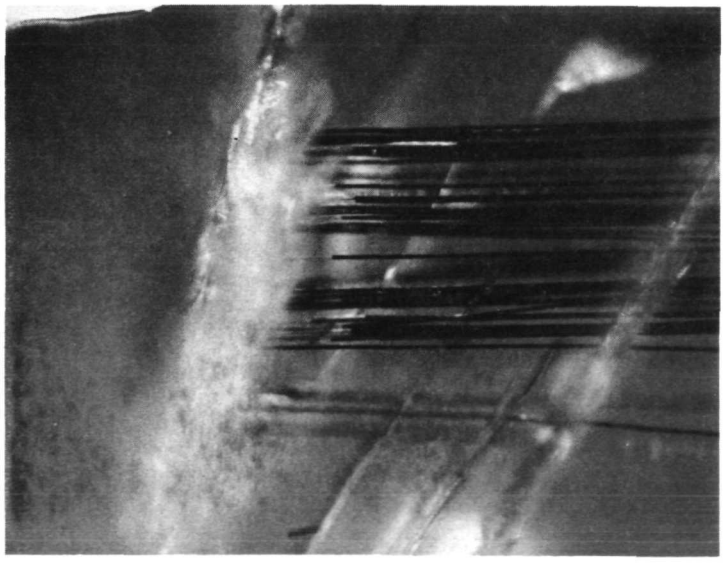

(b) New Untreated HT Fibers in Unmodified Resin - 60 X

Figure 21. Comparison of Two Batches of Untreated HT Fibers in Unmodified Resin

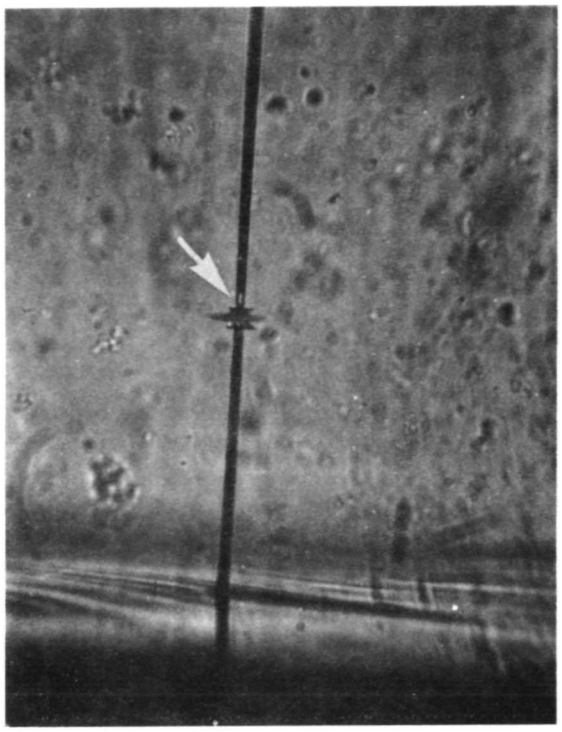

150 X

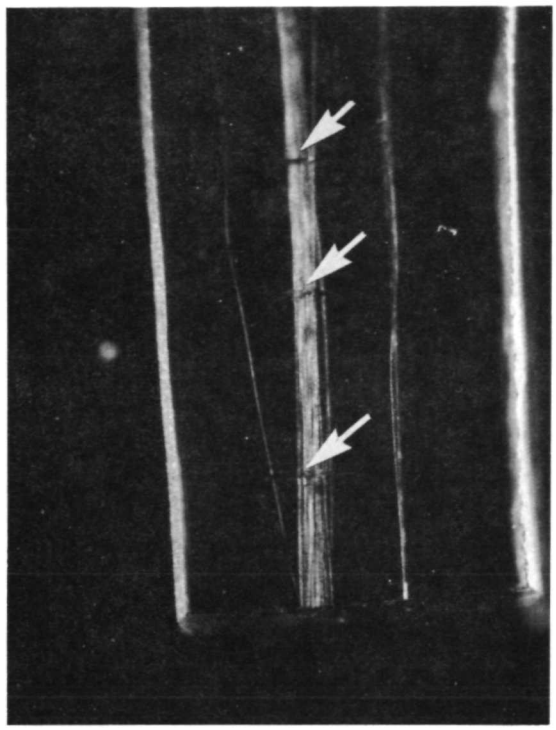

28 X

Original HT Fibers in Modified Resin

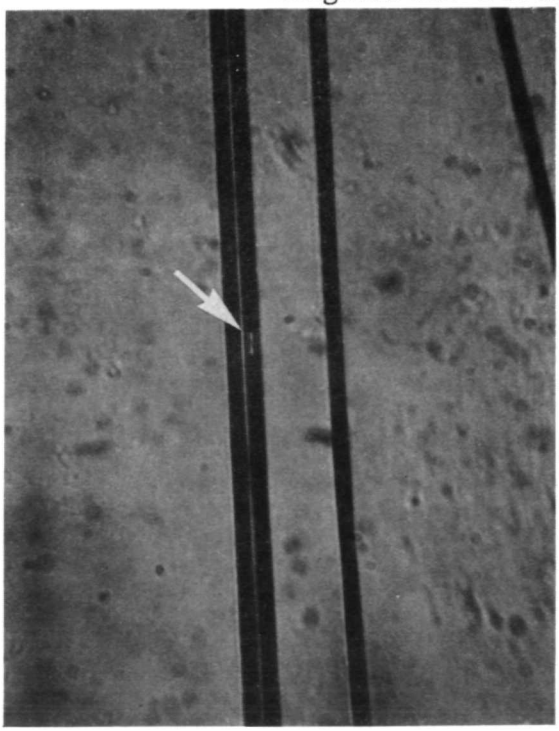

300 X

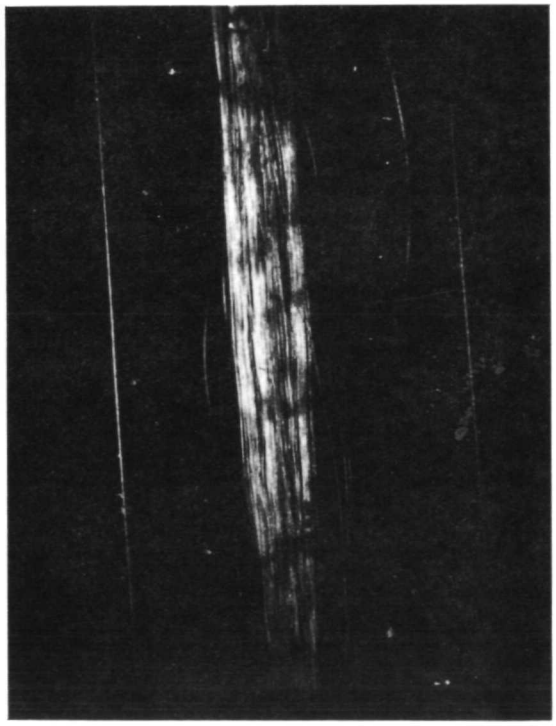

28 X

New HT Fibers in Modified Resin

Figure 22. Comparison of Two Batches of Untreated HT Fibers in Modified Resin (Arrows indicate Fiber Fracture and Matrix Cracks)

These data were then compared to the composite data obtained earlier with the original batch of fibers. The results of these tests are discussed in the following section.

3.2.2 Engineering Composite Properties

Tensile specimens of the new batch of untreated HT fibers were prepared and tested using the same procedures and specimen geometry as had been used with the original HT fibers. Table VII shows the data obtained for each batch of fibers in both modified and unmodified resin. Figure 23 is a plot of tensile strength versus volume fraction for all data obtained on untreated HT fibers. The data from specimens containing the fibers from the original batch are shown as triangles with open triangles representing modified resin and solid triangles representing unmodified resin. Note that there was considerable variation in the fiber volume fraction of specimens made from the original batch with values ranging from 0.20 to 0.55. (The effects of fiber volume fraction on failure modes will be discussed in more detail in Section 3.3). No obvious effect of matrix modification is evident in the data and the lower line represents a reasonable linear fit. Some of the scatter in these data is due to improvements in the specimen preparation technique with the very low volume fraction specimens having been prepared earlier. It should be noted here that because untreated fibers were being studied, specimens were prepared by impregnating individual tows and hot pressing after hand lay-up in a matched metal die mold. This procedure generally gives less uniformity than the use of prepreg tape where fiber orientation and resin content are much more critically controlled.

The circles in Figure 23 represent the tensile strength data for the new batch of fibers in both the unmodified and modified epoxy resin. Even though the strength data reported by the manufacturer is very nearly the same for each batch, the composite strength with the newer fibers is noticeably higher than that of the original batch for equal volume fractions of fibers. The scatter in the test data for the new batch of fibers is also less than that obtained for the specimens made with the original batch. One might expect to obtain greater scatter at lower volume fractions, but even if we ignore the data below a 0.40 fiber volume fraction, the difference in scatter is obvious and cannot be attributed solely to improved processing of specimens. In an attempt to gain further insight into the reasons for this difference in mechanical behavior, gross fracture modes were studied for all the tensile specimens.

Table VII. Comparison of Tensile Strength Data for Two Batches of Untreated HT Carbon Fibers in Both Unmodified and Modified Epoxy-Novolac Resin.

UNMODIFIED RESIN (Original Fibers)				MODIFIED RESIN (Original Fibers)			
Specimen Number	Tensile Strength Ksi	Tensile Modulus $x10^3$Ksi	V_f	Specimen Number	Tensile Strength Ksi	Tensile Modulus $x10^3$Ksi	V_f
HTR-1	41,400	8.23	0.21	HTF-1	138,000	21.6	0.56
HTR-2	32,000	10.0	0.26	HTF-2	55,100	19.6	0.51
HTR-3	36,200	9.85	0.25	HTF-3	56,500	12.1	0.31
HTR-5	55,000	13.0	0.33	HTF-5	60,000	12.0	0.31
HTR-6	74,000	11.9	0.31	HTF-6	90,000	12.7	0.33
HTR-7	93,500	15.0	0.39	HTF-7	99,000	18.9	0.49
HTR-8	111,000	16.2	0.42	HTF-8	114,000	18.0	0.47
HTR-9	88,700	13.0	0.33	HTF-9	58,500	13.5	0.35
HTR-10	68,500	14.2	0.37	HTF-10	61,600	13.6	0.35
HTR-11	95,000	19.5	0.50	HTF-11	108,000	15.5	0.40
HTR-12	130,000	19.5	0.50	HTF-12	87,200	14.5	0.37
Avg.	75,030	13.7	0.35	Avg.	84,355	15.6	0.40

UNMODIFIED RESIN (New Fibers)				MODIFIED RESIN (New Fibers)			
HTUR-1	171,000	21.0	0.55	HTUF-1	149,000	18.5	0.47
HTUR-2	162,000	19.8	0.50	HTUF-2	120,000	17.5	0.44
HTUR-3	157,000	22.0	0.56	HTUF-3	130,000	25.0	0.63
HTUR-4	139,000	19.6	0.50	HTUF-4	139,000	20.0	0.51
HTUR-5	148,000	19.1	0.48	HTUF-5	143,000	17.8	0.45
HTUR-6	134,000	18.9	0.42	HTUF-6	140,000	18.4	0.47
				HTUF-7	159,000	22.0	0.56
				HTUF-8	131,000	17.3	0.44
Avg.	151,830	20.2	0.50	Avg.	138,875	19.6	0.49

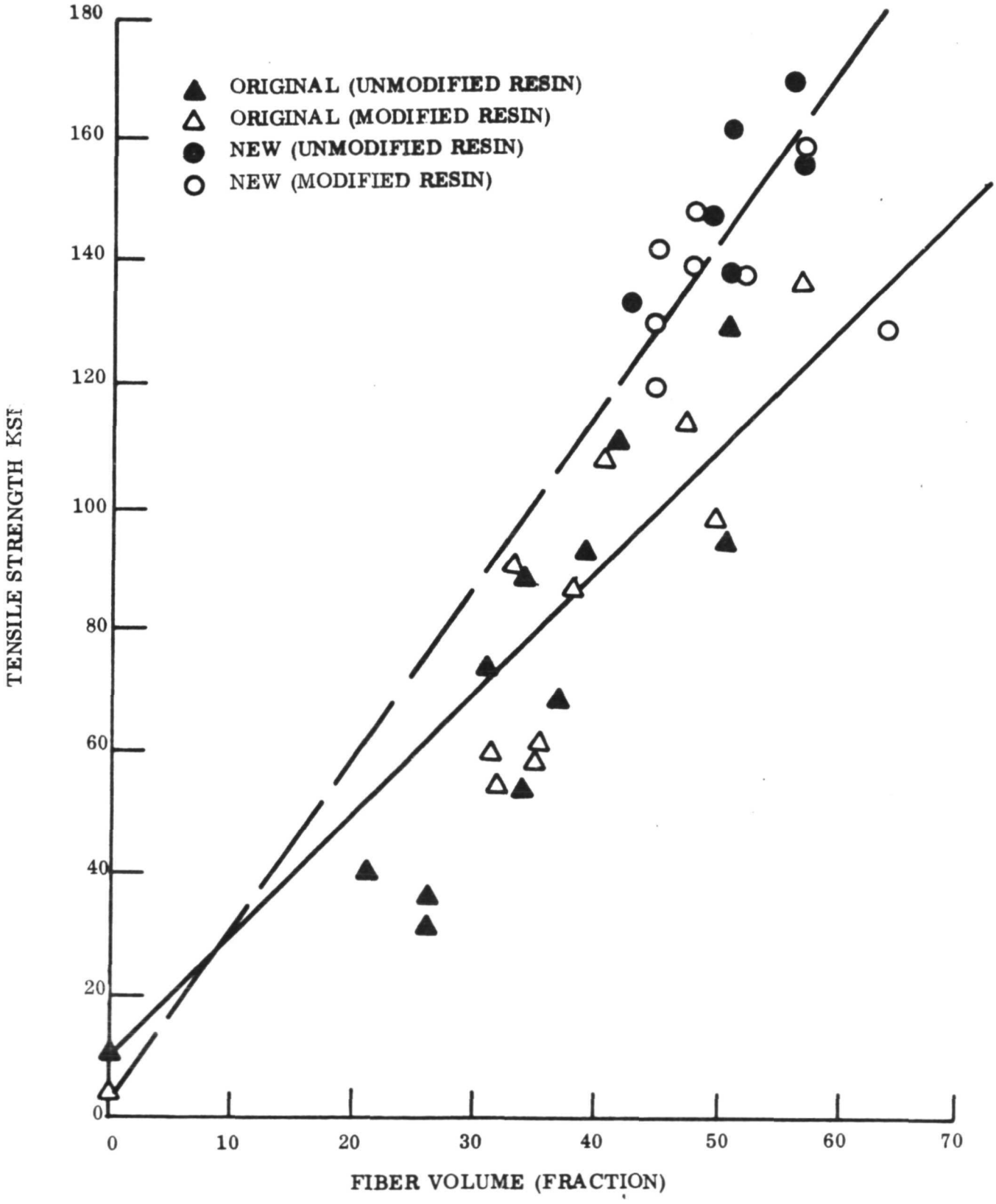

FIGURE 23. TENSILE STRENGTH DATA COMPARISON FOR TWO BATCHES OF HT CARBON FIBERS IN BOTH MODIFIED AND UNMODIFIED EPOXY RESIN

Figure 24 shows a comparison of the fracture modes for the two different batches of fibers in the same unmodified resin system. The upper photo shows typical fracture modes for the original batch of fibers. Care was taken to compare volume fractions in this analysis because fracture modes are also influenced by fiber content. The lower photo shows considerably less cleavage with a good deal of interface separation and fiber pullout for specimens fabricated from the new batch of fibers. This is consistent with the observations discussed previously in model specimens containing single fibers and tows. Note that damage extends over a large portion of the specimen in most cases. The average strength of the specimens made with the new fibers was 30 to 50 percent higher than those fabricated from the old batch. This is not due to deviations from reported strength values for the fibers since fiber strengths have been determined experimentally.

Figure 25 shows a similar comparison in the modified epoxy resin formulation with the gross fracture modes quite similar to those shown previously for the unmodified resin. Although the cleavage with the original batch of fibers (upper photo) is not as distinct as it was in the unmodified resin, this is still the dominant mode of failure. The new batch of fibers on the other hand, behave quite differently with very little cleavage and a good deal of fiber pullout and transverse splitting. The most notable difference here is the greater scatter which occurs with the original fiber specimens (where cleavage is significant) compared to that of the newer fiber specimens (where cleavage is not widespread). Since this scatter is evident even between specimens having nearly the same volume fraction of fibers, it appears that the cleavage failure mode in either modified or unmodified resin is a very random failure process. The more tortuous fracture behavior of the specimens made from the newer batch of fibers showed less scatter, higher strength and, therefore, more predictable behavior even though the fibers have the same mechanical properties as reported in Section 2.2.1.

It appears that the difference in local matrix response at fracture is solely responsible for the differences in composite strength and considerable scatter in the strength data for the old batch specimens. This points up the significance of local matrix cleavage response in bulk composite properties and clearly indicates that interface control is the most likely means for optimizing composite performance.

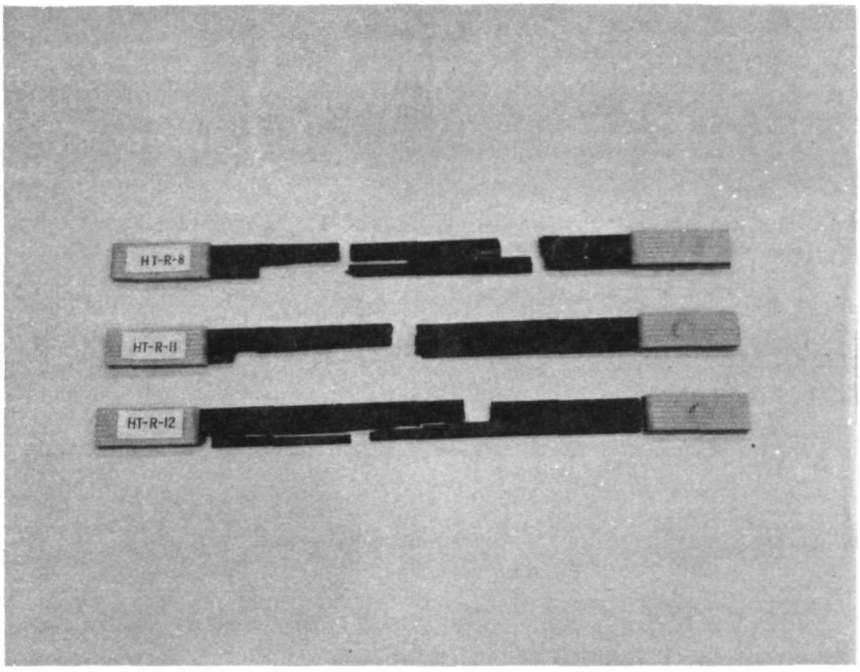

Original Fiber 1st Batch

V_f	σ_c ksi	E x 10^3 ksi
.42	111	16.2
.50	95	19.5
.50	130	19.5

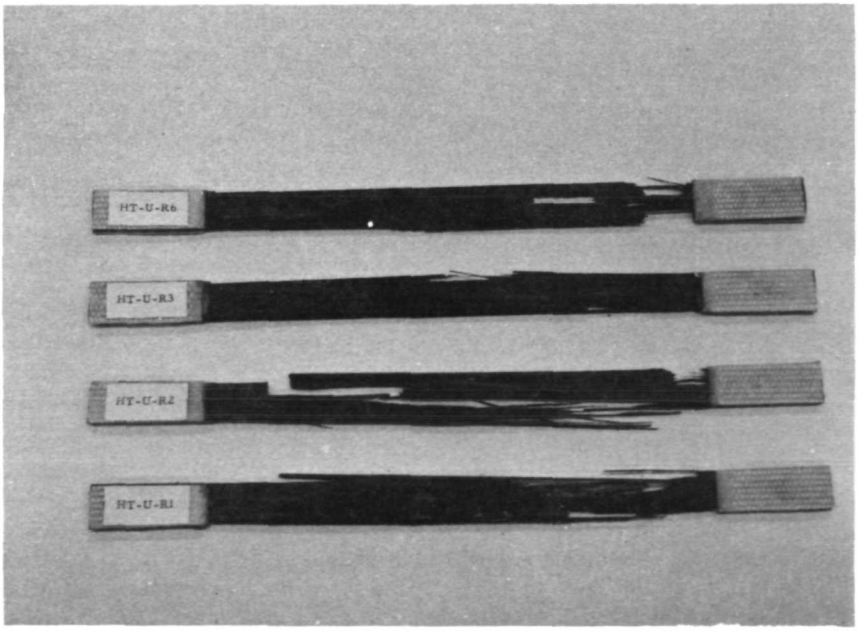

New Fiber Batch

V_f	σ_c ksi	E x 10^3 ksi
.42	134	18.9
.56	157	22.0
.50	162	19.8
.55	171	21.9

Figure 24. Comparison of Gross Failure Modes for Two Batches of Untreated HT Fibers in Unmodified Resin

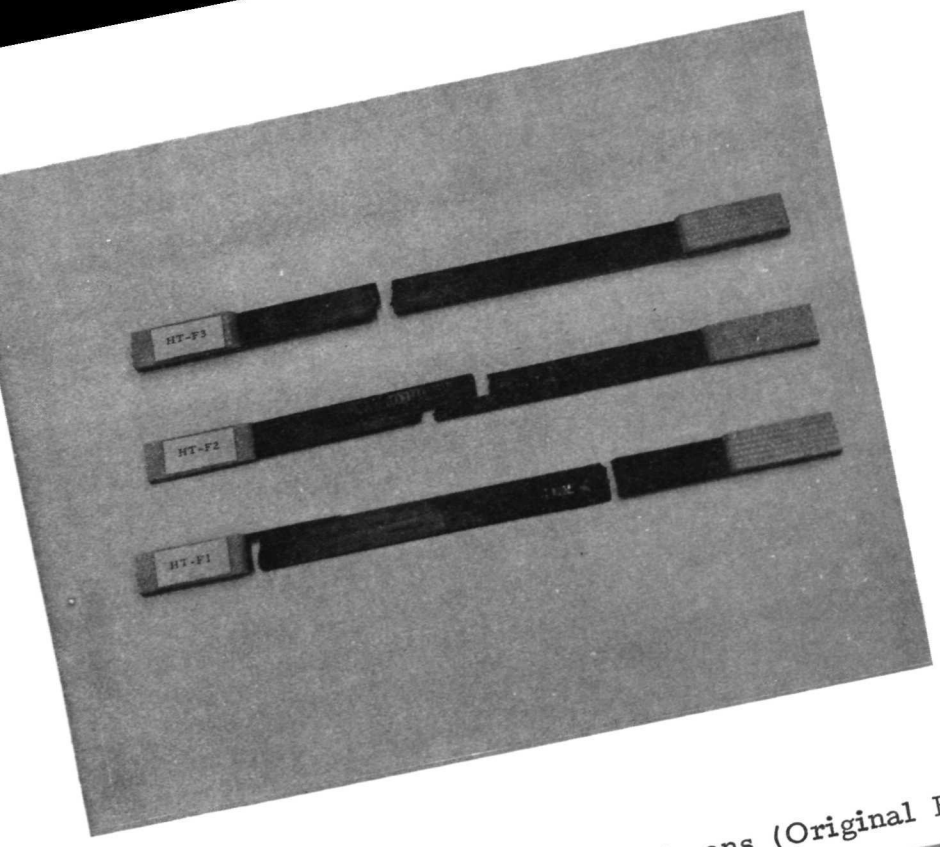

V_f	σ_c ksi	E ksi x 10^3
.31	56.5	12.1
.51	63.8	19.6
.56	138.0	21.6

a) HT-U Fiber Specimens (Original Batch)

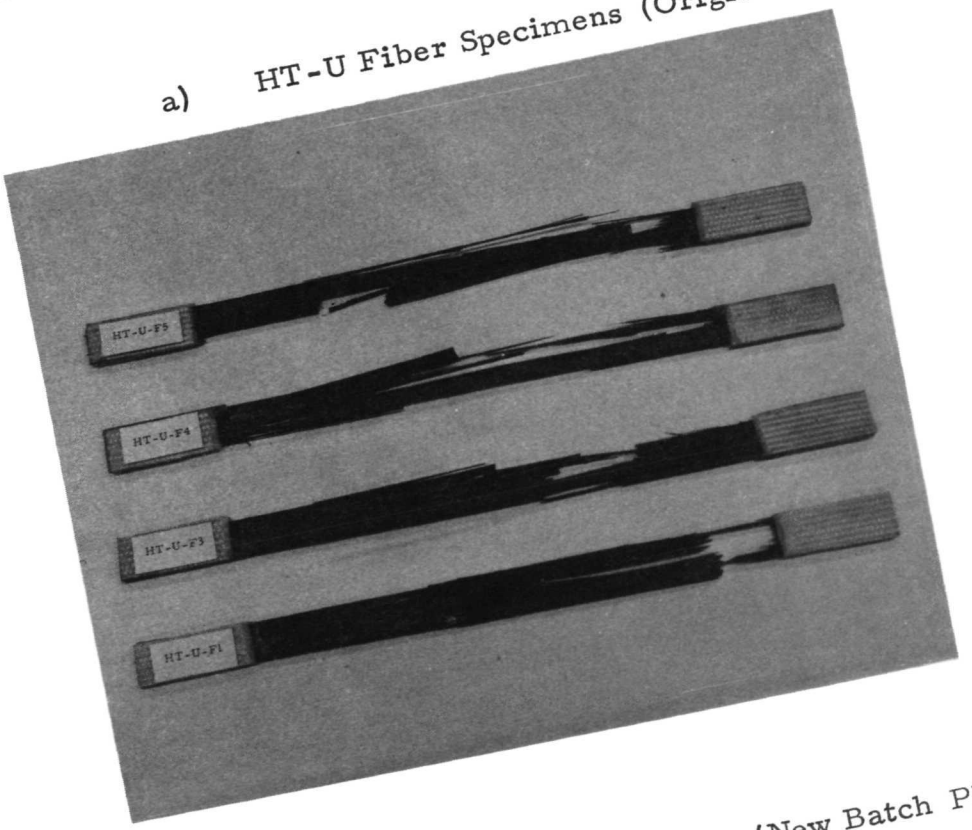

.45	143.0	17.8
.51	139.0	20.0
.63	130.0	25.0
.47	149.0	18.5

b) HT-U Fiber Specimens (New Batch PPH)

Figure 25. Comparison of Gross Failure Modes for Tensile Specimens of HT Fibers in Modified Resin

3.2.3 Acoustic Analysis of Failure Modes

3.2.3.1 Model Composite Failure Mechanisms

As discussed previously in this report, when a carbon epoxy specimen is deformed in tension, one of several failure processes may occur. A fiber break can be associated with subsequent debonding, which can occur in incremental steps, or the break can lead to the formation of a matrix crack. All of these events will produce an elastic wave capable of exciting the accelerometer at its natural frequency of about 48 kHz. In addition, more highly energetic events such as groups of fiber fractures or gross matrix cracking can, in addition to transducer resonance, excite lower frequency components such as specimen vibration. At the present time with carbon fiber composites, we are unable to discriminate between these various failure modes, and the resulting count rate data includes all modes.

A general idea of the frequency of occurrence of events may be obtained from Figure 26. Once failure events begin, they occur at an increasing rate. From time to time a burst of emission is noted, as shown in the top righthand photograph. This could indicate a larger group of fibers failing in close sequence, perhaps in conjunction with incremental debonding. A typical individual event, consisting of an elastic wave exciting the transducer, is shown in the lower photograph. It may be noted that each event would be "counted" a number of times, depending on the discriminator threshhold and the amplitude of the event.

3.2.3.2 Engineering Composite Failure Mechanisms

Since the ability to discriminate between individual failure mechanisms in the carbon epoxy system was limited, a good deal more attention was focused on the response of more heavily reinforced engineering composite specimens. Typical count rate and cumulative count data are shown in Figures 27 through 29. In all these data, the pertinent instrumentation parameters used to record and display the data are as follows:

Data Acquisition:

Amplifier Gain:[1]	60 db
Accelerometer:	Endevco Model 2226C

(1) Ithaco Model 453

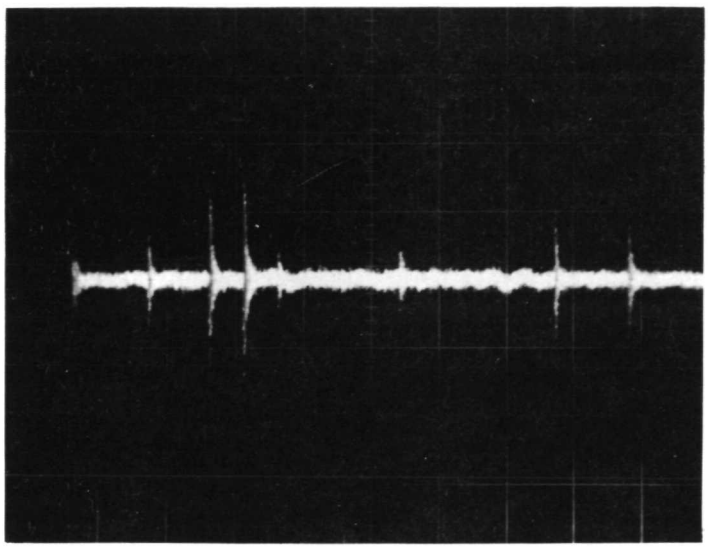

40 msec/cm
Average Emission Rate

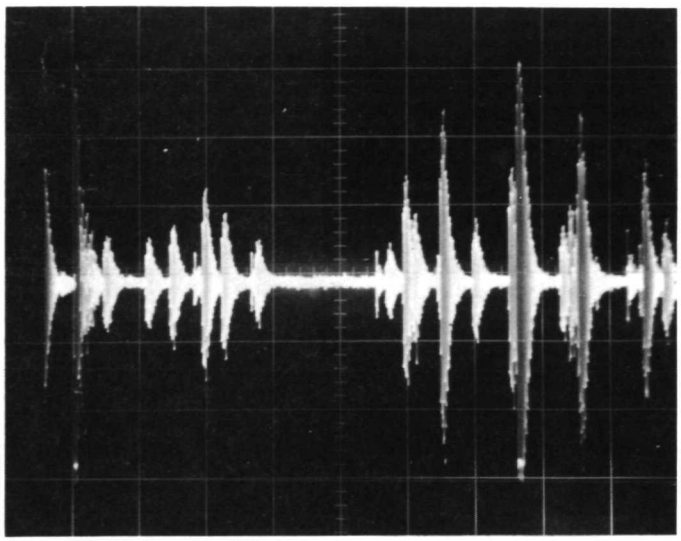

40 msec/cm
"Burst" Emission Rate

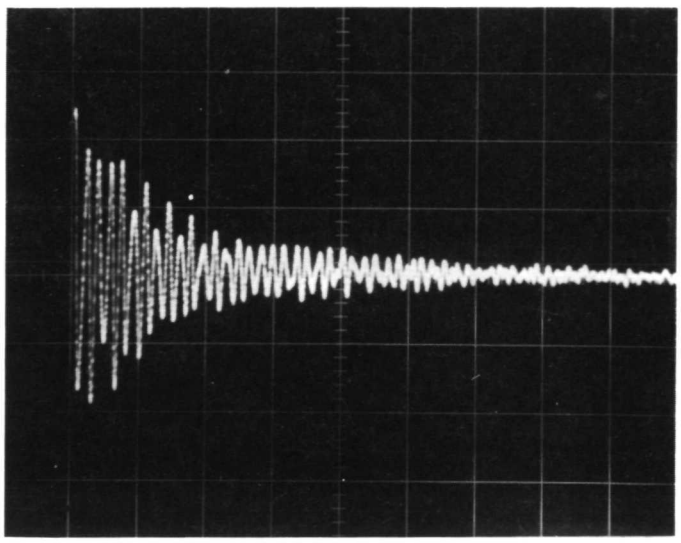

0.125 msec/cm
Typical Acoustic Event

Figure 26. Typical Emissions from a Carbon-Epoxy Specimen Consisting of a Few Type A Fibers in the Modified Resin Formulation

FIGURE 27. ACOUSTIC EMISSION DATA FROM A 45 V_f COMPOSITE SPECIMEN CONSISTING OF TYPE A UNTREATED FIBERS IN UNMODIFIED EPOXY NOVOLAC RESIN

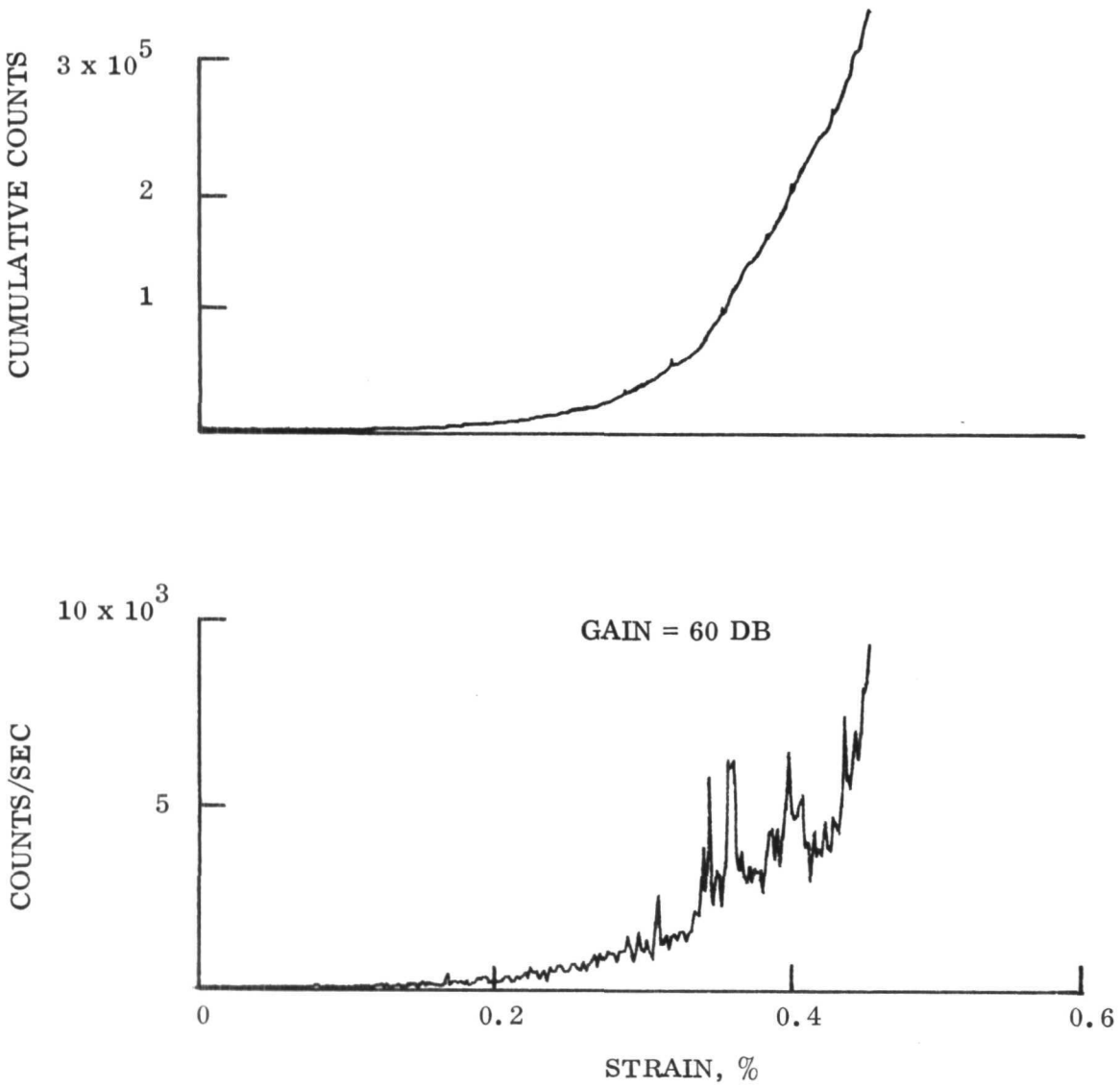

FIGURE 28. ACOUSTIC EMISSION DATA FROM A 30 V_f COMPOSITE SPECIMEN CONSISTING OF HT UNTREATED FIBERS IN UNMODIFIED EPOXY NOVOLAC RESIN

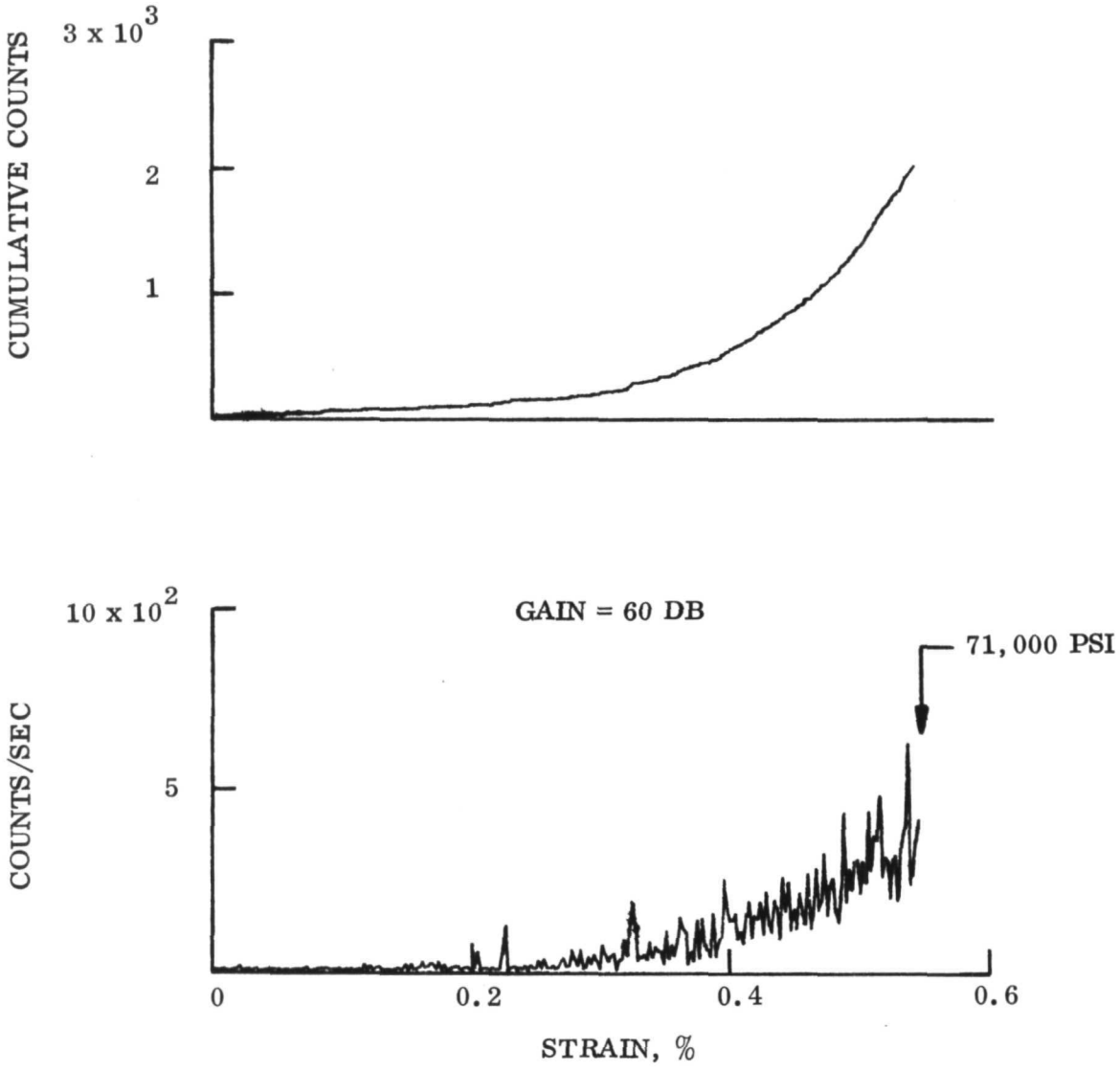

FIGURE 29. ACOUSTIC EMISSION DATA FROM A 55 V_f COMPOSITE SPECIMEN CONSISTING OF HT UNTREATED FIBERS IN A MODIFIED EPOXY NOVOLAC RESIN

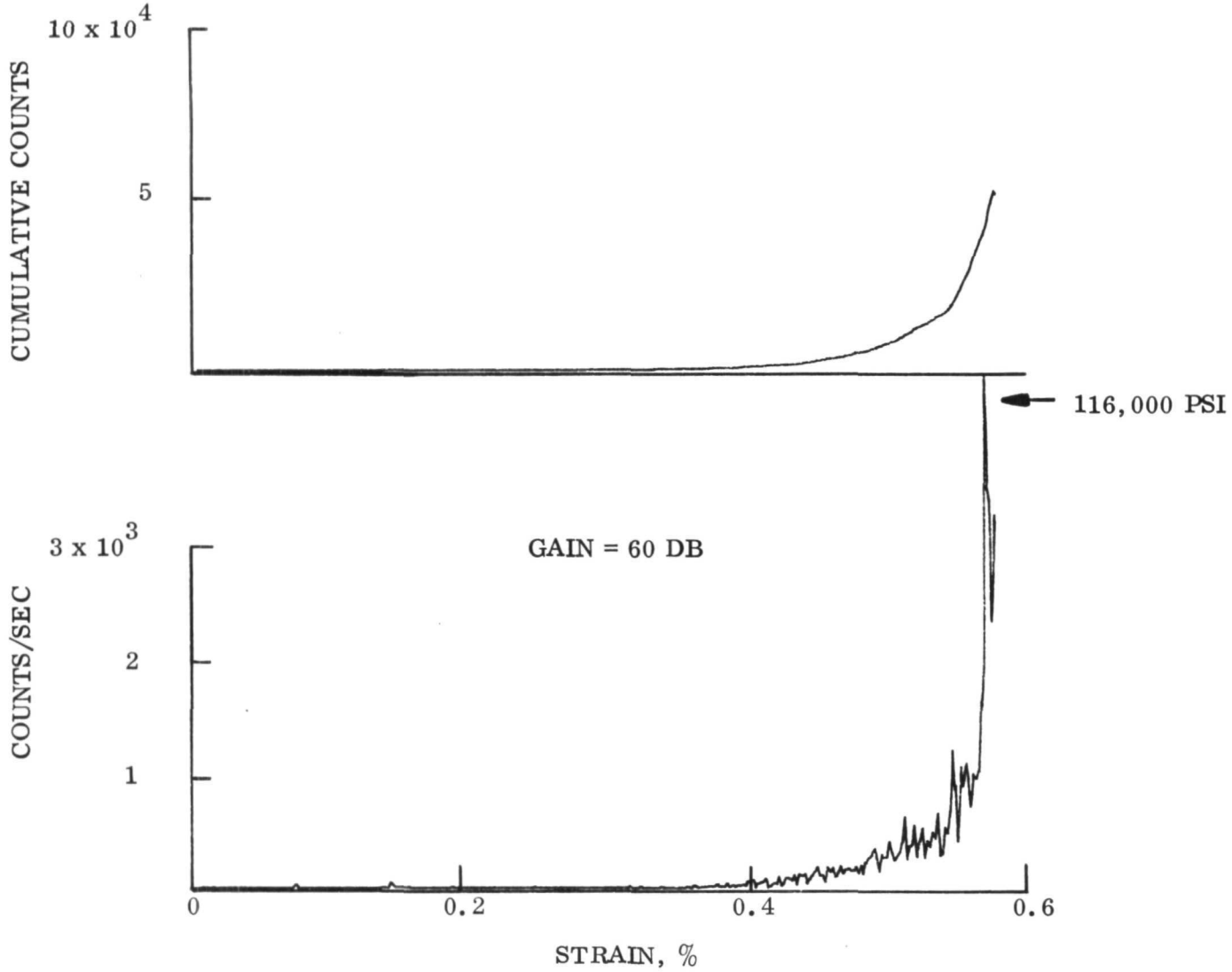

Data Read-Out:

Amplifier Gain:[2]	56 db
Discriminator Level:	42 mv
Band Width:	5 KHz to 100 KHz (approximately)

It may be noted that during the latter part of this program the amplifier used to amplify the transducer signal was changed from an Ithaco Model 252 to an Ithaco 453. It was found that the former amplifier went into oscillations when saturated with a high level signal, and took on the order of one to three seconds to recover. The present amplifier recovers much more quickly and thus assures that no data is lost due to saturation. For this reason, data reported in the previous report may show some deviation from the present data where high amplitude signals are involved.

Pertinent tabular data is presented in Tables VIII and IX. In these and subsequent presentations the count data has been normalized arbitrarily on an area corresponding to $12 \times 10^{-3} in^2$ in order to factor out volume effects (the gage length was the same in all cases). In addition, count data has been evaluated both at failure and at 0.45% strain. The latter comparison is necessary to partially eliminate grip fracture noise, particularly when failure was observed to take place in the grip.

From the data presented in Tables VIII and IX, as well as Figures 27 through 29, the following observations may be drawn:

1. Composites containing untreated Type A fibers show a greater degree of acoustic activity than HT fibers in a similar matrix. This comparison is shown in Table VIII and in bar graph form in Figure 30, where the data is evaluated at .45% strain. This implies that either Type A fibers have a greater strength scatter than HT fibers and hence show more acoustic activity, or a greater degree of debonding or matrix cracking takes place in the case of composites with Type A fibers. The limited fiber data presented in Section 2.2.1 does not support the supposition that Type A fibers have a greater strength scatter: indeed, the opposite could be true. It may also be noted that the total acoustic emissions at failure are greater for composites with the A fibers, even though grip failure and perhaps associated grip noise was probably recorded for the HT fiber specimens. Therefore, it is reasonable to infer that a larger number of matrix associated events such as debonding occur in the A fiber system as compared to the HT system.

---

(2) Hamner Model N301

Table VIII. Comparison of Total Acoustic Emissions from Composites Consisting of Untreated Type A and HT Fibers in an Unmodified Resin - $V_f \cong 0.40$

Specimen	Stress, psi	Counts at Failure		Counts at .45% Strain	
		Total	Normalized(2)	Total	Normalized(2)
AUR-1A	75,600	3.4×10^5	3.4×10^5	2.2×10^5	2.2×10^5
AUR-1B	78,000	1.8×10^5	2.07×10^5	0.8×10^5	0.92×10^5
HTUR-B30(1)	87,000	0.8×10^5	0.6×10^5	0.8×10^5	0.6×10^5
HTUR-A34(1)	66,700	0.8×10^5	0.56×10^5	0.7×10^5	0.49×10^5

(1) Grip Failures

(2) Normalized on $A = 12 \times 10^{-3} in^2$

Table IX. Comparison of Total Acoustic Emissions from Composites Consisting of Untreated HT Fibers in Both Unmodified and Modified Resin - $V_{f.} \cong 0.40$

Specimen	Matrix	Ultimate Stress, psi	Counts at Failure		Counts at 0.45% Strain	
			Total	Normalized(2)	Total	Normalized(2)
HTU-FA(3)	Modified	70,900	7.5×10^4	7.1×10^4	0.7×10^4	0.66×10^4
HTU-FB(3)	Modified	83,000	17×10^4	13.3×10^4	1.5×10^4	1.17×10^4
HTU-F2(3)	Modified	116,000	5×10^4	6.7×10^4	0.5×10^4	0.67×10^4
HTRU-B30(1)	Unmod.	87,000	8×10^4	6×10^4	8×10^4	6×10^4
HTUR-A34(1)	Unmod.	66,700	8×10^4	5.6×10^4	7×10^4	4.9×10^4

(1) Grip Failure

(2) Normalized on $A = 12 \times 10^{-3}$ in^2

(3) This specimen made with new HT fibers

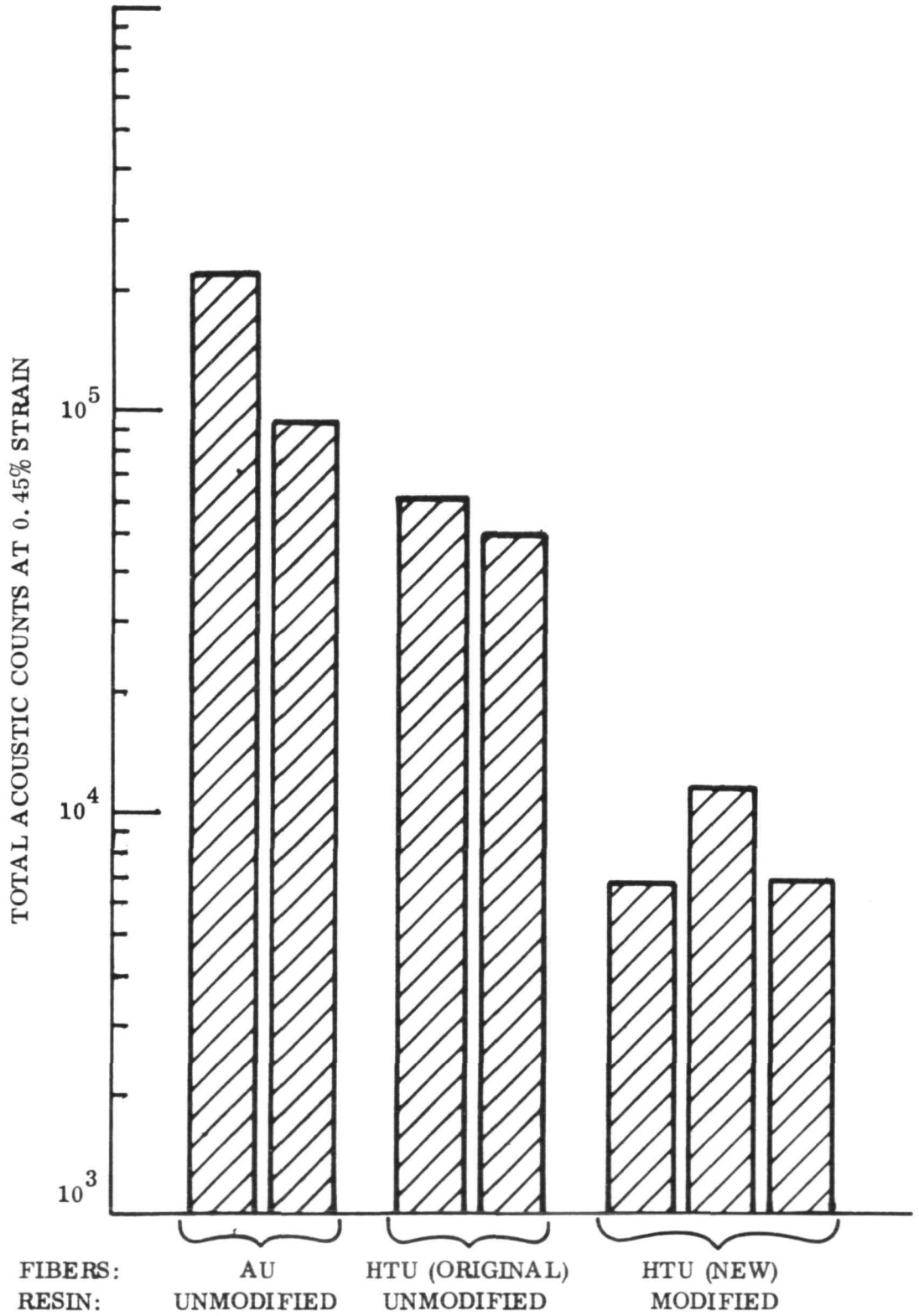

FIGURE 30. COMPARISON OF ACOUSTIC EMISSIONS AT 0.45% STRAIN FOR THREE COMPOSITE FORMULATIONS

2. Composites containing untreated HT fibers in a modified matrix start failing at a larger value of strain than HT fibers in the unmodified resin. This can be seen by comparing Figure 28 and Figure 29.

Unfortunately, the new HT fibers were used in the modified resin, and the old ones in the unmodified epoxy, so the comparison is clouded by the fact that both fibers and resin were changed. The combination of the new fibers in the modified resin, however, does result in the activity taking place within a shorter period of time, as shown in Figure 29. It is known from the micro-fracture work that the HT (new) fibers in a modified matrix produce a large amount of debonding, and this would produce fewer counts because such a process is less energetic than filament fracture, and hence each event would not be counted as many times. Future experiments are planned in which more comparisons between HT fibers in different resins will be made. The failure mechanisms may be quite variable even in the same system, as indicated by the behavior of specimen HTU-FB in Table IX. This specimen, made under similar conditions to the other two HTU-modified specimens had roughly double the amount of acoustic activity. At present, such variable behavior is not understood.

3. For most of the original fiber/unmodified resin composite specimens, acoustic emissions began at about half the fracture strain. By contrast, most specimens of HT fibers (new) in the modified resin give first emissions at two-thirds the fracture strain. These observations are consistent with data presented by Liptai (12) for glass/epoxy specimens in that first emissions were recorded at about half the ultimate strain. This is in general agreement with the cumulative damage predictions of Zweben (16). In addition, to the failure events occurring on a fine scale and at relatively low amplitudes discussed above, larger and far more energetic events are observed as carbon epoxy specimens are loaded in tension. These events are sometimes audible, and typically are recorded at an amplifier attenuation of about 20 db. The origin of these events is probably a large scale longitudinal matrix cracking both below and on the surface. Those specimens which exhibit gross longitudinal splitting after failure typically generate a greater number of these more energetic events. Figure 31 shows such a longitudinal split. The specimen was unloaded prior to failure and the crack was decorated with chalk dust to show greater contrast in the photograph. In some cases, similar acoustic events were observed, but no crack was found, indicating that these failures can occur below the surface of the specimen.

ORIGINAL SURFACE
(12X)

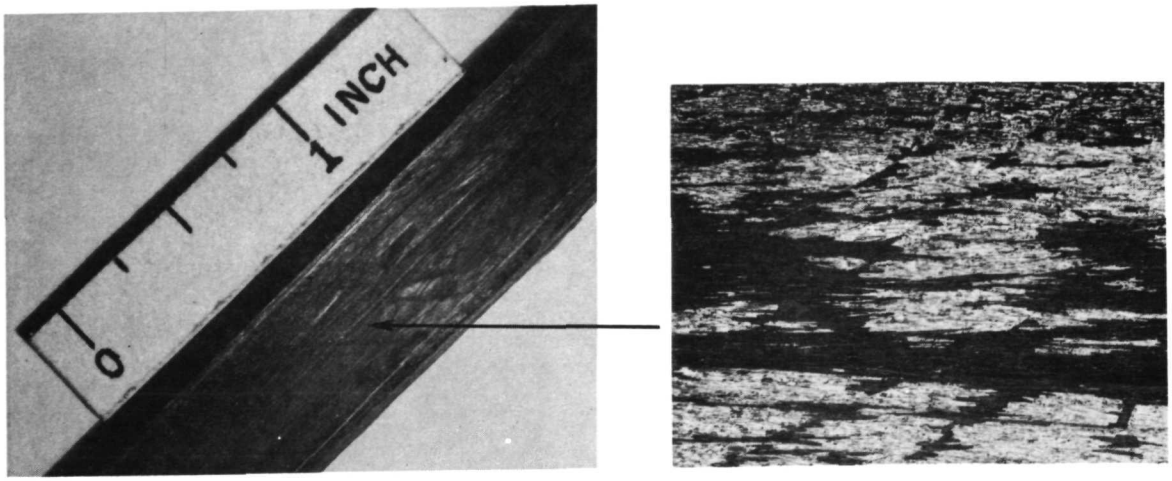

LONGITUDINAL SPLITTING
(12X)

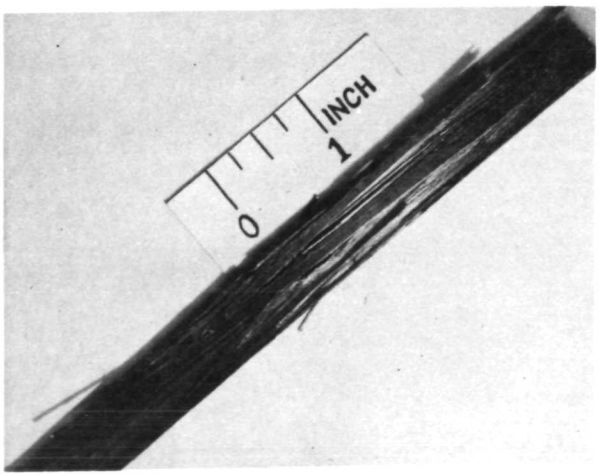

AFTER TEST

Figure 31. Photographs of Specimen HTUR-4 Showing Longitudinal Splitting Prior to Failure

The total accumulation of these failures range from about a half dozen to about 30, depending on the amplifier attenuation level being used and the propensity of the specimen to splitting. For specimens which fail primarily by cleavage, for example, fewer of these events are noted. However, near the point of final failure these large scale events occur with greater frequency. Based on such observations, the following failure process has been constructed for tensile fracture in a uniaxial carbon epoxy composite. Starting at about 50% of the failure load, fibers begin to fail and the rate increases with increasing load. Near groups of failed fibers, the matrix transmits the load between groups of fibers by shear. At intervals, the matrix shear stress is large enough to cause a local matrix crack, which can then propagate longitudinally some distance along the specimen length. This process continues until the longitudinal cracks link up by transverse cracks, and the specimen fails. The amount of such splitting is a strong function of the interfacial bond strength, as discussed in Section 3.1. After failure, the post-fracture shock wave can cause extensive fragmentation if sufficient energy is available and longitudinal splits are present prior to fracture.

3.3 EFFECT OF FIBER CONTENT ON FRACTURE MECHANISMS

In the previous section it was pointed out that significant differences in fiber volume fractions were observed in composite specimens prepared early in the program compared to those prepared later. Since these wide variations in fiber content resulted in a variety of gross fracture modes it was decided that a series of experiments over a range of volume fractions would be most useful in establishing the effect of this critical parameter. At the same time a cleavage dominated system was to be compared to an interface fracture limited system by using the original batch of HT fibers in the unmodified resin. These two systems represent extreme cases of a cleavage limited and an interface limited system, respectively. The goal was to compare fracture modes between small groups of specimens, each group having a controlled fiber content which was uniform within the group and each specimen having the fibers uniformly dispersed. The fabrication techniques used and the degree of uniformity realized have been presented earlier in Section 2.5.2.

Only untreated HT fibers were used in this phase of the study since the inclusion of an additional fiber type or surface condition would result in a prohibitive number of tests. The gross fracture modes were the primary concern in this series of tests but mechanical properties are included in the discussion. Once again it should be noted that a great deal more test data would be necessary to assure the statistical validity of the strength data for design purposes. Our approach was to correlate the limited strength data with specific differences in fracture processes. This approach greatly reduced the constraints on the number of specimens needed to establish reproducible results.

Fiber volume fractions were determined by three independent methods during the early phase of this program and variations of only a few percent were obtained between the three. These were: weight measures of the constituents, area sampling from micrographs of the composite cross-section and rule of mixtures computations from measured moduli of the specimens. The latter method was used in this part of the study and checked against weight measures of the constituents with extremely good agreement.

3.3.1 HT Fibers in the Unmodified Resin Formulation

The first series of tests were performed using the unmodified resin containing fiber volume fractions from approximately 0.30 to 0.60. These specimens were then grouped as shown in Table X so that fracture modes could be examined collectively for specimens having the same fiber content and compared to those of groups having different fiber contents. Note that the average strength for each group increases monotonically with fiber content.

TABLE X. TENSILE STRENGTH GROUPED BY FIBER CONTENT FOR UNTREATED HT FIBERS IN UNMODIFIED EPOXY-NOVOLAC RESIN

Specimen Number	Tensile Strength Ksi	Tensile Modulus $x10^3$ KSI	V_f	
HTUR-D21	74.6	12.8	0.34	
A19	74.0	12.2	0.33	GROUP I
B20	70.6	12.0	0.32	
B3	70.5	10.9	0.29	
D8	66.0	11.3	0.30	
A4	64.6	12.3	0.33	
AVG.	70.1	11.9	0.315	
HTUR-A29	133.0	17.0	0.45	
D11	107.0	16.3	0.43	
B17	106.0	15.0	0.40	GROUP II
D28	106.0	15.5	0.41	
C27	75.1	17.1	0.45	
AVG.	105.4	16.2	0.430	
HTUR-A37	136.0	17.7	0.47	
B26	127.0	17.9	0.48	
C31	122.0	18.9	0.50	GROUP III
B10	116.0	18.2	0.48	
A41	90.0	17.3	0.46	
AVG.	118.1	18.0	0.480	
HTUR-D48	159.0	20.8	0.55	
B38	140.0	19.0	0.51	
B46	123.0	20.6	0.55	GROUP IV
C39	113.0	19.2	0.51	
C35	92.0	20.8	0.55	
AVG.	125.3	20.0	0.53	
HTUR-B33	158.0	26.4	0.63	
D40	131.0	22.0	0.59	
B23	101.0	21.5	0.57	GROUP V
AVG.	142.0	23.2	0.596	

The specimens are listed in order of decreasing strength in each group to facilitate comparison. Note also that the incremental change in fiber content between the first two and between the last two groups are greater than those of the middle three groups.

Figure 32 shows typical fracture modes for both extremes and the middle group representing fiber volume fractions of approximately 0.3, 0.45 and 0.6. Note that in the upper photo (V_f = 0.32) all three specimens have distinct cleavage sites normal to the specimen axis with minimal fracture surface parallel to the fibers. The shorter specimen was the result of a tab failure requiring retabbing and therefore reduced gage length. This tendency to fail by gross cleavage was typical of the lower volume fraction specimens and occurred sometimes in weaker specimens at high volume fractions.

The center photo represents the specimens having a fiber volume fraction of about 0.45 and illustrates some interesting behavior. Note that the upper specimen (HTUR-37) in this photo failed at three locations along the specimen length with a good deal of fracture surface parallel to the fibers. The second specimen in the center photo (HTUR-10) failed at two cleavage locations with similar patterns. Finally, the bottom specimen (HTUR-41) in the center photo failed at a single location by cleavage and showed no fracture parallel to the fibers. This specimen was also the weakest in group III having a strength nearer to that of group I where a single cleavage mode was common. It appears that higher volume fraction of fibers tend to change the fracture mode from cleavage at a single location to a more tortuous process involving several sites over the specimen length except when there is an inherent flaw in the specimen which cancels out the effect of additional fiber content.

The bottom photo in Figure 32 shows the same pattern with the higher strength specimen (HTUR-33) exhibiting extensive interface oriented cracks connecting three distinct cleavage sites. The weaker specimen (HTUR-40) in the group shows the single cleavage mode again which was typical of the weaker specimen in all five groups tested. Note that there was no fiber pull-out or splintering evident in this series of tests with all fracture surfaces clearly defined in the photographs and no splintering.

3.3.2 HT Fibers in the Modified Epoxy-Novolac Resin Formulation

A similar series of tests was performed in the modified resin system with the data falling into three groups having very nearly the same fiber content. These three groups are defined as VI, VII and VIII in Table XI. Again the strength data increases monotonically with fiber content and the data have been arranged in order of declining strength within each group. Note that

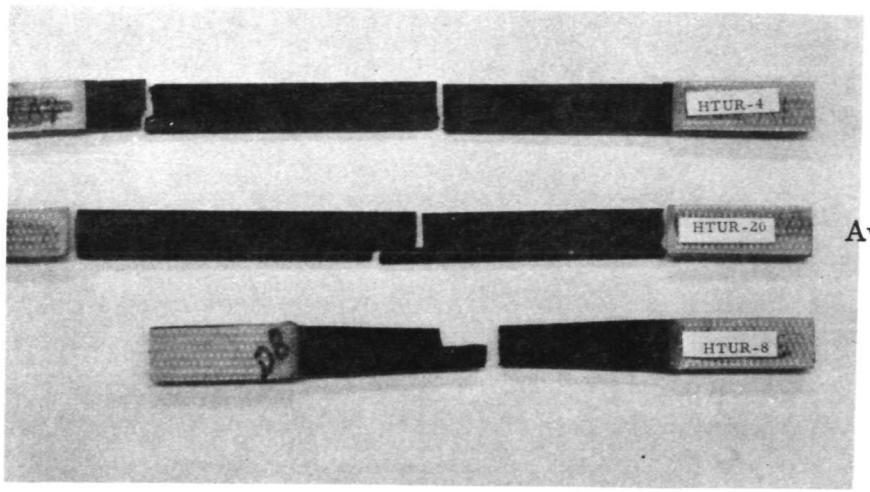

Average $V_f = 0.32$

GROUP I

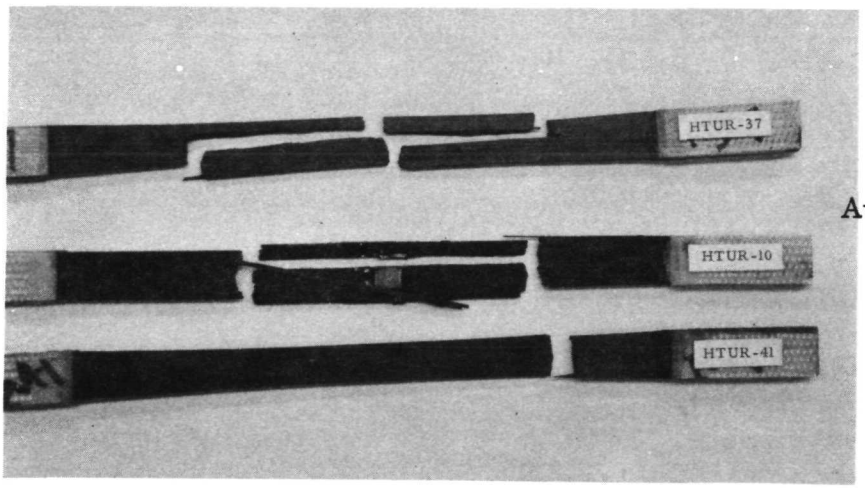

Average $V_f = 0.48$

GROUP III

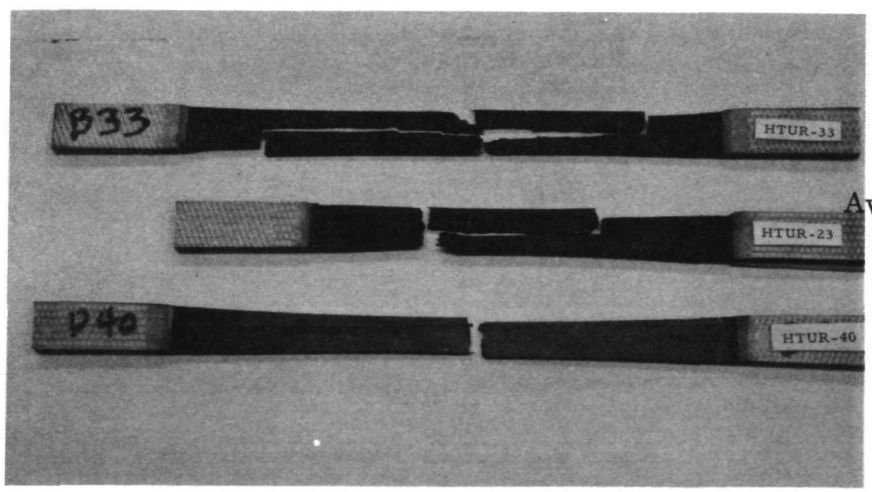

Average $V_f = 0.60$

GROUP V

Figure 32. Fracture Modes for Various Fiber Contents Untreated HT Fibers in Unmodified Epoxy-Novolac Resin

TABLE XI. TENSILE STRENGTH GROUPED BY FIBER CONTENT FOR UNTREATED HT FIBERS IN MODIFIED EPOXY-NOVOLAC RESIN

Specimen Number	Tensile Strength, KSI	Tensile Modulus $X10^3$ KSI	V_f	
HTUF-39C	107.0	10.2	0.26	
37A	107.0	11.8	0.30	
37B	106.0	10.4	0.26	GROUP VI
37D	90.0	12.0	0.30	
39A	87.0	10.6	0.27	
37C	82.0	9.7	0.25	
AVG.	96.6	10.8	0.27	
HTUF-36A	177.0	18.2	0.46	
36D	175.0	19.2	0.49	
18A	173.6	19.4	0.50	GROUP VII
24C	168.4	19.6	0.50	
24D	167.2	18.5	0.47	
36B	164.0	17.3	0.44	
24B	153.1	20.0	0.51	
AVG.	168.3	18.9	0.48	
HTUF-18B	195.3	21.6	0.55	
18C	184.0	21.1	0.54	
18D	179.5	22.5	0.57	GROUP VIII
36C	165.0	23.5	0.59	
AVG.	181.0	22.2	0.56	

there is a good deal of overlap between Groups VII and VIII because of the smaller increment in fiber content between these two groups compared to the increment between Groups VI and VII.

Figure 33 illustrates typical fracture modes for each group. The upper photo represents the lowest fiber content with some very localized transverse fracture sites evident but not nearly so well defined as in the unmodified resin. There is a considerable amount of interface failure with fiber pullout in evidence on each specimen and the more localized fracture is associated with the weaker specimens once again.

The center photo of Figure 33 represents an average fiber volume fraction of 0.48 with significantly improved average strength over the lower fiber content specimens shown in the upper photo. Although there is evidence of interrupted cleavage at numerous sites along the specimen the dominant fracture mode is parallel to the fibers with a splintered appearance at final failure. It is interesting that few of these specimens separate into two pieces even though their load carrying capacity has been exhausted.

The lower photo in this illustration represents the typical fracture modes for an average fiber content of 0.56 and shows dramatic evidence of interface fracture with long splinter type fragments separated along the entire specimen length. The average strength of this group of specimens was about double that of the group shown in the uppermost photograph.

An overall comparison of the data presented in Tables X and XI is given in Figure 34 where the solid triangles represent the unmodified resin formulation and the open triangles represent the modified resin. Note the greater degree of scatter inherent in the unmodified system at higher fiber contents. The modified resin, on the other hand, shows considerably less scatter and gives consistently higher composite strengths than the unmodified system. It is clear that the combination of a less crack sensitive (modified) resin encapsulating fibers which debond at fracture is superior in tension to the opposite combination. Since the strengths of the two batches of fibers have been measured during this program (see Section 2.2.1) the difference must be attributed to differences in matrix and interface response to fiber fracture.

Finally, it should be noted that in order to control the fiber content it was necessary to impregnate bundles of fibers separately rather than use commercial prepreg materials. In doing this we sacrifice some control of fiber alignment and spacing and this results in somewhat lower strength for the same fiber content. However, this same approach was used for both fiber/resin combinations described here so that it cannot be the source of the observed differences in behavior.

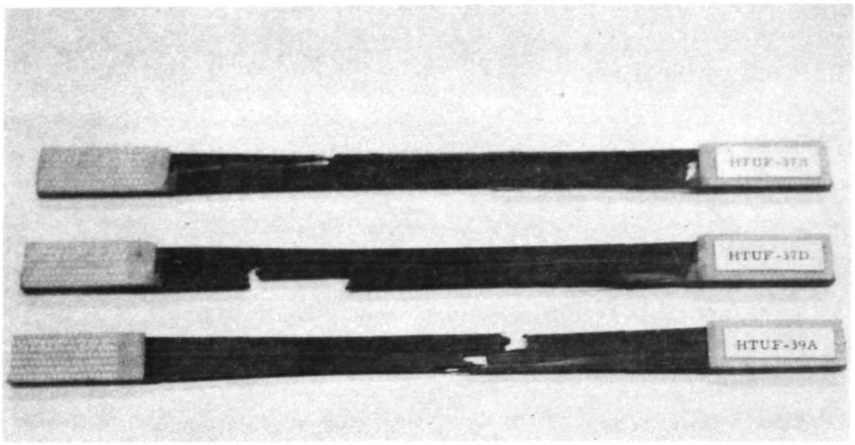

Average $V_f = 0.27$

GROUP VI

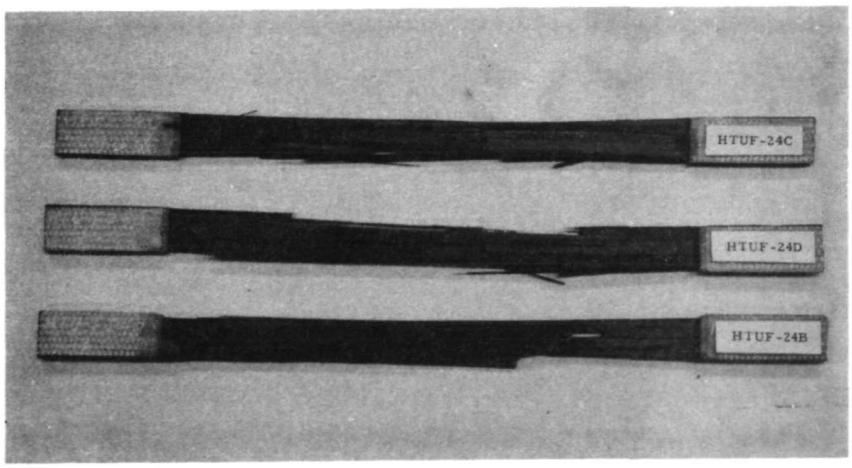

Average $V_f = 0.48$

GROUP VII

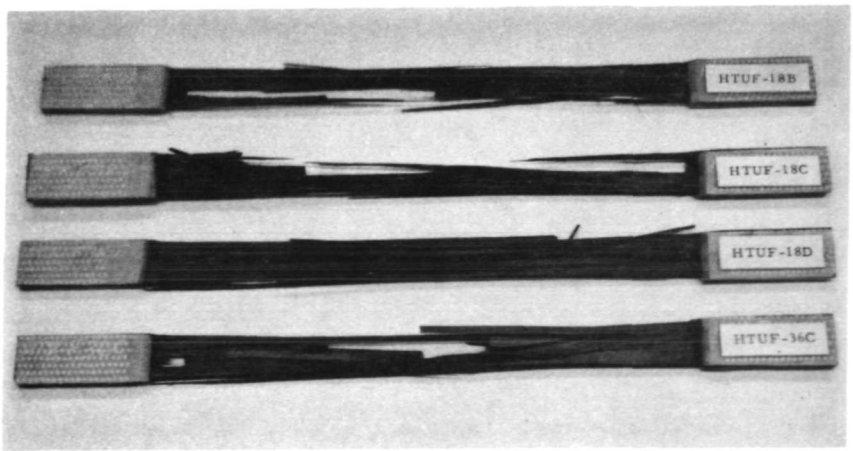

Average $V_f = 0.56$

GROUP VIII

Figure 33. Fracture Modes for Various Fiber Contents Untreated HT Fibers in Modified Epoxy-Novolac Resin

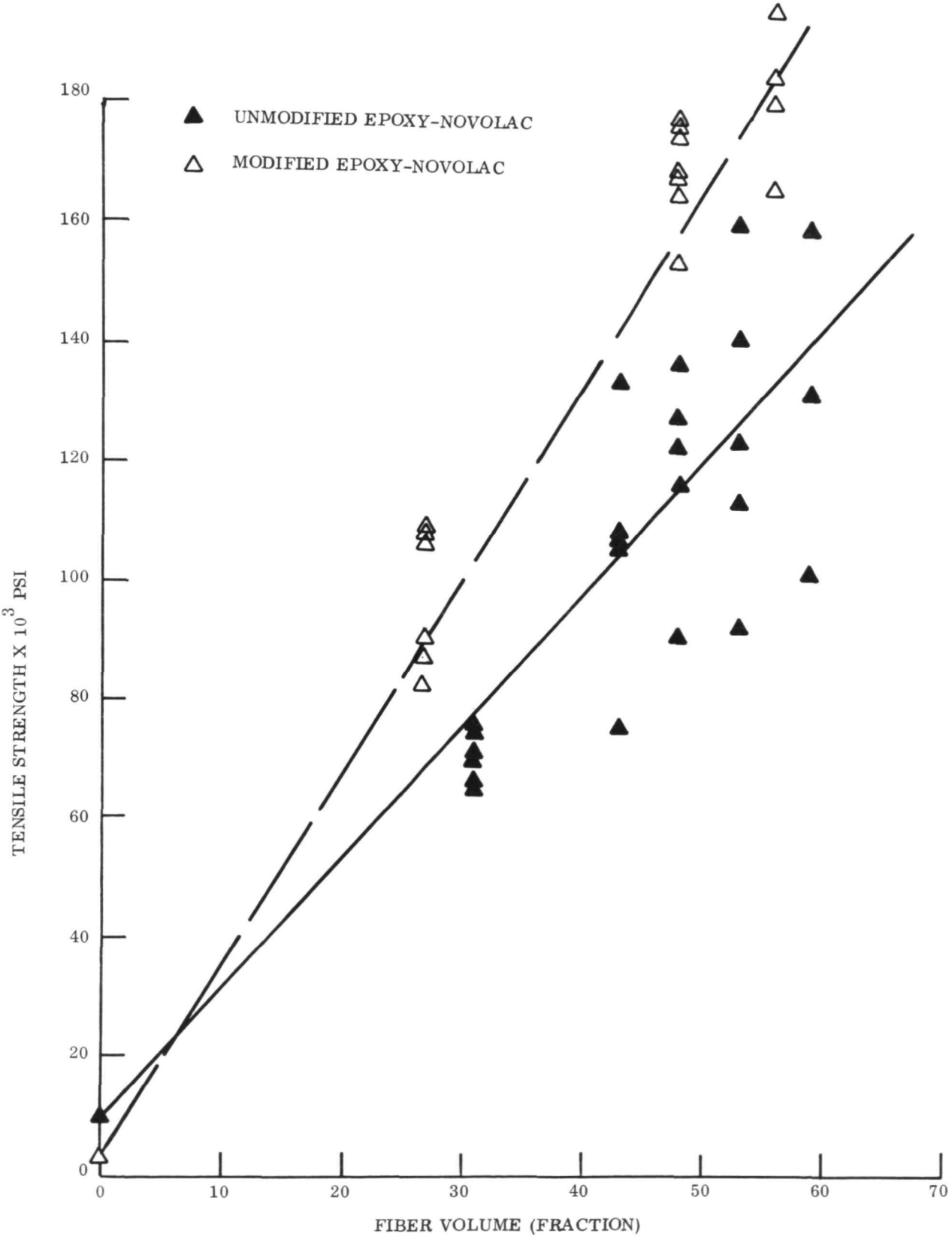

Figure 34. Tensile Strength Data Comparison for Untreated HT Carbon Fibers in Both Epoxy-Novolac Resins

3.3.3 Acoustic Emission Analysis

In addition to studying the effect of volume fraction on strength and elastic modulus, some effort was devoted to determining its influence on acoustic emission. To do this, five specimens with fiber contents of 0.2 to 0.4 untreated HT fibers in an unmodified matrix were prepared and tested in the manner described in Section 3.2.1. The results are given in Table XII and Figure 35.

Unfortunately, most of the specimens failed in the grip section, primarily near the lower pin hole used for preloading the specimen. For this reason, a comparison of 0.45% strain is more accurate than at the failure load, where grip noise may contribute to the total emissions. When this comparison is made (Figure 35), it may be seen that the counts increase in a linear manner with increasing volume fraction. This suggests that the acoustic events are associated with fiber and interface failure rather than slow growth of matrix cracks in lightly reinforced composites. This is a significant point in the use of acoustic emission for quality control of composite fabrication and should be explored in further detail.

3.4 COMPOSITE/METAL SPECIMEN EVALUATION

Because of the increased interest in composites bonded to metal for structural members a series of tests was performed to determine the critical events in the failure process for such specimens. Two geometries were explored: flat specimens in which the carbon/epoxy composite was sandwiched between two metal strips and a concentric tubular specimen where the composite was bonded on the outside of the metal tube. These two configurations were chosen because the first is amenable to most tensile applications while the second is more efficient in axial compression from tests performed at NASA-Langley on boron/epoxy bonded to aluminum. Details on the fabrication of both types of specimens were covered in Section 2.5.3. The following sections will describe the nature of the tests performed and observations made during the failure process.

3.4.1 Flat Specimen Test Data and Failure Modes

Four flat specimens were selected for mechanical test after determining that the composite was uniformly bonded to the metal strips over their entire length. Only the unmodified resin formulation was used with both HT and Type A fibers.

TABLE XII: TOTAL ACOUSTIC COUNTS FOR VARIOUS CONTENTS HT FIBERS IN UNMODIFIED EPOXY-NOVOLAC RESIN

Specimen	Volume Fraction	Ultimate Stress, psi	Counts at Failure		Counts at .45% Strain	
			Total	Normalized (2)	Total	Normalized (2)
HTUR-D5 (1)	0.20	49,700	$1.2X10^4$	$.874x10^4$	$1.2x10^4$	$.874x10^4$
HTUR-C24	0.30	71,000	$2.0x10^4$	$1.42x10^4$	$.9x10^4$	$.64x10^4$
HTUR-A22 (1)	0.30	91,500	$1.8x10^5$	$1.3x10^5$	3×10^4	$2.2x10^4$
HTUR-A34 (1)	0.35	66,700	8×10^4	$5.6x10^4$	7×10^4	$4.9x10^4$
HTUR-B30 (1)	0.40	87,000	8×10^4	6×10^4	8×10^4	$6 X 10^4$

(1) Grip Failure

(2) Normalized on $A = 12 \times 10^{-3}$ in ^{2}

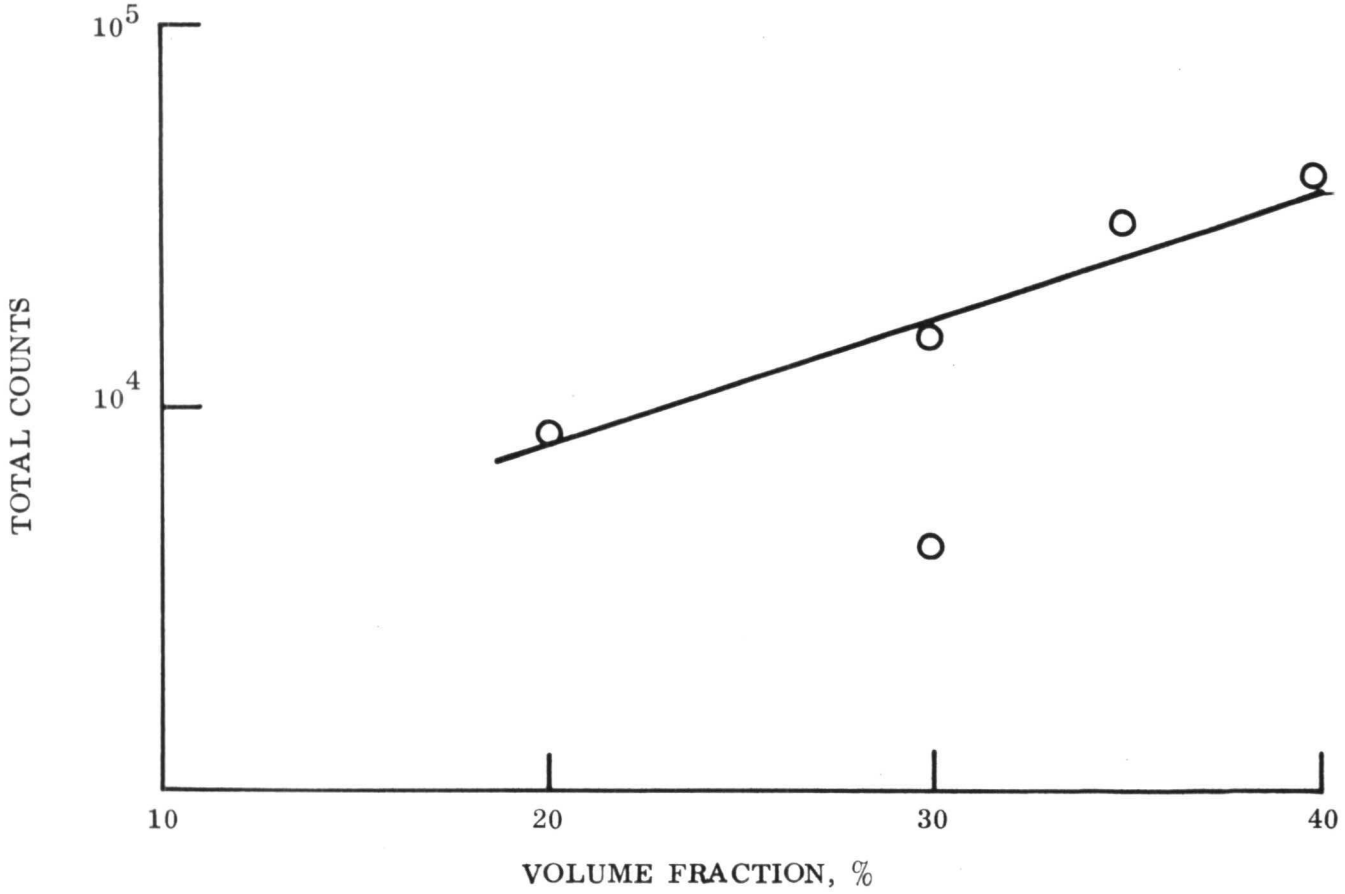

FIGURE 35: TOTAL ACOUSTIC EMISSION AT 0.45% STRAIN VS. VOLUME FRACTION FOR HTU FIBERS IN AN UNMODIFIED EPOXY-NOVOLAC RESIN. DATA HAS BEEN NORMALIZED ON A = 12×10^{-3} in^2.

Tensile tests were performed with an Instron machine. A wide range extensometer was used to obtain an accurate measure of strain throughout the entire test. The extensometer output and corresponding specimen load were fed into an x y recorder and this record constituted the primary data to be correlated with gross failure modes. Since the stress is dependent on area and modulus of the composite and metal, it varies for both materials throughout the test. Average specimen stress is therefore meaningless in this analysis so specimen load is plotted against strain in Figure 36. This figure compares typical data obtained for the HT fiber composites (HRM) and the Type A fiber composites (ARM). In each case there are two distinct linear ranges which precede the ultimate load point and a third linear response after the ultimate load is reached. The lower curve is the load-strain diagram for the aluminum face sheets as derived from the stress-strain curve given in Section 2.4 using the actual dimensions of the fact sheets. Note that at each point of inflection in the diagram the stress in the aluminum and the composite are noted. During the first phase of loading both the aluminum and the composite are straining together with each carrying load proportional to its modulus and cross-sectional area. The aluminum begins to yield when its stress is between 28 and 49.5 ksi and as it yields its modulus gradually reduces from 10.3×10^6 psi to 0.48×10^6 psi. This means the composite now controls the stiffness of the specimen and gradual separation of the aluminum/metal interface can be observed. This second linear region has a somewhat lower slope because of the gradual loss of stiffness of the aluminum as it yields even though the metal still supports load at its yield stress.

Finally, the composite fails with the metal sheets still intact and the load drops off suddenly in the region of 7000 microinches per inch of strain. Because there is a good deal of elastic recovery when the composite fails, the stress in the metal after recovery can be below its 0.2 percent yield point and thus its modulus is again 10.3×10^6 psi since it is again behaving elastically. The metal will therefore continue to support additional load until it again yields and its modulus decreases to that of strain hardening (0.48×10^6 psi). Dimensional instability is soon reached and the metal fails bringing an end to the test. In Figure 36 the HRM specimen exhibits a somewhat steeper slope than the ARM specimen in the first two phases of loading. This is due primarily to a difference in gross area of the two specimens since the composite modulus in each case was about the same. Table XIII gives the significant data for the two specimens represented in Figure 36 with the knee being defined as the point of transition between the first and second linear region. The general behavior of the two specimens was the same except that the knee was more sharply defined in the ARM specimen than for the HT fiber reinforced HRM specimen. The load point corresponding to the knee was also lower in the HRM specimen beginning at an

TABLE XIII: PROPERTIES OF FLAT COMPOSITE/METAL SPECIMENS

PROPERTY	HRM	ARM
Area of aluminum	0.01145 in^2	0.0113 in^2
Area of composite	0.0118 in^2	0.0094 in^2
Modulus of aluminum elastic plastic	 10.3×10^3 Ksi 0.48×10^3 Ksi	 10.3×10^3 Ksi 0.48×10^3 Ksi
Modulus of composite	15.2×10^3 Ksi	15.6×10^3 Ksi
Ultimate load	1880 lbs.	1540 lbs.
Load at knee	840 lbs.	1090 lbs.

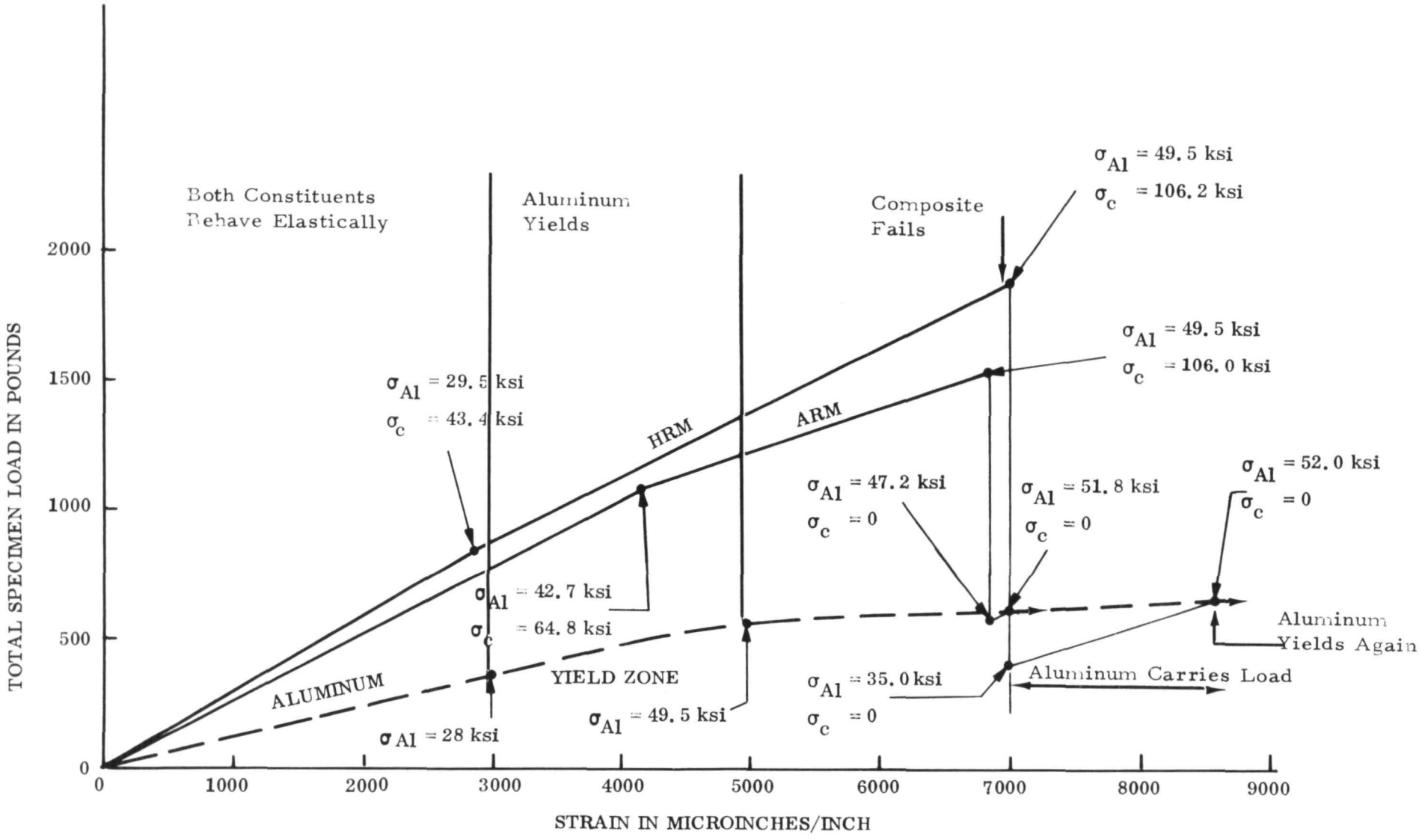

Figure 36. Typical Load-Strain Diagram for Tensile Test of Composite/Metal Sandwich Specimens

aluminum stress of 29.5 ksi while the ARM specimen didn't reach tranition until the aluminum stress was at 42.7 ksi. This difference could be more related to the bond between the metal and the composite than to the behavior of the materials themselves with the knee becoming evident once separation has occurred.

It is interesting to note that the fracture modes for the composites are generally unaffected by bonding to the metal. Figure 37 shows photographs of both specimens. Note the very definite cleavage and separation of the HT fiber composite in the upper photo. The lower photo shows the more jagged fracture pattern which was evident in the Type A fiber specimens with the crack decorated in white for contrast. Note the amount of metal deformation after composite failure in the upper photo as evidenced by the separation of the composite fracture surfaces. This points up rather vividly that the metal has a good deal of deformation and load carrying capacity left after the composite has failed. Whatever the fracture mode for the composite, it is clear that the use of a composite in combination with a metal offers some interesting design advantages. When the application is deformation limited so that relaxation allows the metal to support the load after the composite has failed. Such a system can minimize the effects of a local failure by allowing the failure of the composite without complete loss of load carrying capacity of the structural member.

3.4.2 Tubular Specimen Test Data and Failure Modes

3.4.2.1 Unmodified Epoxy-Novolac Resin Formulation

Several tubular specimens were prepared in the manner described in Section 2.5.3 with the intention of performing compression tests on them. Prior to performing the tests, the specimen ends were cut-off in order to remove the aluminum end and obtain a uniform portion of tube to test. It was noted that when the first specimen was cut, loud cracking sounds emanated from it. Some longitudinal cracks were present before cutting, and the severity of these cracks gradually increased with time after the ends were cut. In some cases the cracks extended all the way through the composite so that the aluminum tube was exposed. The upper tube in Figure 38 shows a typical crack of this type.

More quantitative data was obtained for the second specimen. After one end was cut-off, an accelerometer was quickly bonded to the free end, and then the other end cut. The acoustic emissions were then recorded. About 30 seconds elapsed between cutting the first end and then the data recording started. The test record for the first 10 minutes is shown in Figure 39. Emission continued at a gradually reducing rate for about 30 minutes.

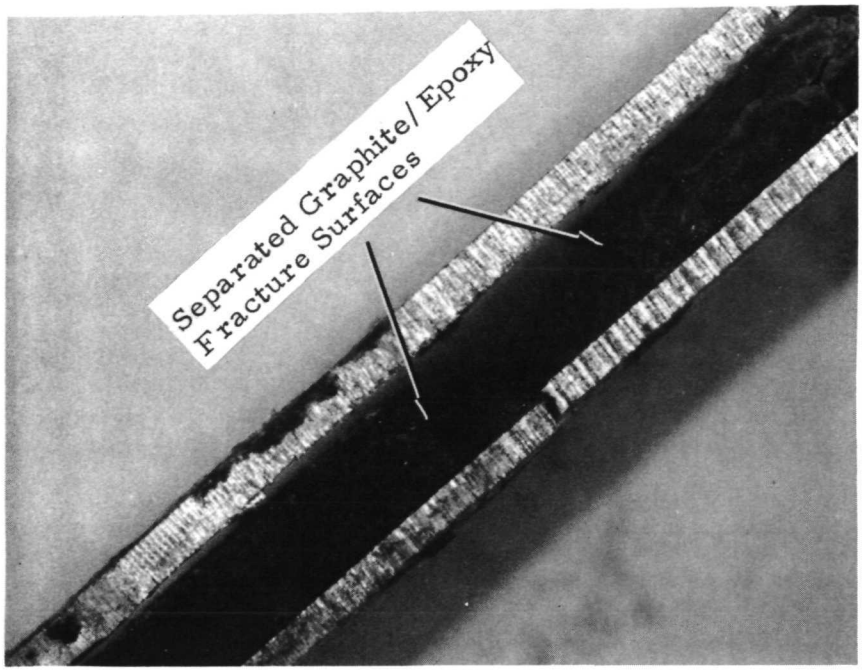

HT Fibers in Epoxy Bonded to Aluminum 7.5X

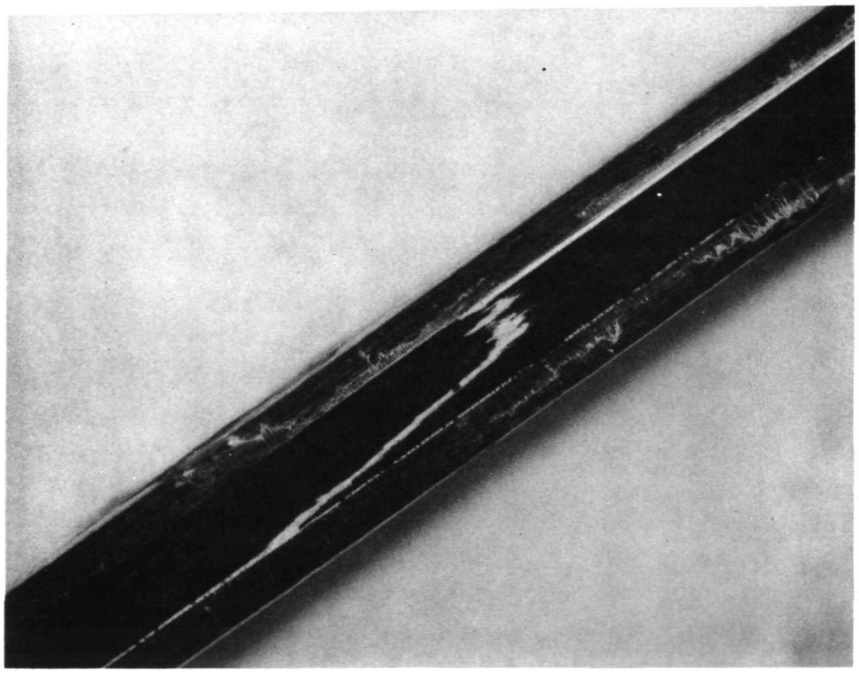

Type A Fibers in Epoxy Bonded to Aluminum 7.5X

Figure 37: Typical Fracture Modes for Composite/Metal Sandwich Specimens (Edge View)

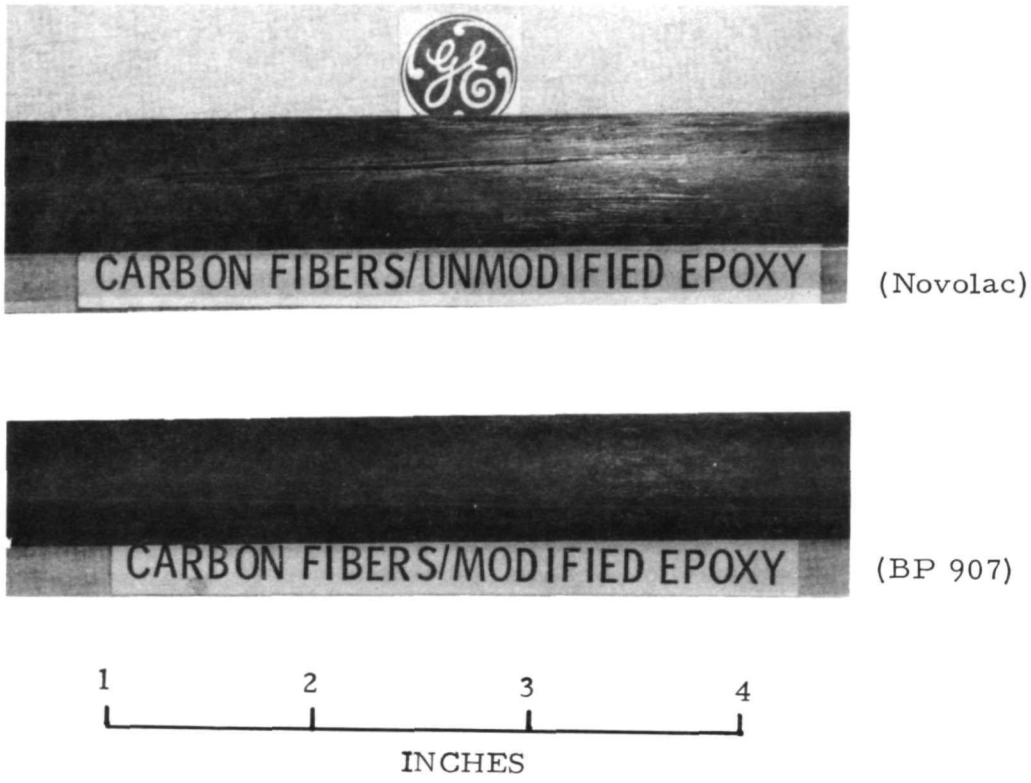

Figure 38. Photograph of Composite Tubes in As-Fabricated Condition and Before Cutting Off Ends

FIGURE 39: ACOUSTIC EMISSIONS FROM A METAL/COMPOSITE TUBE AFTER CURING AND AND CUTTING OFF THE ENDS (TIME = 0 MIN). THE RESIN WAS AN UNMODIFIED EPOXY NOVOLAC.

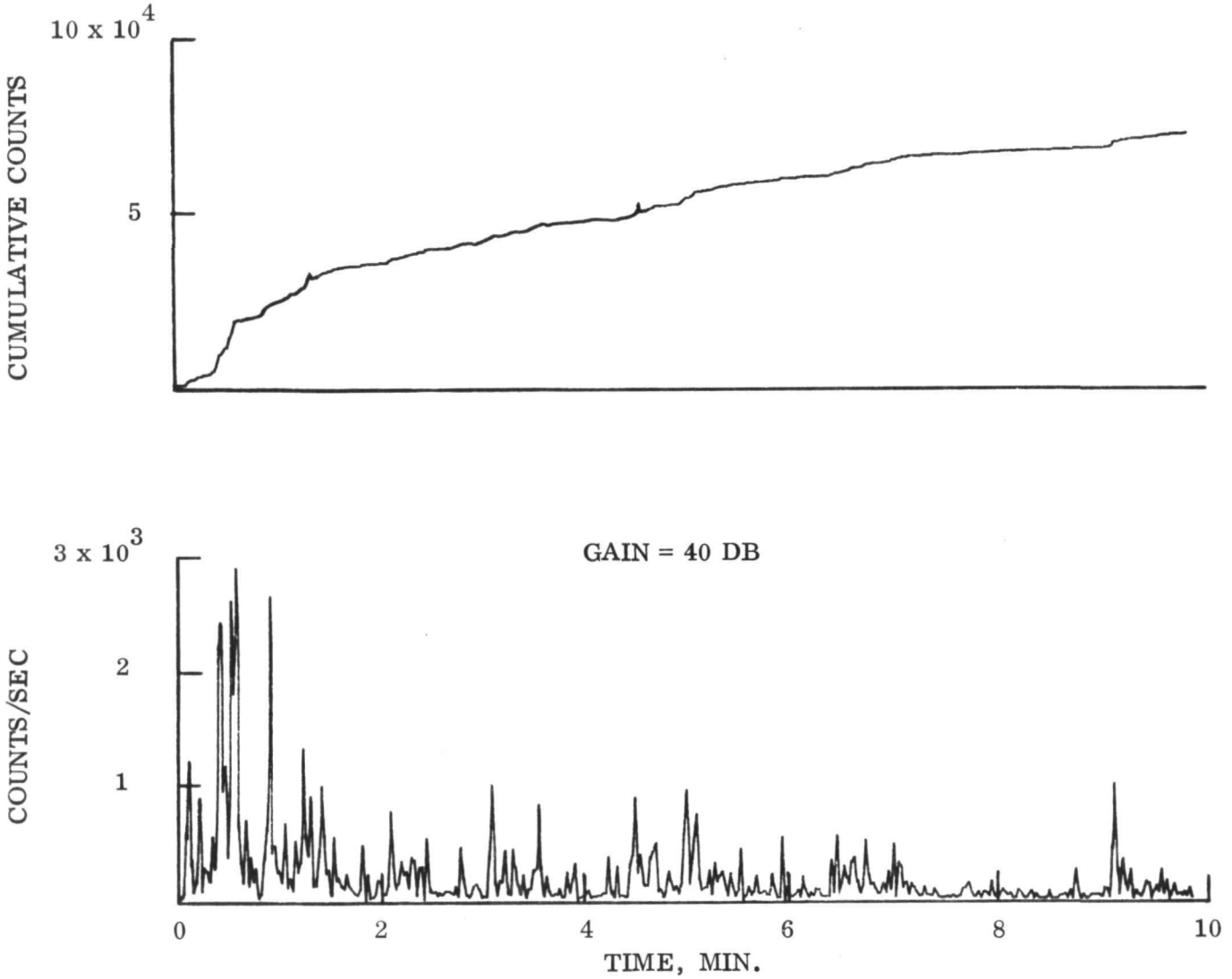

The source of this longitudinal splitting is believed to be the relief of residual stresses caused by cooling down the composite tube from the fabrication temperature, and the magnitude of these stresses can be calculated from standard cylindrical shrink-fit equation. In the following, ΔT is the temperature difference between the curing temperature and room temperature, α is the coefficient of thermal expansion. E the elastic modulus, and ν, Poisson's ratio. Subscripts c and a refer to the composite and aluminum, respectively. The tube dimensions are given by a, b, and c, where a is the aluminum inner radius, b the aluminum outer radius (or composite inner radius), and c the composite outer radius. Using the above nomenclature, the following numerical values may be assigned:

$\Delta T = 125^{\circ}C$

$\alpha_c = 60 \times 10^{-6}/^{\circ}C$ [17]

$\alpha_a = 23 \times 10^{-6}/^{\circ}C$

$E_c = 1.54 \times 10^{-6}$ psi (transverse direction) [18]

$E_a = 10 \times 10^{3}$ Ksi

$\nu_c = 0.25$

$\nu_a = 0.30$

$a = 0.216$ in.

$b = 0.250$ in.

$c = 0.254$ in

When the composite tube cools from $150^{\circ}C$ to room temperature, a radial interference will be present due to the expansion differences. This value is

$$\delta = (\alpha_c - \alpha_a)\, b\, \Delta T$$

$$= 37 \times 10^{-6} \times 0.25 \times 125$$

$$= 1.16 \times 10^{-3} \text{ in}$$

The pressure p produced at the interface because of this mismatch is given by [19]

$$\frac{bp}{E_c}\left[\frac{b^2 + c^2}{c^2 - b^2} + \nu_c\right] + \frac{bp}{E_a}\left[\frac{a^2 + b^2}{b^2 - a^2} - \nu_a\right] = \delta$$

Inserting numerical values, we find

$$p = 955 \text{ psi}$$

At the inner surface of the carbon epoxy sleeve, a tensile stress will be generated equal to [3]

$$\sigma_t = p\left[\frac{b^2 + c^2}{c^2 - b^2}\right]$$

and using the value of p = 955 psi, we have

$$\sigma_t = 5920 \text{ psi}$$

This is a significant stress, and could well lead to cracking in an unmodified system especially when ends of fibers are exposed by cutting the specimen. It is interesting to note that in the axial direction a compressive stress is developed. Assuming that no slip occurs at the interface (not a particularly good assumption) and using $E_c = 20 \times 10^6$ psi and $\alpha_c = 0$ [17] we have

$$\frac{P_c L}{E_c A_c} = \alpha_a \Delta T L + \frac{P_a L}{E_a A_a}$$

where $P_c = P_a$ is the load in the carbon epoxy and aluminum, respectively, and L is the composite tube length (8"). The axial compressive stress can then be computed to be

$$\sigma_c = 59,400 \text{ psi}$$

The actual value will be less than this due to shear deformation or slip at

the interface.

For the unmodified system, then, significant residual stresses are developed due to cool-down strains, and the resin is not sufficiently viscoelastic to relieve the stress. The stresses are of sufficient magnitude to cause some failure in the transverse direction, which is manifested as longitudinal splitting. When the tube is cut, exposing a fresh surface, profuse longitudinal crack propagation occurs, as shown by the acoustic record in Figure 39. Because of this loss of integrity at the outset, no actual compression tests were attempted for this resin formulation.

3.4.2.2 Modified Resin Formulation

Although the same thermal expansion differences exist for this composite system, the modified resin (BP907) system is apparently sufficiently viscoelastic to relieve much of the thermally induced residual stesss. This can be seen by the lack of any cracks in the lower tube in Figure 38. More importantly, when the tube was cut no acoustic activity was detected.

One tube using the modified resin system was tested in compression. The specimen ends were imbedded into 1 1/2" deep holes drilled in steel blocks, and to maintain axial alignment the specimen was bonded into the blocks in the testing machine under a slight compressive load. Load was applied through a swivel assembly to minimize the effect of any small degrees of misalignment.

The stress-strain curve for this specimen is shown in Figure 40. The ultimate load, based on the total cross-sectional area, was 36,400 psi. The failure was by delamination between the plies, as shown in Figure 41. It would appear that interlaminar strength is very important for such composite tubes used in compression loading. The present results are low compared to the values obtained by Zender and Dexter[20] for aluminum/boron epoxy compression tubes. They obtained crushing strength on short tubes (2.8 inches long) of the order of 200 ksi. This is a fertile area for further study to determine whether the differences are inherent in the fiber properties such as modulus and strength, or in the fiber diameter which is many times greater for the boron filament. The scope of this program would not allow an extensive study of compressive failure mechanisms in addition to the parameters which influence tensile behavior.. It is clear however, that transverse properties are critical to the strength of the composite tube specimens discussed here and that the properties of the matrix and interface can seriously limit the axial compressive strength through poisson effects.

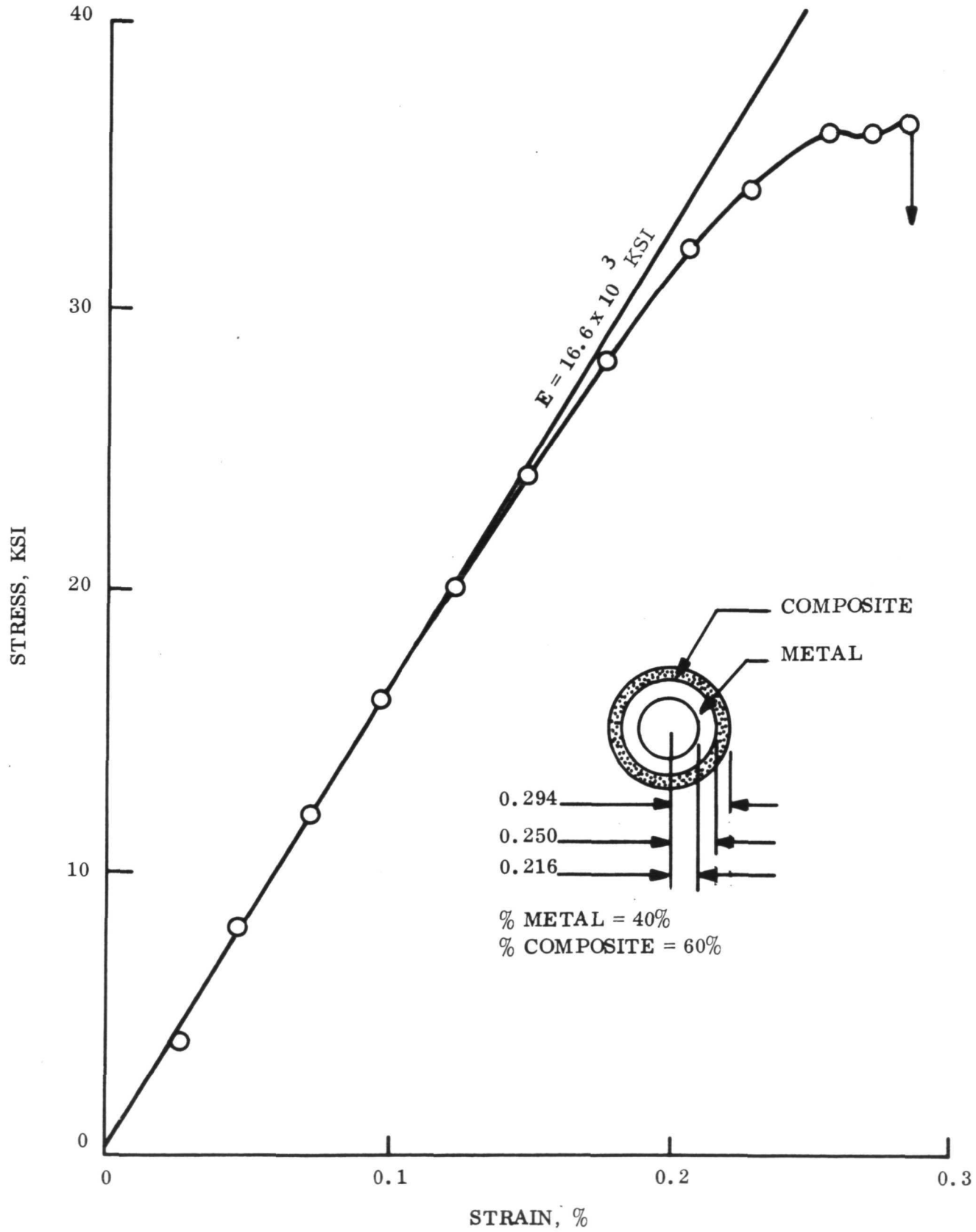

FIGURE 40: COMPRESSIVE STRESS-STRAIN CURVE FOR HTS FIBERS IN BP907 BONDED TO ALUMINUM

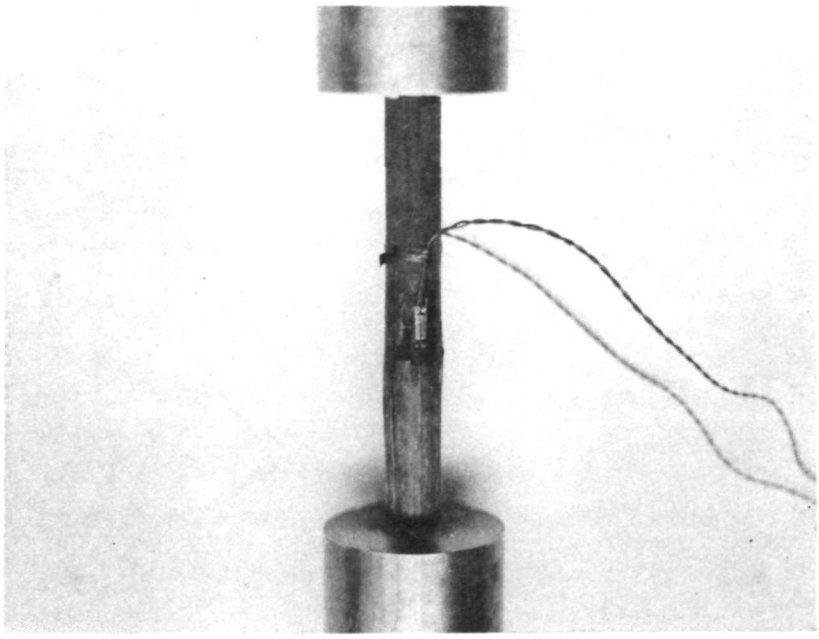

A. Composite Tube After Fracture. Note Longitudinal Splits

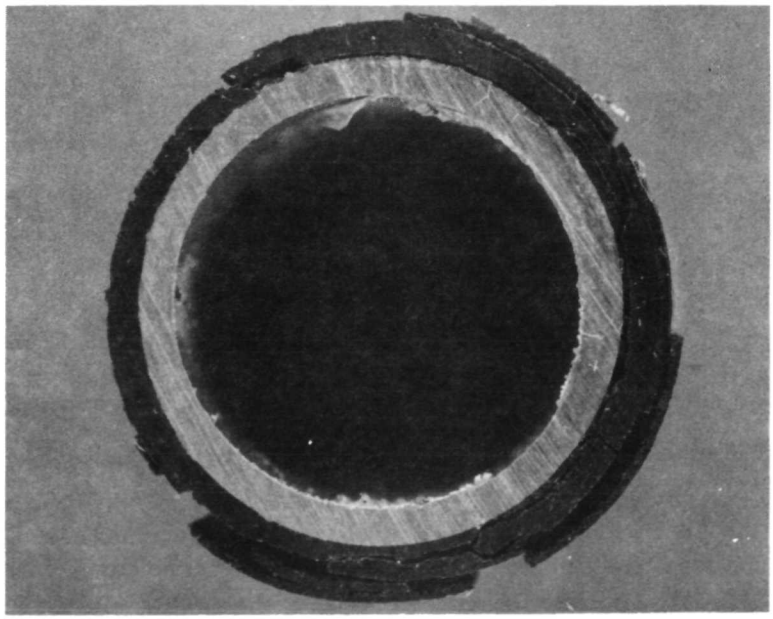

B. Cross Section After Fracture. Note Delaminations. Mag: 5X

Figure 41. Photographs of Composite/Metal Tube After Compression Testing

3.5 COMPRESSION TESTS

In order to conduct a preliminary investigation of the effect of volume fraction on compression strength, five test specimen were prepared in an identical fashion to that employed for the tensile specimens. The test specimen, shown in Figure 42, was first surface ground to 0.062 $\pm$ 0.001 inch. The scotchply end tabs were bonded on and then the specimen was ground to final size. Because of the sensitivity of compression strength to eccentric loads, considerable care was taken to machine the specimens to the tolerances shown in Figure 42.

The jig used to perform the compression tests is shown in Figure 43, and is based on a design obtained from the Celanese Corporation, Summit, New Jersey*. Tests were performed in an Instron machine at a crosshead speed of 0.02 in/min between parallel plattens ($\pm$ 0.002"), with the load on the upper platten being transmitted through a ball joint.

The data is presented in Table XIV and typical stress-strain curves are shown in Figure 44. All the specimens were strain gaged with two 180° opposed gages, and three out of five tests were performed while reading each strain gage separately during the course of the test. In all cases the data were similar to that shown in the upper curve of Figure 44; that is, no discernible bending strains were present up to failure (in Figure 44, one strain gage failed before the failure load was reached).

The shape of the compression stress-strain curve differs from the tension curve in that the response is nonlinear. As can be seen from Figure 44, the non linearity increases with decreasing volume fraction. The exact cause for this behavior is not known, but has been reported in other tests involving compression of carbon-epoxy specimens [21.] Possible reasons include local fiber buckling and/or fiber-resin shear. The cause does seem to be related to the fiber diameter, since published data for the same fiber content of boron-epoxy shows a smaller degree of non-linearity, as well as a substantial region of linearity early in the loading process. [22] For the carbon-epoxy case, the compression curve starts to deviate from linearity at the outset.

---

*

The courtesy of Dr. Sward, Celanese Corporation, for supplying blueprints of the fixture is gratefully acknowledged.

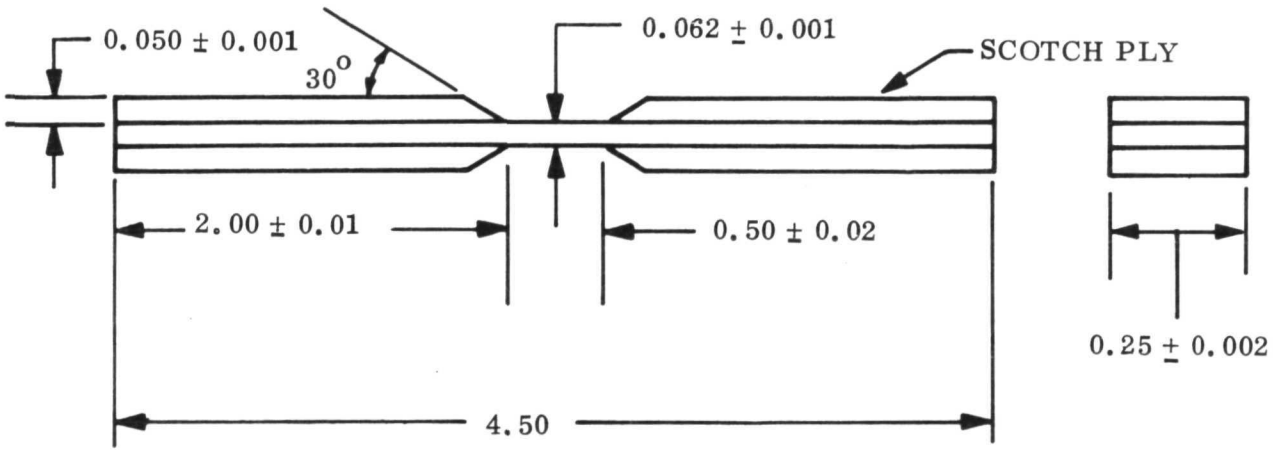

FIGUR E 42. Compression Test Specimen

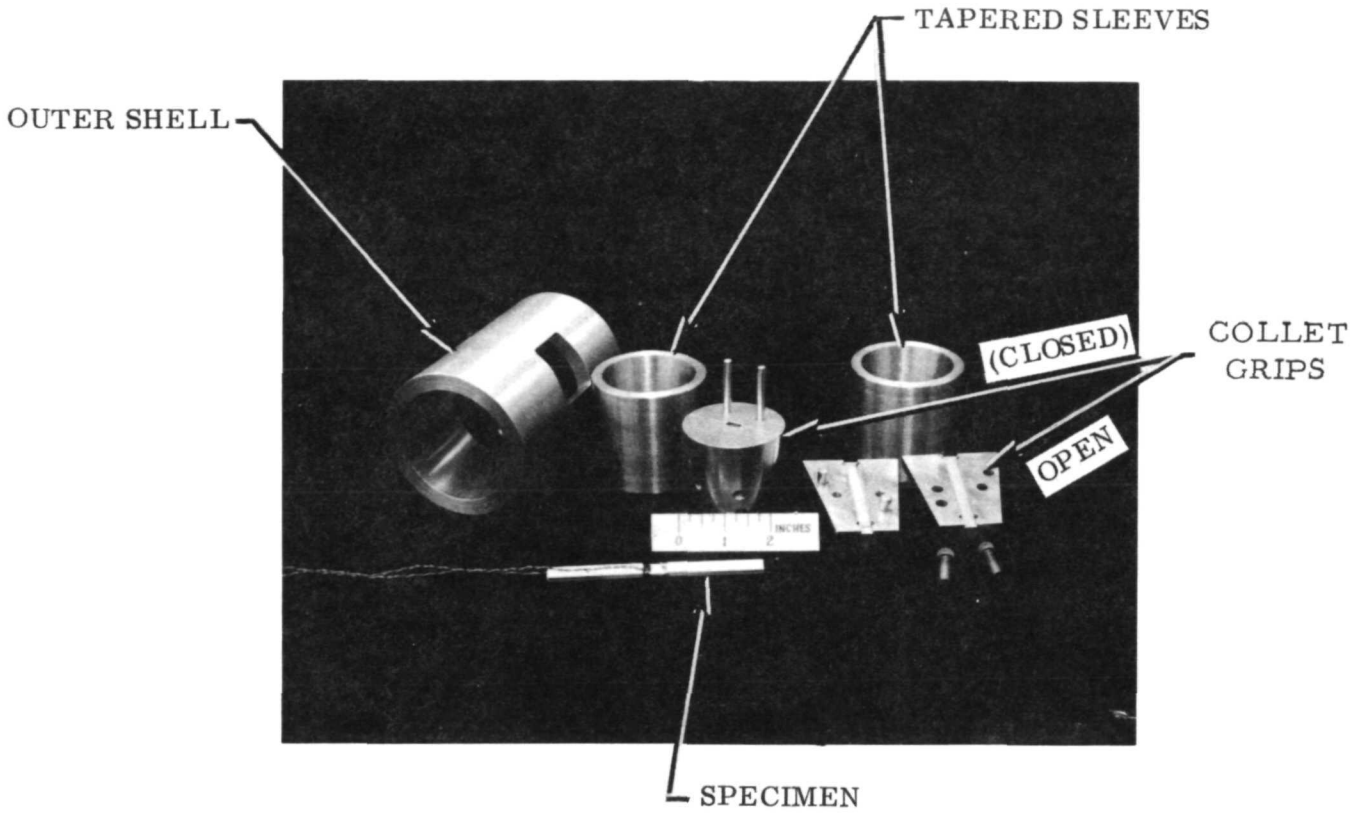

Figure 43. Photograph of Compression Test Fixture

TABLE XIV: COMPRESSIVE PROPERTIES OF HT FIBERS IN BOTH RESIN FORMULATIONS

Resin	Nominal Volume Fraction	Elastic Modulus $\times 10^4$ Ksi	Ultimate Strength Ksi
Unmodified	0.20-0.25	12.9	76
Unmodified	0.30-0.35	12.0	96
Unmodified	0.30-0.35	11.8	107
Unmodified	0.40-0.45	21.4	160
Modified	0.50-0.55	17.3	93

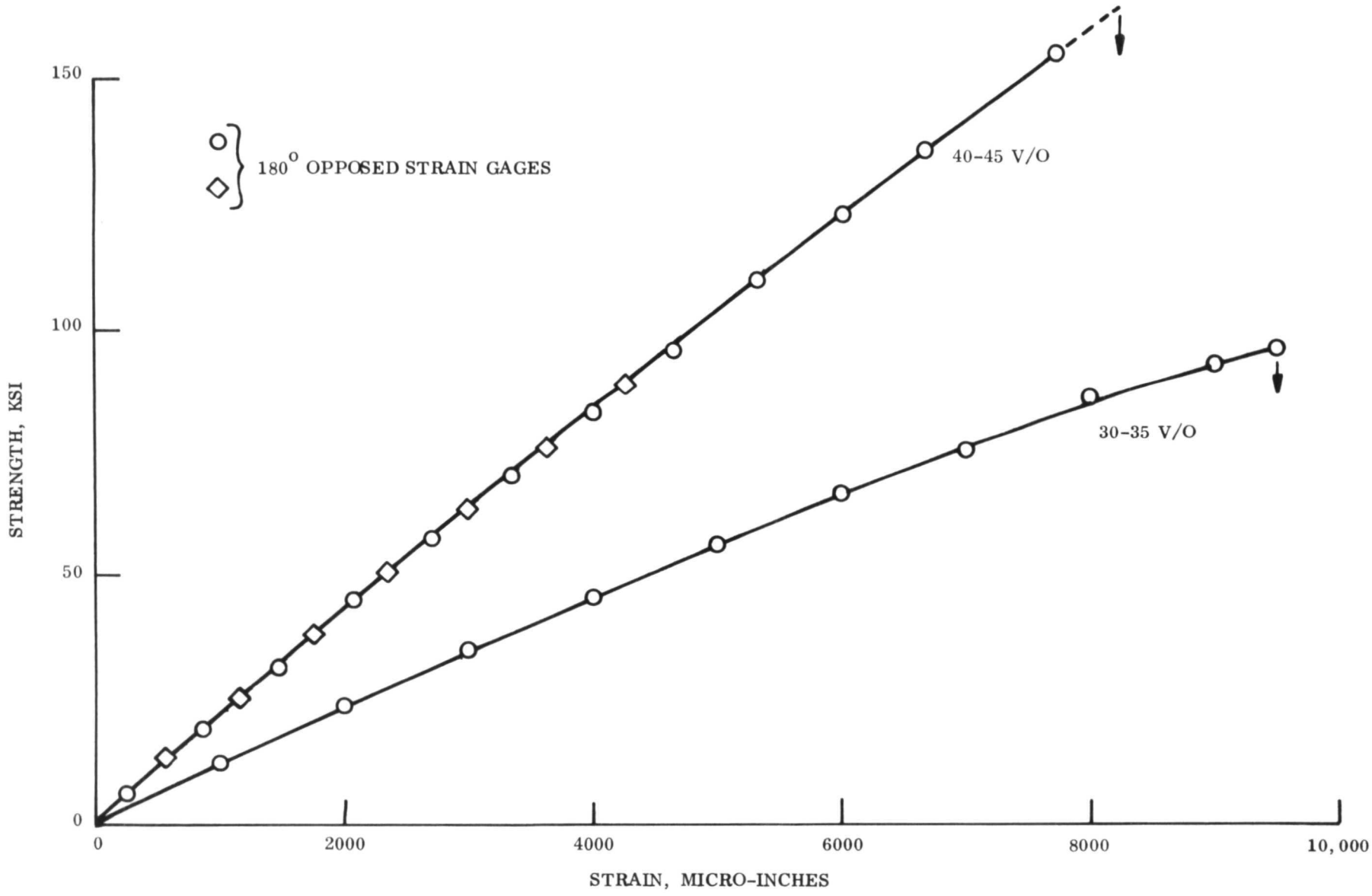

Figure 44. Compression Stress-Strain Curves of Carbon-Epoxy Composites

The failed specimens are shown in Figure 45, both in an overall view and with one specimen photographed at a higher magnification to show more details of the fracture. All the specimens failed abruptly, and showed various degrees of longitudinal splitting and, in some cases, shear type failures. An exception was the specimen prepared using the modified resin (see Table I). In this case, only a small amount of spliting was observed and some degree of brooming at the fracture surfaces was noted. In addition, the strength appears low when compared to the data for the unmodified resin. Additional tests will have to be performed to determine if such behavior is due to a poorly prepared specimen or to the difference in moduli of the two resin formulations.

4.0 CONCLUSIONS AND RECOMMENDATIONS FOR FUTURE WORK

Effects of Fiber Surface Treatment on Fracture Mechanisms For Tensile Tests Of Unidirectional Reinforced Composites

1. Surface treatment of both HT and Type A graphite fibers results in a cleavage failure mode when individual fibers fail in model composite specimens. This is in contrast to the debonding which occurs when the fibers are untreated.

2. There is a very definite correlation between local failure mechanisms observed in model specimens and gross fracture modes in engineering composite specimens for both modified and unmodified DEN 438, or the ERL 4617 system.

3. Although both model composite and engineering composite fracture modes are affected by fiber surface treatment, there appears to be no appreciable difference in the ultimate tensile strength of engineering composites using treated and untreated fibers in either resin system.

Comparison of Fracture Mechanisms for Different Fiber Types

4. Two separate batches of untreated HT fibers have been found to produce distinctly different local fracture mechanisms in the modified epoxy-resin. Although manufacturer's data and tests performed during this program showed no difference in fiber strength, we concluded that differences in the interfacial bonding for the two fiber batches resulted in this behavior.

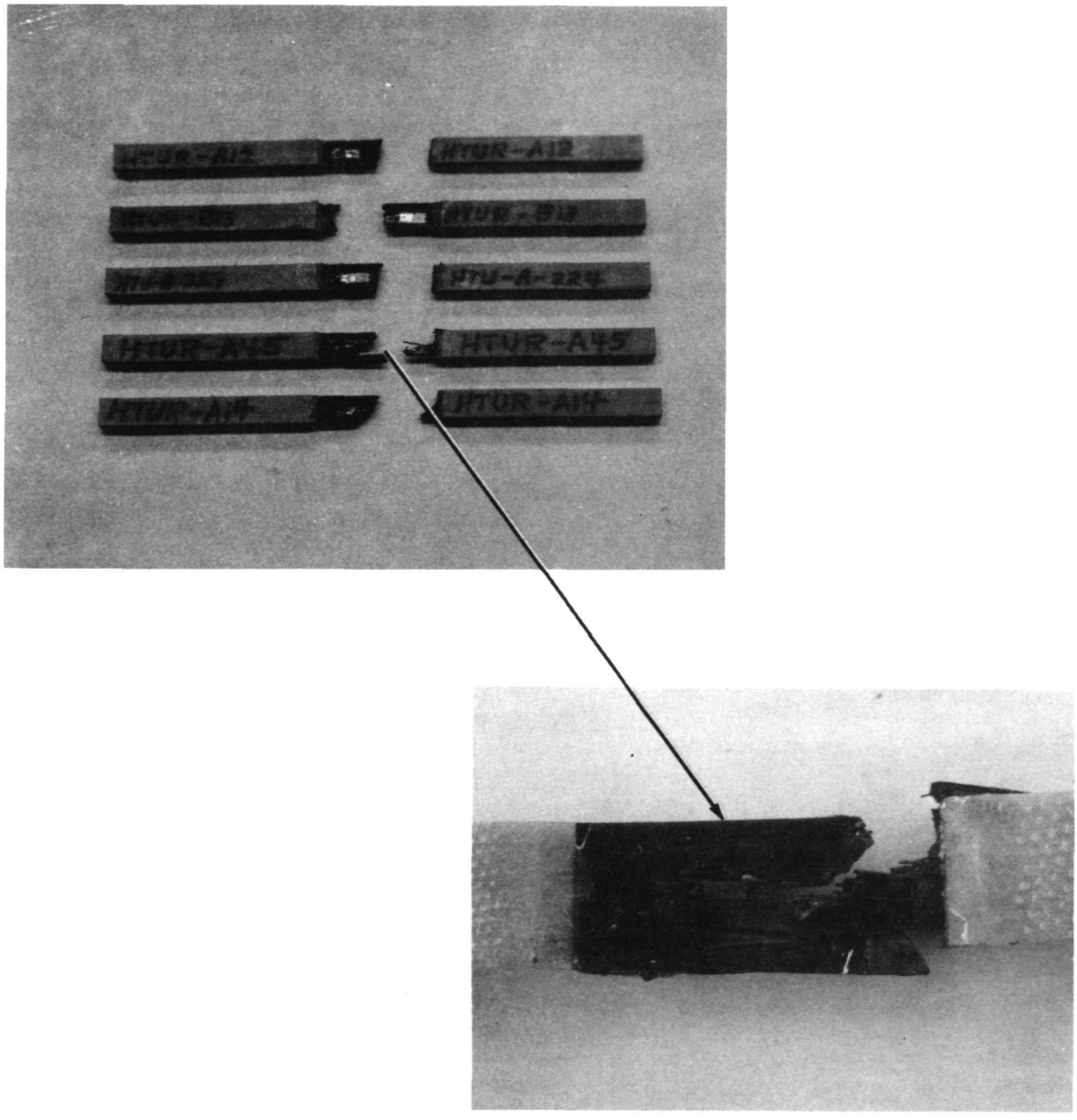

Figure 45. Compression Fracture Modes for HT Fibers in Both Epoxy-Novolac Resin Formulations

5. The difference between the two fiber batches is also quite evident in the fracture modes observed in engineering composites. Cleavage type fracture was the dominant fracture for the original batch of fibers whereas interfacially oriented cracks were predominantly observed for the new batch of fibers. We concluded that the latter is the more efficient failure mode since it involves a greater specimen volume.

6. The tensile strength of the engineering composites made from the two fiber batches support the above conclusion. Composites made with the new batch of fibers are stronger than those made with the original batch for the same fiber content. Because both batches have the same strength properties and specimens are fabricated identically, we conclude that the difference in interfacial response is the source of this difference in composite tensile strength.

7. Composites containing untreated Type A fibers generally show a greater degree of acoustic activity than HT fibers in the same matrix. Since the dominant failure mode for the Type A fibers is interface oriented while that of the HT fibers (original batch) is cleavage, we conclude that either more Type A fibers are able to reach their potential before the specimen fails, or that the interface failure generates more noise than the cleavage process.

Effect of Fiber Content on Fracture Mechanisms

8. For untreated HT fibers (original batch) in unmodified epoxy resin, lower fiber content results in cleavage fracture at a single location while high fiber content involves several cleavage sites connected by long interface oriented cracks. In every case the weaker specimens at a given fiber content failed by a single cleavage crack. We conclude that the failure at a single location normal to the fibers is due to the inability of the matrix and interface to contain the first fiber fractures thus generating an unstable crack which causes premature failure. This situation is aggravated by local flaws when the resin is unmodified.

9. For untreated HT fibers (new batch) in the modified epoxy resin, lower fiber content results in more localized fracture zones but with considerably more interface oriented fracture surface. As fiber content increases a greater volume of specimen is fractured and separation at the interface is the dominant failure mode.

10. The new batch of HT fibers in the modified resin formulation gives consistently higher tensile strengths than the original batch of fibers in the unmodified resin at all fiber content levels. Further, the scatter in strength values for the latter system appears to increase with fiber content. Since the fiber strengths are the same for each batch of fibers we conclude that these differences are related to the ability of the matrix and interface to contain local fiber fractures effectively.

11. Acoustic activity increases with fiber content for untreated HT fibers in the unmodified resin. This is consistent with visually observed fracture modes where numerous cleavage sites develop at higher fiber content and these are joined by a few longitudinal cracks. This results in more fracture surface and more broken fibers.

12. Compression behavior of axially aligned HT fibers in modified epoxy resin shows a nonlinear stress-strain diagram which becomes more pronounced as fiber content decreases. There are several possible reasons for this behavior which involve both fiber and matrix parameters.

Composite/Metal Specimen Behavior

13. When a flat composite is sandwiched between two aluminum face sheets and tested in tension with all fibers parallel to the load direction, there are three regions of mechanical response each leading to a more compliant behavior. In the final phase the metal can support load elastically when the composite has failed at a fixed deformation level. This behavior can provide a valuable fail-safe design advantage in certain applications and requires further study to optimize this performance.

14. Tubular specimens which employ carbon epoxy over an aluminum substrate with fibers parallel to the tube axis can be seriously limited by longitudinal splitting resulting from fabrication induced residual stresses. The unmodified epoxy resin is much more sensitive to this condition than the modified resin. We conclude that a tougher resin should be used in such applications where thermal mismatch between the substrate and composite is significant.

There is much yet to be explored regarding the effects of fiber properties, surface treatment and matrix crack sensitivity on fracture of composites for more complex loading conditions. Certainly a resin formulation which is effective in tensile applications may be undersirable in a composite where interlaminar shear or compression is the dominant load condition. Only by examining failure modes and identifying critical parameters for each can we hope to truly "tailor" these

materials. Emphasis here has been placed on tensile strength because this is the most common property measured in comparing composite systems without the complication of a stress gradient. A parallel study of compressive failure processes would help to resolve the problem of why carbon/epoxy composites generally yield lower compressive strengths than boron/epoxy while their tensile strengths are comparable. Another area of interest is the effect of thermal cycling on composite integrity. This will be the focal point for further research during the coming year.

REFERENCES

1. Gatti, A., et al, "Investigation of the Reinforcement of Ductile Metals with Strong, High Modulus Discontinuous, Brittle Fibers," Final Report NASw-1543, November 1967.

2. Tyson, W. R., and Davies, G. I., "A Photoelastic Study of the Shear Stresses Associated with the Transfer of Stress During Fiber Reinforcement," British Journal of Applied Physics, Vol. 16 (1965).

3. Schuster, D. M. and Scala, E., "The Mechanical Interaction of Sapphire Whiskers with a Birefringent Matrix," Transactions of the Metallurgical Society of AIME, Vol. 230, December 1964.

4. Marsh, D.M., "Micro-Tensile Testing Machine," J. Sci. Inst. Vol. 38, 1961, p. 229.

5. Mullin, J. V., Mazzio, V. F. and Mehan, R. L., "Basic Failure Mechanisms in Advanced Composites," NASA Progress Report, Contract NASw-2093, October 1971.

6. Mullin, J. V. and Mazzio, V. F., "Basic Failure Mechanisms in Advanced Composites," NASA Final Report, Contract NASw-2093, April 1971.

7. Mullin, J. V. and Mazzio, V. F., "Basic Failure Mechanisms in Advanced Composites," NASA Progress Report, Contract NASw-2093, November 1970.

8. Santelli, M. L. and Simon, R. A., "Water Exposure of Stressed Graphite Fiber Composites," NOLTR 70-258, 8 February 1971.

9. Arridge, R. G. C., "Mechanical Properties of Fibre Reinforced Resins-Part 2 - A Theory of Fracture of Fibre Reinforced Viscoelastic Materials," University of Oxford, Oxford, England, 1969 Report No. 1084/69, U. S. Department of Commerce/N.B.S. Report N70-26202.

10. Kaiser, J., "Erkenntnisse und Folgorungen aus dor Messung von Gerauschen bei Zugbeans pruchung von metallischen Workstoffen," Arch, Eisenhutt Wes. 1 43 (1953).

11. Schofield, B. H. "Acoustic Emission under Applied Stress," ARL-150 (1961).

12. Liptai, R. G., et al, "Acoustic Emission Techniques in Materials Research, " Univ. of California, Lawrence Radiation Laboratory, Report UCRL-72582, Sept. 1970.

13. Tatro, C. A., "Experimental Considerations for Acoustic Emission Testing," Mat. Des. and Stds., 11, 17 (1971).

14. Mullin, J. V., Mehan, R. L., "Prediction of Composite Materials Performance through Acoustic Emission Analysis," to be published.

15. Dunnegan, H.L., et al, "Fracture Analysis by Acoustic Emission," Eng. Fract. Mech. 1, 105 (1968).

16. Zweben, C., "Tensile Failure of Fibrous Composites, " AIAA J. 6, 2325 (1968).

17. Fahney, A. A., Ragai, A. N., "Thermal Expansion of Graphite-Epoxy Composites", J. Appl. Phys., 41 , 5112 (1970).

18. Ashton, J.E., et al, "Primer on Composite Materials: Analysis". Technomic Publishing Co., Conn. 1969, p. 110.

19. Timoschenko, S., "Strength of Materials - II". D. Van Nostrand, Princeton, 1956, p. 211.

20. Zender, G. W., Dexter, H. B., "Compressive Properties and Column Efficiency of Metals Reinforced on the Surface with Bonded Filaments". NASA TN-4878, NW 1968.

21. Hercules, Incorporated. Bulletin ACM-9.

22. Structural Design Guide for Advanced Composite Applications First Edition, August 1969, North American Rockwell, prepared under AFML Contract F33615-69-C-1368.

DISTRIBUTION LIST

	COPIES
National Aeronautics and Space Administration Lewis Research Center 21000 Brookpark Road Cleveland, Ohio 44135	
Attn: Contracting Officer, MS 500-313	1
Technical Report Control Office, MS 5-5	1
Technology Utilization Office MS 3-16	1
AFSC Liaison Office, MS 4-1	2
Library, MS 60-3	2
Office of Reliability & Quality Assurance, MS 500-111	1
G. M. Ault, MS 3-13	1
R. H. Kemp, MS 49-3	1
S. S. Manson, MS 49-12	4
Polymer Matrix Composite Section, MS 49-3	15
National Aeronautics and Space Administration Washington, D.C. 20546	
Attn: G. C. Deutsch, Code RW	1
J. J. Gangler, Code RWM	1
B. G. Achhammer, Code RWM	1
National Technical Information Service Springfield, Virginia 22151	40
National Aeronautics and Space Administration Ames Research Center Moffett Field, California 94035	
Attn: Library	1
National Aeronautics and Space Administration Flight Research Center P. O. Box 273 Edwards, California 93523	
Attn: Library	1

National Aeronautics and Space Administration
Goddard Space Flight Center
Greenbelt, Maryland 20771

Attn: Library 1

National Aeronautics and Space Administration
John F. Kennedy Space Center
Kennedy Space Center, Florida 32899

Attn: Library 1

National Aeronautics and Space Administration
Langley Research Center
Langley Station
Hampton, Virginia 23365

Attn: E. E. Matthauser 1
R. A. Pride 1
H. W. Herring 1

National Aeronautics and Space Administration
Manned Spacecraft Center
Houston, Texas 77001

Attn: Library 1
Code EP 1

National Aeronautics and Space Administration
George C. Marshall Space Flight Center
Huntsville, Alabama 35812

Attn: J. Curry 1
J. Stuckey 1

Jet Propulsion Laboratory
4800 Oak Grove Drive
Pasadena, California 91103

Attn: Library 1

Office of the Director of Defense
Research and Engineering
Washington, D.C. 20301

Attn: H. W. Schulz, Office of Assistant Director (Chem. Technology) 1

Defense Documentation Center
Cameron Station
Alexandra, Virginia 22314 1

Research and Technology Division
Bolling Air Force Base
Washington, D.C. 20332

Attn: RTNP 1

Air Force Materials Laboratory
Wright-Patterson Air Force Base
Dayton, Ohio 45433

Attn: D. L. Schmidt 2
T. J. Reinhart 2
S. W. Tsai 1
N. J. Pagano 1
J. M. Whitney 1

Office of Aerospace Research (RROSP)
1400 Wilson Boulevard
Arlington, Virginia 22209

Attn: Major Thomas Tomaskovic 1

Arnold Engineering Development Center
Air Force Systems Command
Tullahoma, Tennessee 37389

Attn: AEOIM 1

Air Force Rocket Propulsion Laboratory
Edwards, California 93523

Attn: RPM 1

Air Force Flight Test Center
Edwards Air Force Base, California 93523

Attn: FTAT-2 1

Air Force Office of Scientific Research
Washington, D.C. 20333

Attn: SREP, J. F. Masi 1

Commanding Officer
U. S. Army Research Office (Durham)
Box GM, Duke Station
Durham, North Carolina 27706 1

U. S. Army Missile Command
Redstone Scientific Information Center
Redstone Arsenal, Alabama 35808

Attn: Chief, Document Section 1

Bureau of Naval Weapons
Department of the Navy
Washington, D.C. 20360

Attn: DLI-3 1

Commander
U. S. Naval Missile Center
Point Mugu, California 93041

Attn: Technical Library 1

Commander
U. S. Naval Ordnance Test Station
China Lake, California 93557

Attn: Code 45 1

Director (Code 6180)
U. S. Naval Research Laboratory
Washington, D.C. 20390

Attn: H. W. Carhart 1

Picatinny Arsenal
Dover, New Jersey

Attn: SMUPA-VP3 1

Aeronautic Division of Philco Corporation
Ford Road
Newport Beach, California 92600

Attn: L. H. Linder, Manager 1
Technical Information Department

Aeroprojects, Inc.
310 East Rosedale Avenue
West Chester, Penna. 19380

Attn: C. D. McKinney 1

Aerospace Corporation
P. O. Box 95085
Los Angeles, California 90045

Attn: Library-Documents 1

Aerotherm Corporation
800 Welch Road
Palo Alto, California 94304

Attn: Roald Rindal 1

ARO, Incorporated
Arnold Engineering Development Center
Arnold Air Force Station, Tennessee 37389

Attn: B. H. Goethert, Chief Scientist 1

Atlantic Research Corporation
Shirley Highway and Edsall Road
Alexandria, Virginia 22314

Attn: Security Office for Library 1

AVCO Corporation
Space Systems Division
Lowell Ind. Park
Lowell, Mass. 01851

Attn: Library 1

Battelle Memorial Institute
505 King Avenue
Columbus, Ohio 43201

Attn: Report Library, Room 6A 1

Bell Aerosystems, Inc.
Box 1
Buffalo, New York 14205

Attn: T. Reinhardt 1

The Boeing Company
Aero Space Division
P. O. Box 3707
Seattle, Washington 98124

Attn: Ruth F. Peerenboom (1190) 1

Chemical Propulsion Information Agency
Applied Physics Laboratory
8621 Georgia Avenue
Silver Spring, Maryland 20910 1

University of Denver
Denver Research Institute
P. O. Box 10127
Denver, Colorado 80210

Attn: Security Office 1

General Dynamics/Astronautics
P. O. Box 1128
San Diego, California 92112

Attn: Library & Information Services (128-00) 1

General Electric Company
Re-Entry Systems Department
P. O. Box 8555
Philadelphia, Pennsylvania 19101

Attn: Library 1

General Electric Company
Aircraft Engine Group
Cincinnati, Ohio

Attn: M. Grande 1

General Technologies Corporation
708 North West Street
Alexandria, Virginia

Attn: H. M. Childers 1

Hercules Incorporated
P. O. Box 98
Magna, Utah 84044

Attn: H. R. Macpherson 1

Institute for Defense Analyses
400 Army-Navy Drive
Arlington, Virginia 22202

Attn: Classified Libary 1

ITT Research Institute
Technology Center
Chicago, Illinois 60616

Attn: Library 1

Lawrence Livermore Laboratory
Livermore, California

Attn: T. T. Chiao 1

Lockheed-Georgia Company
Marietta, Georgia

Attn: Library 1

Lockheed Missiles & Space Company
Propulsion Engineering Division (D.55-11)
1111 Lockheed Way
Sunnyvale, California 94087 1

Lockheed Propulsion Company
P. O. Box 111
Redlands, California 92374

Attn: Library 1

Material Sciences Corporation
1777 Walton Road
Blue Bell, Penna. 19422

Attn: Library 1

McDonnell Douglas Aircraft Company
Santa Monica Division
3000 Ocean Park Boulevard
Santa Monica, California 90406 1

Monsanto Research Corporation
Dayton Laboratory
Station B, Box 8
Dayton, Ohio 45407

Attn: Library 1

North American Rockwell Corporation
Space & Information Systems Division
12214 Lakewood Boulevard
Downey, California 90242

Attn: Technical Information Center - D/096-722 (AJ01) 1

Northrop Corporate Laboratories
Hawthorne, California 90250

Attn: Library 1

Rocketdyne, A Division of
North American Rockwell Corporation
6633 Canoga Avenue
Canoga Park, California 91304

Attn: Library, Dept. 596-306 1

Sandia Corporation
Livermore Laboratory
P. O. Box 969
Livermore, California 94551

Attn: Technical Library (RPT) 1

V.P.I.
Department of Eng. Mech.
230 Norris Hall
Blacksburg, Virginia 24061

Attn: Professor G. W. Swift 1

SCI
6344 Irwindale Avenue
Azusa, California 91702

Attn: I, Petker 1

TRW, Inc.
TRW Equipment Laboratories
Cleveland, Ohio

Attn: W. E. Winters 2

United Aircraft Corporation
United Aircraft Research Laboratories
East Hartford, Conn. 06118

Attn: D. A. Scola 1

United Aircraft Corporation
Pratt and Whitney Aircraft
East Hartford, Conn.

Attn: Library 1

United Aircraft Corporation
United Technology Center
P. O. Box 358
Sunnyvale, California 94088

Attn: Library 1

Whittaker Corporation
Research and Development/San Diego
3540 Aero Court
San Diego, California 92123

Attn: K. Berg 1